Morphology of PLA/PBAT/PA ternary blends

Yang Fu

THÈSE DE DOCTORAT

de l'Université de recherche Paris Sciences et Lettres
PSL Research University

Préparée à MINES ParisTech

Morphology of PLA/PBAT/PA ternary blends

Morphologie des mélanges ternaires PLA/PBAT/PA

Ecole doctorale n°364

SCIENCES FONDAMENTALES ET APPLIQUEES

Spécialité Mécanique numérique et Matériaux

COMPOSITION DU JURY :

M. Jérémie SOULESTIN
IMT Lille Douai, Président du jury

M. Peter VAN PUYVELDE
KU Leuven, Rapporteur

Mme Trang PHAN
Université d'Aix-Marseille, Membre du jury

M. Jean-Jacques FLAT
ARKEMA, Membre du jury

Mme Edith PEUVREL-DISDIER
MINES ParisTech, Membre du jury

M. Patrick NAVARD
MINES ParisTech, Membre du jury

Soutenue par **Yang FU**
le 18 décembre 2017

Dirigée par
Edith PEUVREL-DISDIER
Patrick NAVARD

Table of contents

I Introduction and objectives of the study 1

Résumé du travail de thèse 8

II Literature survey 13

II.1 PLA based polymer blends 15

II.1.1 PLA as a bioplastic 15

II.1.2 Mechanical improvement of PLA by polymer blending 15

II.2 Immiscible ternary polymer blends 19

II.2.1 Polymer blend principles 19

II.2.1.1 Drop deformation and breaking 19

II.2.1.2 Drop coalescence 24

II.2.1.3 Combination of break up and coalescence 25

II.2.2 Immiscible ternary polymer blends 27

II.2.2.1 Macroscopic and microscopic considerations 28

Macroscopic view 28

Microscopic view 29

Contribution of the viscosity 31

II.2.2.2 Parameters controlling the microstructure 32

Parameters controlling the number of sub-inclusions 32

Parameters controlling the size of dispersed phase 33

Influence of mixing parameters 35

II.3 Measurement of interfacial tensions between polymers 36

II.3.1 Calculation of interfacial tension from intrinsic properties of each polymer 36

II.3.2 Calculation from the rheological response of a polymer blend 38

II.3.3 Dynamic/static observations of a drop/fibre/disk in a polymer melt 40

II.3.3.1 Equilibrium situation for a drop deformed by the 40

Pendent drop 40

Sessile drop 42

II.3.3.2 Relaxation to equilibrium after a deformation 43

Drop retraction 43

Fibre retraction 44

Thread breakup 45

Disk retraction 46

General comment 48

II.3.3.3 Equilibrium between interfacial tension and an imposed flow 48
II.3.4 Examples of interfacial tension measurements 49
II.4 Conclusion 51
References 52

III Materials and experimental methods 59
III.1 Polymers 61
III.2 Experimental Methods 62
III.2.1 Blend preparation 62
III.2.2 Compression moulding 64
III.2.3 Rheometer 64
III.2.4 Scanning electronic microscopy (SEM) and image analysis 64
III.2.4.1 SEM machines and observation modes 64
III.2.4.2 Sample preparation and image analysis 65
III.2.5 Rheo-optical observations 66
III.2.6 Tensile and impact test 71
III.2.7 DSC 72
III.2.8 X ray diffraction 72
III.2.9 Molecular analysis 72
References 73

IV Measurement of interfacial tension and morphologies of non compatibilized ternary blends 75
IV.1 Measurement of interfacial tension by Palierne model 77
IV.1.1 Working flow chart of characterization of interfacial tension by the Palierne model 77
IV.1.2 PBAT/PLA as an example 79
IV.2 Measurement of interfacial tension by drop retraction 82
IV.2.1 Working flow chart of drop retraction 83
IV.2.2 Retraction of PBAT drop in PLA as example 83
IV.2.3 Influence of molecular weight and inversed matrix on interfacial tensions on PLA/PBAT 84
IV.2.4 Drop deformation along the vorticity axis of PA in PBAT 85
IV.2.5 Influence of angle correction on the result of interfacial tension 86
IV.3 Summary of interfacial tension measurement 86
IV.4 Prediction and validation of ternary blend morphology 87
IV.4.1 Prediction on the morphology basing on interfacial force balance 87

IV.4.2 Interpretation of morphology from thermodynamic aspect **89**
IV.4.3 Mechanism to form this morphology **91**
IV.5 Influence of blend condition on the morphology of the ternary blend **92**
IV.6 Conclusion **94**
References **94**

V Compatibilized ternary blends **97**
V.1 Compatibilization with a commercial compatibilizer **99**
V.2 Synthesis and characterization of PBAT-b-PLA and PA-b-PBAT block copolymers **104**
V.2.1 Synthesis of block copolymers PBAT-b-PLA and PA-b-PBAT **104**
V.2.1.1 PBAT-b-PLA **104**
V.2.1.2 PA-b-PBAT **106**
V.2.2 Characterization of the PBAT-b-PLA and PA-b-PBAT block copolymers **108**
V.2.2.1 Molecular analysis **108**
V.2.2.2 DSC **112**
V.2.2.3 XRD **113**
V.2.2.4 Rheology **114**
V.2.3 Verification of compatibilization effect of diblock copolymer **115**
V.2.3.1 Influence on interfacial tension **116**
V.2.3.2 Influence on the size of inclusion in binary blends **116**
V.2.3.3 Influence on the hierarchy of ternary blend **117**
V.3 Compatibilized ternary blends **118**
V.3.1 Strategy to better control the morphology of a ternary blend **118**
V.3.2 Morphology of compatibilized ternary blends **123**
V.3.3 Mechanical properties of ternary and binary blends **126**
V.3.3.1 Tensile test **127**
V.3.3.2 Charpy test **131**
V.3.3.3 Understanding of the impact performance – deformation analysis during tensile test **132**
V.3.3.4 Fracture surfaces **135**
IV.4 Conclusion **136**
References **137**

VI General conclusion and future outlook **139**

Chapter I

Introduction and objectives of the study

I Introduction and objectives of the study

Polylactic acid (PLA) is the most widely used bio-based/biodegradable polymer. However, it suffers the disadvantage of having a low toughness. To overcome this weakness has been the subject of numerous studies.

A conventional method to overcome the brittleness of a glassy polymer is to combine it with an elastomeric phase, either in a chemical way (i.e. synthesis in a reactor) or in a physical way (i.e. by blending). The advantage of using reactor synthesis is that it can give morphologies which are difficult to obtain by polymer blending. For instance, in high impact polystyrene (HIPS) or high impact poly(methyl methacrylate) (PMMA), core–shell inclusions with an elastomeric shell and a rigid core dispersed in the polymer matrix are obtained by synthesis. Such morphologies can provide higher toughness enhancement than the biphasic morphology where an elastomeric phase is dispersed in the rigid matrix.

In the case of PLA, to our knowledge no process has yet been developed to produce complex morphologies with elastomeric phases by synthesis. The only way to improve its toughness is thus to blend it with other polymers, preferentially bio-based or/and biodegradable ones if there is a will to keep the environmentally friendly feature of PLA.

In the 1990s, research was carried out to study the morphology of non-miscible ternary blends. It was found that it is possible to achieve core–shell morphologies with ternary polymer blends. But all those studies were based on conventional polymers. In the present work, we will explore the possibility of achieving core–shell morphologies with PLA-based ternary polymer blends and verify whether this kind of morphology can indeed bring better toughness improvement than binary blends.

To reach this goal, the first question to answer is how to control the morphology of immiscible polymer blends. It is known that the key factor dominating the ternary blend morphology structuration is the three binary interfacial tensions between the three polymers. If the values of these interfacial tensions are known, the morphology of a ternary blend can then be predicted. This was our guideline. We first measured the interfacial tensions between the chosen polymers and the results of these measurements were used to theoretically predict the morphology of their ternary blends. We showed that the prediction and experimental observations are indeed in agreement and that semi-encapsulated morphologies can be obtained with PLA-based blends. However, this was

not our goal, which was to prepare core–shell morphologies. To modify the morphology of the ternary blends in such a way as to have a core–shell morphology, the interfacial tensions needed to be selectively changed. This was achieved by adding interfacial tension modifiers (often called compatibilizers) to the blends. We tried to use commercially available compatibilizers to tune the morphology but we failed since selective compatibilization was needed to induce a change in the ternary blend morphology. With the collaboration of a group from the University of Aix Marseille, two specific diblock copolymers were synthesized and their selective compatibilization effect was verified. With the help of these diblock copolymers, we succeeded in creating the core–shell morphology we were looking for. The mechanical properties of the obtained composites were measured and compared to those of binary blends.

Outside this general introduction (chapter I), the manuscript is organized around five chapters. The following paragraphs summarize their main content and our main results.

II Literature survey

This chapter describes what is known about PLA and PLA-based blends. Attention is paid to the mechanism of toughness improvement from core–shell morphologies and to the ways to control the morphology of polymer blends. The key factor controlling the morphology of ternary blends is the spreading coefficient, the relation between this parameter and ternary blend morphology being illustrated in Fig. I.1:

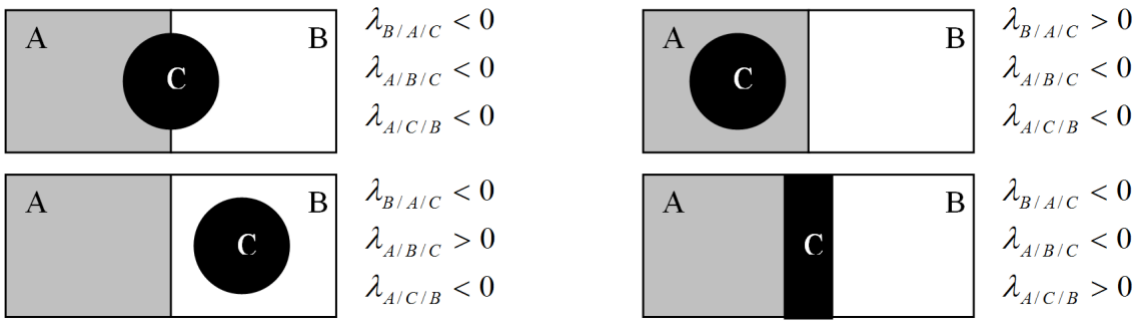

Fig. I.1 *Relation between spreading coefficients λ and the morphology of ternary blends composed of three polymers A, B and C.*

In Fig. I.1, λ is the spreading coefficient. It is calculated from the values of the interfacial tensions between polymers A, B and C:

$$\lambda_{B/A/C} = \gamma_{BC} - \gamma_{AB} - \gamma_{AC}$$
$$\lambda_{A/B/C} = \gamma_{AC} - \gamma_{AB} - \gamma_{BC}$$
$$\lambda_{A/C/B} = \gamma_{AB} - \gamma_{AC} - \gamma_{BC}$$

A summary of the methods used to measure the interfacial tension between two polymers is given. In order to have reliable measurements, two methods were chosen for this study: the first method is based on the Palierne model, the second on the kinetics of relaxation of a deformed drop.

III Materials and experimental methods

In this chapter, we describe the three polymers which were used in this work: PLA, poly(butylene adipate-co-terephthalate) (PBAT) and a copolyamide (PA). In the targeted morphology PLA was defined as the matrix, PBAT and PA as dispersed phases where PA should be encapsulated by PBAT. The apparatuses used to prepare the polymer blends and characterization methods are described.

IV Measurement of interfacial tensions and study of non-compatibilized ternary blends

In this chapter the characterization of the interfacial tensions between PLA, PBAT and PA was carried out with two methods (Palierne's model and drop retraction). The values of the interfacial tension we measured are given below:

	Palierne model (mN/m)	Drop retraction (mN/m)
PBAT/PLA	3.8	3 ± 0.4
PA/PLA	5.2	5.6 ± 0.3
PA/PBAT	2	3.3 ± 0.4

The values of the interfacial tensions from drop retractions were preferred to predict the morphology of the ternary blend (we obtained larger errors in interfacial tensions with the Palierne model). From the values of the interfacial tensions, the spreading coefficients in the PLA/PBAT/PA ternary blend can be calculated:

$$\lambda_{PBAT/PA/PLA} = \gamma_{PBAT/PLA} - \gamma_{PA/PBAT} - \gamma_{PA/PLA} < -5\ mN/m$$
$$\lambda_{PA/PBAT/PLA} = \gamma_{PA/PLA} - \gamma_{PBAT/PLA} - \gamma_{PA/PBAT} = -0.5 \pm 1\ mN/m$$
$$\lambda_{PA/PLA/PBAT} = \gamma_{PA/PBAT} - \gamma_{PBAT/PLA} - \gamma_{PA/PLA} < -5\ mN/m$$

Based on these spreading coefficient values, it was expected that the morphology should be either a core–shell one, where PA droplets are sub-inclusions in PBAT, or a semi-encapsulated one where PA droplets are sitting at the border of the PBAT and PLA phases. By preparing a ternary blend 60PLA/20PBAT/20PA in an internal mixer, it was confirmed that the morphology is indeed a semi-encapsulated one (Fig. I.2). The model was thus validated.

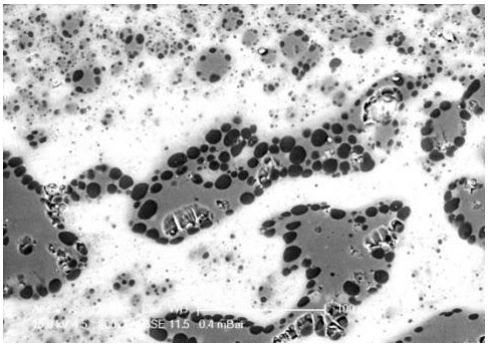

Fig. I.2 *Morphology of the ternary blend 60PLA/20PBAT/20PA prepared by melt mixing. The white matrix is PLA, the grey phase is PBAT and the black phase is PA.*

V Compatibilization of ternary blends

Although the morphology of ternary blends had been successfully predicted, our goal (i.e. to obtain a core–shell morphology) was not attained. The spreading coefficients, and thus the interfacial tensions, needed to be modified in order to push the morphology evolution in the aimed direction (Fig. I.3).

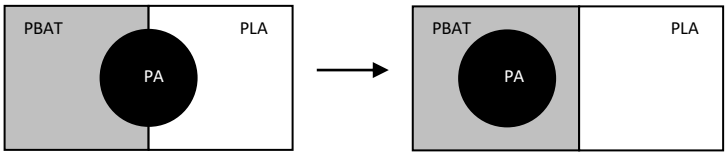

Fig. I.3 *Schematic representation of the morphology evolution from semi-encapsulation to core–shell*

Spreading coefficients satisfying the conditions below were thus needed:

$$\lambda_{PBAT/PA/PLA} = \gamma_{PBAT/PLA} - \gamma_{PA/PBAT} - \gamma_{PA/PLA} < 0 mN/m$$
$$\lambda_{PA/PBAT/PLA} = \gamma_{PA/PLA} - \gamma_{PBAT/PLA} - \gamma_{PA/PBAT} > 0\ mN/m$$
$$\lambda_{PA/PLA/PBAT} = \gamma_{PA/PBAT} - \gamma_{PBAT/PLA} - \gamma_{PA/PLA} < 0\ mN/m$$

Compared to the results of Chapter IV, $\lambda_{PA/PBAT/PLA}$ needed to be increased from negative to positive. There were two options to achieve this goal: either increasing the value of $\gamma_{PA/PLA}$ or reducing the value of $\gamma_{PBAT/PLA}$ and $\gamma_{PA/PBAT}$.

From the practical point of view, the latter option is easier to implement, as the interfacial tension can be reduced by adding a compatibilizer to the system. Ideally, it is preferable for the compatibilizer to be a selective one that reduces only the interfacial tension of PBAT/PLA and PA/PBAT blends, but not of PA/PLA blends. Based on this approach, a first trial was carried out with a commercial compatibilizer (Lotader), but it was found that this non-selective compatibilizer could not achieve the core–shell morphology since it reduces all three interfacial tensions in the ternary blend at the same time. Compatibilization with a selective block copolymer is mandatory in this case to achieve the desired core–shell morphology. Two block copolymers, PLA-*b*-PBAT and PBAT-*b*-PA, were synthesized and characterized. After checking their compatibilization effect, a strategy to achieve core–shell morphology was designed and applied to achieve the targeted core–shell morphology.

Afterwards, the mechanical performance of the ternary blends was evaluated and compared with PLA/PBAT binary blends since the purpose of this work was to see whether the core–shell morphology could bring some advantage in toughness compared with binary blends. However, the ternary blends did not show any advantage compared to binary blends in terms of either the stiffness or toughness properties. This may be due to the too low value of the modulus of the core phase relative to the two other polymers, making it unable to induce the multi-cavitation effect as in HIPS or to the imperfect morphology with the presence of a few droplets of PA at the interface.

VI Conclusions and perspectives

This work aimed at achieving direct core–shell morphologies in ternary PLA/PBAT/PA polymer blends by melt mixing. Interfacial tensions were determined and the three spreading coefficients were calculated. The blends prepared by melt mixing showed a partial encapsulation of the PA phase at the interface between the PLA and PBAT. This morphology was in agreement with the sign of the spreading coefficients. Two diblock copolymers were synthesized in order to have a selective compatibilization and to modify the PA sub-inclusion location. The presence of the block copolymers enabled us to modify the interfacial tension balance and to successfully change the morphology from partial encapsulation to full encapsulation of PA sub-inclusions in the PBAT drops. Due to the low modulus of the PA phase relative to the other phases, the

core–shell morphology of the ternary blend did not lead to an enhanced reinforcement relative to the binary blend.

Résumé du travail de thèse

L'acide polylactique (PLA) est le polymère le plus largement utilisé. C'est un polymère biosourcé et biodégradable. Cependant, il souffre d'un inconvénient qui est d'avoir une faible ténacité. De nombreux auteurs ont tenté de pallier à cette faiblesse.

Un procédé classique pour vaincre la fragilité d'un polymère vitreux consiste à le mélanger avec une phase élastomère, soit d'une manière chimique (synthèse au sein d'un réacteur), soit d'une manière physique (mélange de polymères à l'état fondu). L'avantage d'utiliser la voie synthèse est de pouvoir obtenir des morphologies difficiles à réaliser par mélange de polymères. Par exemple, dans le polystyrène choc (HIPS) ou dans le poly(méthacrylate de méthyle) (PMMA) choc, des morphologies coeur–peau avec des inclusions constituées d'un noyau rigide entouré d'une coque élastomère dispersées dans la matrice polymère ont été obtenues par voie synthèse. Une telle morphologie permet d'améliorer la ténacité de la matrice par rapport à au mélange binaire où une phase élastomère est dispersée dans la matrice rigide.

Dans le cas du PLA, aucun procédé, à notre connaissance, n'a encore été développé pour produire des phases élastomères de morphologies complexes par voie synthèse. La seule manière d'améliorer sa ténacité est donc de le mélanger avec d'autres polymères, de préférence biosourcés et/ou biodégradables pour conserver le caractère environnemental du PLA.

Dans les années 1990, des recherches ont été menées pour étudier la morphologie de mélanges ternaires non miscibles. Il a été constaté qu'il est possible d'obtenir des morphologies coeur–peau avec un mélange de polymère ternaire. Mais toutes ces études étaient basées sur des polymères conventionnels. Dans notre travail, nous avons exploré la possibilité d'obtenir une morphologie cœur–peau dans des mélanges de polymères ternaires à base de PLA et de vérifier si ce type de morphologie permet effectivement d'apporter une amélioration de la ténacité par rapport aux mélanges binaires.

Pour atteindre cet objectif, le premier point a été de comprendre comment contrôler la morphologie dans les mélanges de polymères non miscibles. Le paramètre clé qui domine la structuration de la morphologie d'un mélange ternaire est la tension

interfaciale des trois mélanges binaires. Si les valeurs des tensions interfaciales sont connues, la morphologie du mélange ternaire peut alors être prédite. Ce fut notre ligne directrice. Nous avons d'abord mesuré les tensions interfaciales entre les polymères de l'étude et les résultats de ces mesures ont été utilisés pour prédire théoriquement la morphologie des mélanges ternaires. Nous avons montré que les prédictions et les morphologies observées sur les mélanges ternaires sont en accord et que des morphologies avec une encapsulation seulement partielle des nodules de PA par le PBAT étaient obtenues dans les mélanges à base de PLA. Cependant, ce n'était pas l'objectif visé (morphologie cœur-peau avec une encapsulation complète des nodules de PA dans le PBAT). Pour modifier la morphologie des mélanges ternaires, les tensions interfaciales devaient être modifiées. Ce but a été atteint en ajoutant des agents compatibilisants (copolymères). Nous avons essayé d'utiliser des agents compatibilisants disponibles dans le commerce pour ajuster la morphologie, mais nous avons échoué car une affinité sélective avec les différentes phases était nécessaire pour modifier la morphologie du mélange ternaire. Avec la collaboration d'une équipe de l'université Aix Marseille, deux copolymères diblocs spécifiques ont été synthétisés et leur effet de compatibilisation sélective a été vérifié. Avec l'aide de ces copolymères diblocs, nous avons réussi à créer la morphologie cœur–peau que nous recherchions. Les propriétés mécaniques des composites obtenus ont été mesurées et comparées à celles des mélanges binaires.

Sans compter cette introduction générale (chapitre I), le manuscrit est organisé autour de cinq chapitres. Nous donnons ci-dessous un résumé du contenu et des principaux résultats de chaque chapitre.

II Etude bibliographique

Ce chapitre décrit ce qui est connu sur les mélanges à base de PLA. L'attention a été portée sur le mécanisme d'amélioration de la ténacité à partir de morphologies cœur-peau et sur les moyens de contrôler la morphologie des mélanges de polymères par voie mélange. Le paramètre clé contrôlant la morphologie des mélanges ternaires est le coefficient d'étalement, la relation entre ce paramètre et la morphologie du mélange ternaire étant illustrée sur la Fig. I.1.

Sur la Fig. I.1, λ est le coefficient d'étalement. Il est calculé à partir des valeurs des tensions interfaciales entre les polymères A, B et C:

$$\lambda_{B/A/C} = \gamma_{BC} - \gamma_{AB} - \gamma_{AC}$$
$$\lambda_{A/B/C} = \gamma_{AC} - \gamma_{AB} - \gamma_{BC}$$
$$\lambda_{A/C/B} = \gamma_{AB} - \gamma_{AC} - \gamma_{BC}$$

Un résumé des méthodes utilisées pour mesurer la tension interfaciale entre deux polymères est fait. Deux méthodes ont été choisies pour ces mesures dans cette étude: Une méthode est basée sur le modèle de Palierne, l'autre est basée sur la cinétique de relaxation d'une goutte déformée.

III Matériaux et méthodes expérimentales

Dans ce chapitre, nous avons introduit les trois polymères étudiés dans ce travail, le PLA, le poly (butylène adipate-co-téréphthalate) (PBAT) et le copolyamide (PA). La morphologie ciblée a été définie avec le PLA comme matrice, le PBAT et le PA comme des phases dispersées où les inclusions de PA sont encapsulées dans le PBAT. Les appareils utilisés pour préparer les mélanges de polymères et les méthodes de caractérisation sont décrits.

IV Mesure de tensions interfaciales et étude de mélanges ternaires non compatibilisés

Dans ce chapitre, la caractérisation des tensions interfaciales entre le PLA, le PBAT et le PA a été effectuée avec deux méthodes (modèle de Palierne et rétraction de goutte). Les valeurs des tensions interfaciales sont données ci-dessous:

	Palierne model (mN/m)	Rétraction de goutte (mN/m)
PBAT/PLA	3.8	3 ± 0.4
PA/PLA	5.2	5.6 ± 0.3
PA/PBAT	2	3.3 ± 0.4

Considérant les larges erreurs de nos mesures avec le modèle de Palierne, seules les valeurs de tension interfaciale issues des essais de rétraction de gouttes ont été utilisées pour calculer les coefficients d'étalement et pour prédire la morphologie des mélanges ternaires:

$$\lambda_{PBAT/PA/PLA} = \gamma_{PBAT/PLA} - \gamma_{PA/PBAT} - \gamma_{PA/PLA} < -5\ mN/m$$
$$\lambda_{PA/PBAT/PLA} = \gamma_{PA/PLA} - \gamma_{PBAT/PLA} - \gamma_{PA/PBAT} = -0.5 \pm 1\ mN/m$$
$$\lambda_{PA/PLA/PBAT} = \gamma_{PA/PBAT} - \gamma_{PBAT/PLA} - \gamma_{PA/PLA} < -5\ mN/m$$

Sur la base de ces coefficients d'étalement, la morphologie pourrait être soit une morphologie cœur–peau avec des inclusions de PA encapsulées (sous-inclusions) dans le PBAT ou partiellement encapsulées dans le PBAT (inclusions de PA localisées à la frontière entre le PBAT et le PLA). En préparant un mélange ternaire 60PLA / 20PBAT / 20PA en mélangeur interne, il a été confirmé que la morphologie est bien une morphologie semi-encapsulée. Le modèle est donc validé (Fig. I.2).

V Compatibilisation de mélanges ternaires

Même si la morphologie du mélange ternaire a été prédite avec succès, notre objectif (morphologie coeur–peau) n'était pas atteint. Pour pousser la morphologie à évoluer dans la direction visée (Fig. I.3), les coefficients d'étalement, et donc les tensions interfaciales, devaient être modifiés. Les coefficients d'étalement à atteindre sont donnés ci-dessous:

$$\lambda_{PBAT/PA/PLA} = \gamma_{PBAT/PLA} - \gamma_{PA/PBAT} - \gamma_{PA/PLA} < 0 mN/m$$
$$\lambda_{PA/PBAT/PLA} = \gamma_{PA/PLA} - \gamma_{PBAT/PLA} - \gamma_{PA/PBAT} > 0\ mN/m$$
$$\lambda_{PA/PLA/PBAT} = \gamma_{PA/PBAT} - \gamma_{PBAT/PLA} - \gamma_{PA/PLA} < 0\ mN/m$$

Par rapport aux résultats du chapitre III, $\lambda_{PA/PBAT/PLA}$ doit être augmenté pour devenir positif. Il y a deux options pour atteindre cet objectif, soit augmenter la valeur de $\gamma_{PA/PLA}$ ou réduire la valeur de $\gamma_{PBAT/PLA}$ et $\gamma_{PA/PBAT}$.

D'un point de vue pratique, cette dernière option est plus facile à mettre en œuvre, car la tension interfaciale peut être réduite en ajoutant un agent compatibilisant dans le mélange. Idéalement, un agent compatibilisant sélectif réduisant seulement la tension interfaciale des couples PBAT/PLA et PA/PBAT, et non dans le couple PA/PLA, est préférable. Sur la base de cette approche, un premier essai a été réalisé avec un compatibilisant commercial (Lotader), mais il a été constaté que ce compabilisant non sélectif ne permettait pas d'obtenir la morphologie cœur–peau, car il réduisait les trois tensions interfaciales dans le mélange ternaire en même temps.

La compatibilisation avec des copolymères à blocs sélectifs était donc indispensable pour obtenir la morphologie cœur–peau recherchée. Deux copolymères à blocs, PLA-*b*-PBAT et PBAT-*b*-PA, ont été synthétisés et caractérisés. Après avoir vérifié leur effet de compatibilisation, une stratégie pour parvenir à la morphologie coeur–peau a été mise au point et réalisée pour obtenir la morphologie ciblée.

Les performances mécaniques des mélanges ternaires ont aussi été évaluées et comparées à celles des mélanges binaires PLA / PBAT puisque le but de ce travail était de voir si la morphologie cœur–peau des mélanges ternaires pouvait permettre d'augmenter la ténacité par rapport aux mélanges binaires. Cependant, dans le cas présent, les mélanges ternaires ne présentent aucun avantage par rapport aux mélanges binaires en termes de rigidité et la ténacité. Cela est probablement dû au fait que le module des sous-inclusions (phase PA) n'est pas assez élevé pour avoir l'effet de multicavitation trouvé dans le polystyrène choc.

VI Conclusions et perspectives

Ce travail visait à obtenir des morphologies dites cœur–peau dans des mélanges de polymères ternaires PLA/PBAT/PA par voie fondue. Les tensions interfaciales ont été déterminées et les trois coefficients d'étalement calculés. Les mélanges préparés par voie fondue ont montré une encapsulation partielle de la phase PA à l'interface entre le PLA et le PBAT en accord avec le modèle. Deux copolymères à blocs ont été synthétisés afin d'avoir une compatibilisation sélective. Ces copolymères ont permis de modifier l'équilibre des tensions interfaciales et de la localisation des sous-inclusions de PA dans les gouttes de PBAT. Des mélanges avec une morphologie cœur–peau ont été obtenus par voie mélange. En raison du faible module de la phase PA par rapport aux autres phases, la morphologie cœur–peau du mélange ternaire n'a pas conduit au renforcement escompté par rapport à un mélange binaire ou à la non perfection de la morphologie obtenue (présence de gouttelettes de PA à l'interface entre le PBAT et le PLA.

Chapter II

Literature survey

II Literature survey

In this chapter, the first point of focus is PLA, which is the most widely used bioplastic. One of the factors limiting a wider application of this polymer is its weak toughness, which can be improved by blending it with an elastomeric phase. However, a morphology with a core–shell structure can improve even further the toughness (i.e. HIPS), but such a morphology has never been created with PLA.

Conventionally, a core–shell morphology is created by chemical synthesis, but this is not easily feasible with PLA. The literature shows that it should be possible to achieve this morphology by polymer blending. Thus, in the following part the principle used to control the morphology of immiscible polymer blends is introduced – from binary to ternary blends. It was found that interfacial tension plays the most important role in controlling the morphology of ternary blends. Various methods for the measurement of interfacial tension are thus described.

II.1 PLA-based polymer blends

II.1.1 PLA as a bioplastic

As early as in 1962, the term "renewable resource" was coined by Paul Alfred Weiss [Weiss, 1962] as "the total range of living organisms providing man with food, fibers, drug, etc…" With time, this definition has evolved in two different ways, renewable energy and renewable materials, which are regarded as alternatives to the diverse environmental and energy issues caused by the use of traditional fossil-based fuel and materials.

The present work deals with a specific type of renewable material, bioplastics, which refers to plastics derived from living substances such as plant oil, sugar or starch, etc. It is often confused with another concept, "biodegradable plastics", which only indicates that a certain type of plastic is biodegradable. Many bioplastics are biodegradable, with some exceptions like bio-based polyamide (PA) Rilsan®, some cellulose derivatives or bio-based polyethylene (PE). On the contrary, not all biodegradable plastics are bio-based, such as polycaprolactone (PCL) or polybutylene succinate (PBS). Thanks to environmental considerations, the trend to develop and use bio-based polymers will increase, as predicted in the European Bioplastics report [European Bioplastics, 2012] and seen in Fig. II.1.

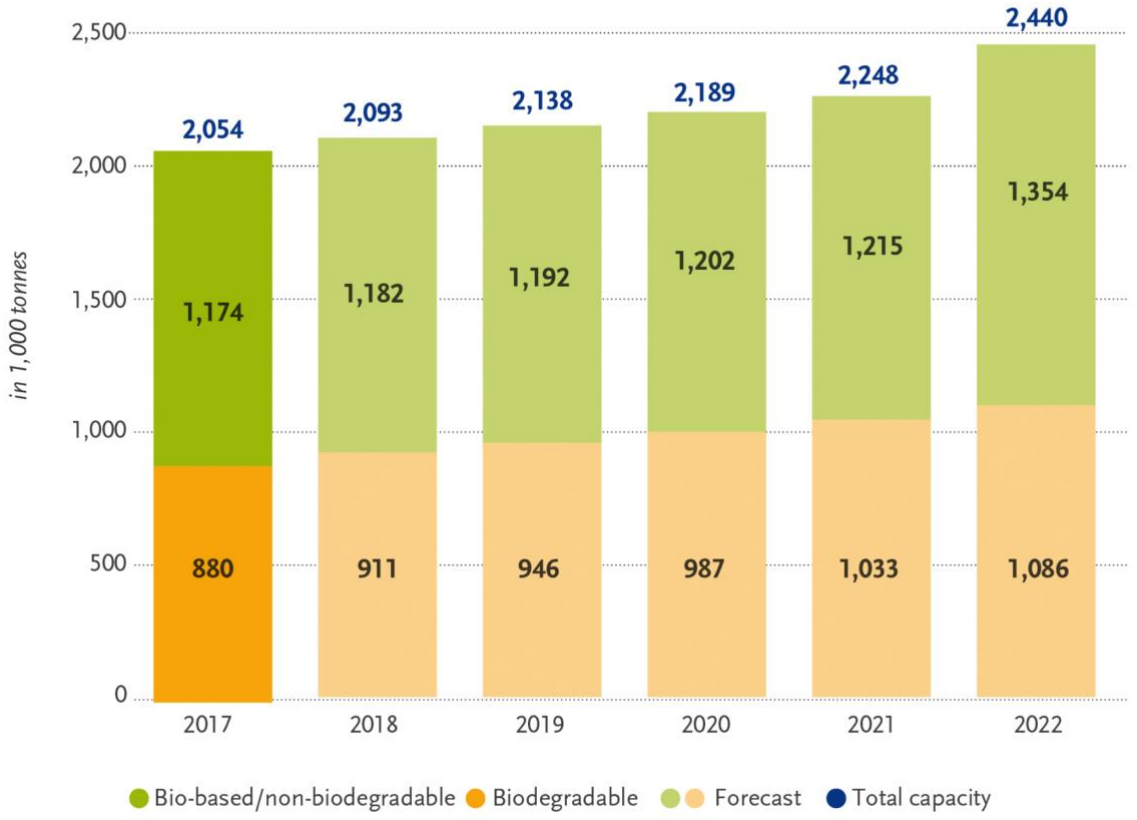

Fig. II.1 *Global production capacity of bioplastics* [European Bioplastics, 2017]

According to the predictions of European Bioplastics, the annual bioplastic production capacity in the year 2022 will be larger by 120% than that of 2017. Among those plastics, the one making the major contribution is polylactide (PLA), which accounted for 10.3% of the total bioplastic production in 2017 [European Bioplastics, 2017].

The main reason for the success of PLA is its bio-based characteristics associated with a good Life Cycle Assessment. In addition, it has good, but not outstanding, mechanical properties, the Young's modulus of pure PLA being between 3 and 6 GPa [Shen et al., 2009], showing a brittle rupture at around 4% deformation at room temperature. Another advantage is its processability to form classical pieces of equipment. For these reasons, it has been used to replace common plastics such as polypropylene or

polyethylene in different cases. The disadvantages limiting the further application of PLA are its weak chemical/environmental resistance and its poor ductility, which limit the use of PLA to packaging applications where large mechanical properties and durability are not needed.

II.1.2 Mechanical improvement of PLA by polymer blending

Blending with an elastomer phase is a traditional way to improve the ductility of brittle polymers [Wu, 1985]. As a matter of fact, a lot of work has been devoted to studying the blending of PLA with polymers such as PCL [Broz et al., 2003] [Todo et al., 2007], PBS [Wang et al., 2009] [Harada et al., 2007] and poly(butylene adipate-co-terephthalate) (PBAT) [Jiang et al., 2006] [Zhang et al., 2008], which are ductile at room temperature, in order to achieve a better toughness. These soft inclusions are often bio-based and/or biodegradable in order to preserve the ecologically friendly properties for the whole blend.

This enhancement of ductility by preparing a binary blend can be obtained by two correlated mechanisms, (1) cavitation of the dispersed phase and (2) redistribution of the stress in the matrix [Halary et al., 2008]. Under an external strain, for example a uniaxial traction, stress will concentrate around the heterogeneous part (the dispersed phase) and create a hydrostatic pressure inside the drop. As the traction continues, the pressure accumulates a potential energy inside the inclusion. Once the stored potential energy reaches a given threshold level, it will be released in the form of creating a new surface: a cavity is formed inside the inclusion. After the appearance of cavities, the normal stress around the inclusion reduces and leads to a redistribution of stress: the stress around the inclusions changes from triaxial to plane. Triaxial stress favours craze formation which is a signature of brittle rupture, while plane stress tends to induce chain slippage by shear. A shear band can thus be formed between inclusions if the distance between them is small enough [Wu, 1985]. The formation of these shear bands in the whole matrix will consume a considerable amount of energy, and that is the reason for the improvement of ductility.

Thanks to the relatively easy procedure to realize this approach, it has been widely applied to enhance the toughness of various rigid polymers. However, if backtracking on the history of strategies to improve the ductility of polymers, polystyrene (PS) binary blends with the elastomer polybutadiene (PB) were the first generation of enhancement. Nowadays, instead of preparing binary blends, further mechanical improvements can be achieved by replacing homogeneous elastomeric inclusions by complex inclusions composed of an elastomer shell and a rigid core, the so-called “core–

shell" structure or "salami" for the case with multiple cores. It is this kind of morphology that was created in high impact poly(methyl methacrylate) and high impact polystyrene (HIPS) [Halary et al., 2008]. The mechanism by which such structure provides better toughness is that under a mechanical strain, a multi-cavitation is created instead of the mono-cavitation in the case of a homogeneous inclusion. Hence, even more energy is consumed during deformation by this effect, as illustrated in Fig. II.2:

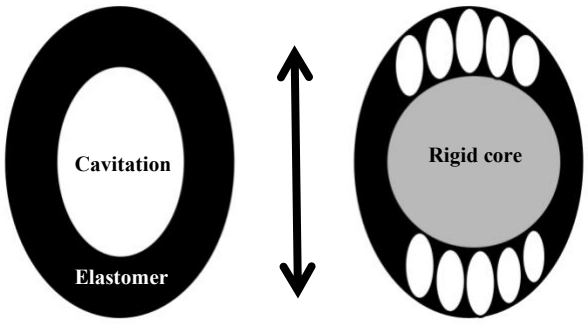

Fig. II.2 *Cavitation mechanisms in a pure elastomer inclusion and in a core–shell inclusion* [Schirrer et al., 1996]

Fig. II.2 illustrates the cavitation mechanisms in the case of two types of inclusions under a uniaxial stress. One single cavity is created in the pure elastomeric inclusions. But for the complex inclusion, since the modulus of the matrix and rigid core is much larger than that of the elastomer shell, little stress is transmitted to the core via the shell. During the strain, the rigid core barely deforms. Hence the elastomer in the polar location is being stretched and this finally leads to the creation of multiple small cavities. Supposing that the cavity volume is identical for both cases, there is obviously more area created in the case of multi-cavitation. As a consequence, more energy is consumed in this case and this mechanism of cavitation leads to a higher toughness [Schirrer et al., 1996].

In ternary blends, using a rigid core as sub-inclusion can also lead to an increase of the Young's modulus in comparison with binary blends. Overall, a core–shell structure can achieve both better rigidness and ductility at the same time. The only difficulty is to obtain such morphology. The realization of such a specific structure is difficult using traditional polymer blending methods. The complex inclusions used in HIPS and high impact PMMA are actually obtained by in situ chemical synthesis [Halary et al., 2008]. Although these two common plastics have been industrialized for a

long time, improvement aiming at simpler and more economical synthesis is still under development [Desbois et al., 2006].

Outside the chemical synthesis method, recent results on multiphase polymer blends have shown the possibility of obtaining such core–shell structures [Reignier and Favis, 2003] by classical mechanical blending, but these studies were mostly limited to some fossil-based polymers and they only focused on the morphology. The present work aimed at expanding such multiphase blending approaches using bio-based polymers and measuring the associated mechanical properties.

II.2 Immiscible ternary polymer blends

II.2.1 Polymer blend principles

The aim of polymer blending is to create a given morphology, usually by dispersing one immiscible polymer inside another one with a defined and controlled size and shape of dispersed inclusions, by distributing these inclusions or drops well, with the purpose of obtaining synergetic properties, i.e. better properties than the sum of those of individual polymers. In the case of thermoplastics which are in a solid state at room temperature, the mixing process is realized in their molten state. This process is conducted in an apparatus that is able to provide enough thermal and mechanical power to overcome the high viscosity of molten polymer.

For a more comprehensive understanding of the blending process, some principles for the blending of two immiscible liquids will be presented here considering two aspects: the local behaviour of a single drop and a global view on the whole polymer blend.

II.2.1.1 Drop deformation and breaking

When discussing the behaviour of a drop in the blend, two phenomena should be taken into consideration, first the mechanical stress τ which tends to deform the drop, and second the interfacial stress which counterworks with the shear stress and tries to minimize the interfacial area between the drop and the matrix. Such a competition is expressed in a parameter called the capillary number, defined as the ratio of the shear stress and the interfacial stress [Taylor, 1934]:

$$Ca = \frac{\tau_{12} R}{\gamma_{AB}} \qquad \text{Eq. 1}$$

where R is the radius of the drop and γ_{AB} is the interfacial tension. In a simple shear flow, the shear stress is written as $\tau_{12} = \eta_m \dot{\gamma}$, η_m is the viscosity of the matrix and $\dot{\gamma}$ is the shear rate. Thus the expression of the capillary number can be rewritten as:

$$Ca = \frac{\eta_m \dot{\gamma} R}{\gamma_{AB}} \qquad \text{Eq. 2}$$

During an increase of the shear rate, the shear stress progressively takes the dominant role. There is a critical value of Ca above which the drop will be broken by the flow: this value is the so-called critical capillary number Ca_{crit}. Taylor [Taylor, 1934] was the first to interpret the value of Ca_{crit} as a function of the viscosity ratio p (Eq. 3) between the viscosities of the dispersed phase (η_d) and the matrix.

$$p = \frac{\eta_d}{\eta_m} \qquad \text{Eq. 3}$$

Several scientists have extended his work [Grace, 1982], [Hinch and Acrivos, 1979, 1980] to both shear and elongational flows as shown in Fig. II.3:

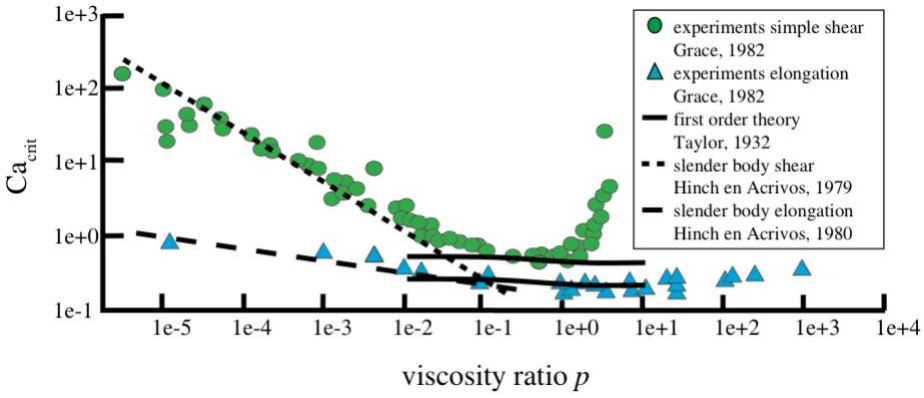

Fig. II.3 *Relationship between* Ca_{crit} *and* p *in different types of flow* [Stegeman et al., 2002]

As the curve corresponding to the elongational flow is always below that of the shear flow, it is an indication that an elongational flow has a higher efficiency in breaking a drop than shear. The explanation is simply that in a shear flow, only part of the shear is used to deform the drop, and the other part is only rotating the drop. On the curve corresponding to simple shear, there is a minimum Ca_{crit} existing when the value of p is around 1. When p is larger than 4, it is predicted that no drop breakage is possible, no matter how large the shear rate is.

To summarize the behaviour of a drop as a function of Ca, Utracki [Utracki, 2003] proposed the following rules:

$Ca < 0.1\, Ca_{crit}$, no deformation

$0.1\, Ca_{crit} < Ca < Ca_{crit}$, drop is deformed but not broken

$Ca_{crit} < Ca < 2\, Ca_{crit}$, drop is deformed and broken into two smaller drops by flow

$Ca > 2\, Ca_{crit}$, drop is deformed into a stable thread

An important and interesting issue about this well accepted conclusion by Utracki [Utracki, 2003] is that it is only valid under the hypothesis that the initial deformation of the drop is zero. To have a complete description of drop behaviour in flow, the amount of its deformation at the initial state should also be taken into consideration, as shown in Fig. II.4, which shows the drop behaviour for two initial deformation conditions. Fig. II.4 represents the deformation rate ratio between the dispersed phase and matrix as a function of the initial deformation of the drop (L equals the ratio between the length of the major axis of the deformed drop and its original radius). The viscosity of the dispersed phase and matrix are supposed to be identical in the two cases.

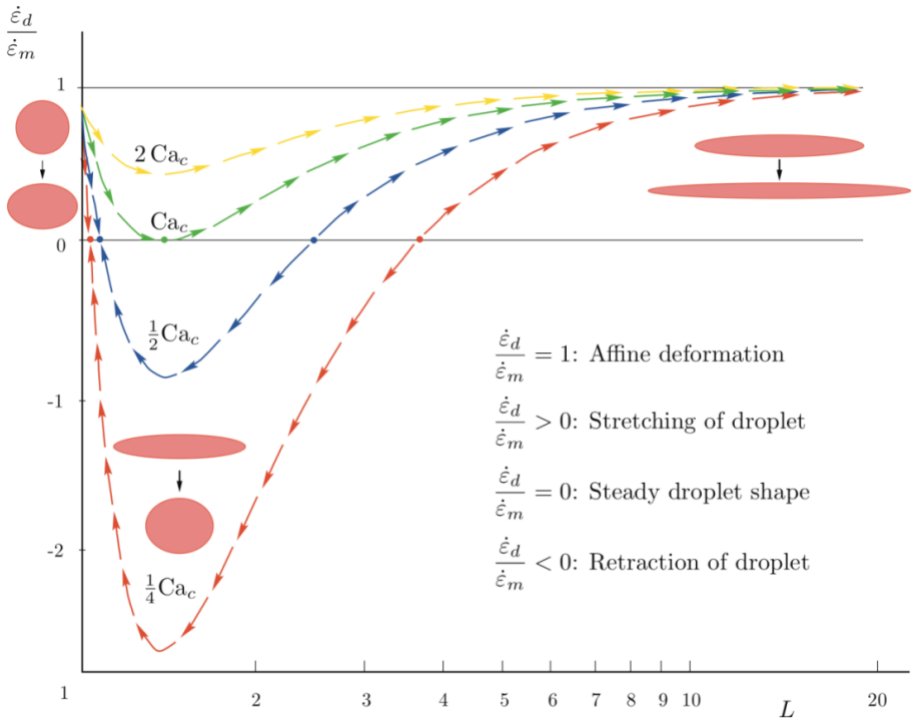

Fig. II.4 *Dependence of the drop deformation in shear on the initial drop deformation* [Stegeman et al., 2002]. *L represents the ratio of the length of the major axis of the deformed drop on its original radius*

If there is sufficient deformation at the beginning, the drop can be stretched into a long filament even with only $0.25\,Ca_{crit}$, as if the value Ca was larger than Ca_{crit} for an initially non-deformed drop.

When the value of Ca reaches the value of Ca_{crit} in the flow, Meijer et al. [Meijer et al., 2009] introduced the distinction between two mixing mechanisms to break the drop: distributive mixing ($Ca >> Ca_{crit}$) and dispersive mixing ($Ca \sim Ca_{crit}$). For distributive mixing, as the shear effect takes the dominant position, the dispersed phase deforms affinely with the matrix and does not develop capillary waves. In the mechanism of dispersion, drops deform into filaments and are finally broken into smaller drops due to the stretching effect of the flow, and locally the interfacial stress competes with the shear stress. The working principle of some static mixers is to perform such stretching by elongational flow and then to refold the blended material in order to repeat the elongation action [Meijer et al., 2009]. For dispersive mixing where the interfacial effect has an important effect, the drop is first stretched into a filament, then broken up into smaller drops by the growth of instabilities formed at the interface [Rayleigh, 1879].

A significant difference between the distributive and dispersive mixings is the role of time. During distributive mixing, the exclusive parameter is the maximum value of Ca. But for dispersive mixing, beside Ca, time should also be taken into consideration. An example is shown in Fig. II.5.

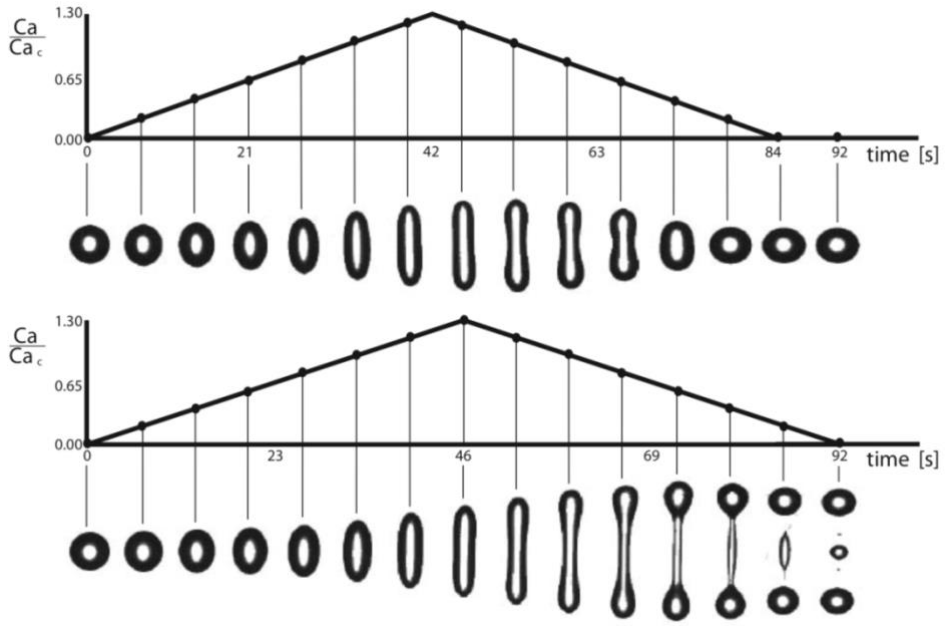

Fig. II.5 *Response of a drop under a similar triangle load of shear. All parameters are the same: maximum* $Ca/Ca_{crit} = 1.3$, $p = 1.3$ *but a difference of 8 s in the total duration of the experiment* [Meijer et al., 2009]

In Fig. II.5, the maximum ratio between Ca and Ca_{crit} is 1.3, and therefore it is under the case of dispersive mixing. The maximum value of Ca is identical in both cases, the only difference being the duration of shear: 84 s for the top scheme and 92 s for the bottom. Then, these 8 seconds of difference are enough for an instability to form at the interface, which finally leads to the drop breakup.

From the practical point of view, small inclusion sizes are often regarded as an indication of "good" dispersion. It is, however, interesting to discuss this issue. Between the two mechanisms of distributive and dispersive mixing, as defined by Meijer et al. [Meijer et al., 2009], which one is more efficient to obtain a fine dispersion? The well-known conclusion is that when the viscosity ratio is equal to unity, Ca_{crit} reaches a minimum value in shear flow, and then the drop size decreases easily by the shear effect, giving a distributive mixing mechanism for the breaking of drops. However, in the case of the stretching of a large drop into a long filament disintegrating into smaller drops by the interfacial instability effect, small satellite drops are formed during the last stage of the thread breakup [Elemans et al., 1990]. The size of these satellite drops is very small and impossible to attain by the simple effect of drop breakage by shearing [Meijer et al., 2009]. As a result, it is rather the dispersive mixing which can lead to very small drops.

II.2.1.2 Drop coalescence

Contrary to drop breakup which leads to a fine morphology, during coalescence two drops assemble into one and the morphology will coarsen by this mechanism. This procedure of coalescence can be divided into two steps: collision and drainage of the film sitting between the two drops.

Preceding coalescence, two drops have first to approach each other. The reason for this approaching motion is the flow dynamics, as the contribution of Van de Waals forces can be neglected considering the high viscosities of molten polymers. Once the two drops are close enough, the interface between them deforms from curved to flat to form a film. During the contact time of the drops, the thickness of the film decreases until a critical value h_{crit} is reached, where an instability begins to grow at the interface of the film and finally leads to the coalescence of the drops. There are three existing models to describe film drainage depending on the mobility of the interface: immobile, partially mobile or fully mobile. In the case of polymer blends, the partially mobile model is used since in this model the flow inside the drop is considered. Coalescence depends on two factors, the probability of collision between two drops and film drainage. In a simple shear flow, on average a drop collides with another drop after every time t_{coll} expressed as [Meijer et al., 2009]:

$$t_{coll} = \frac{\pi}{8\dot{\gamma}\varphi} \qquad \text{Eq. 4}$$

where $\dot{\gamma}$ is the shear rate and φ is the volume fraction of dispersed phase.

The probability of collision is defined as an exponential of the ratio between the collision time t_{coll} and the whole process time t_{proc} [Meijer et al., 2009]:

$$P_{coll} = \exp(-\frac{t_{coll}}{t_{proc}}) = \exp(-\frac{\pi}{8\dot{\gamma}\varphi t_{proc}}) \qquad \text{Eq. 5}$$

The probability of film drainage occurring is defined in a similar approach, the drainage probability being the exponential of the ratio between the time needed for the film drainage and the interaction time. Assuming that the sizes of the two colliding drops are identical, the probability can be written as:

$$P_{drain} = \exp(\frac{\sqrt{3}}{4}\frac{R}{h_{crit}} pCa^{3/2}) \qquad \text{Eq. 6}$$

In the equation above, R refers to the radius of the drop and p indicates the viscosity ratio between the dispersed phase and the matrix. Therefore, the probability of

coalescence is expressed as the product of those two probabilities. Fig. II.6 [Meijer et al., 2009] illustrates the combination of collision and film drainage.

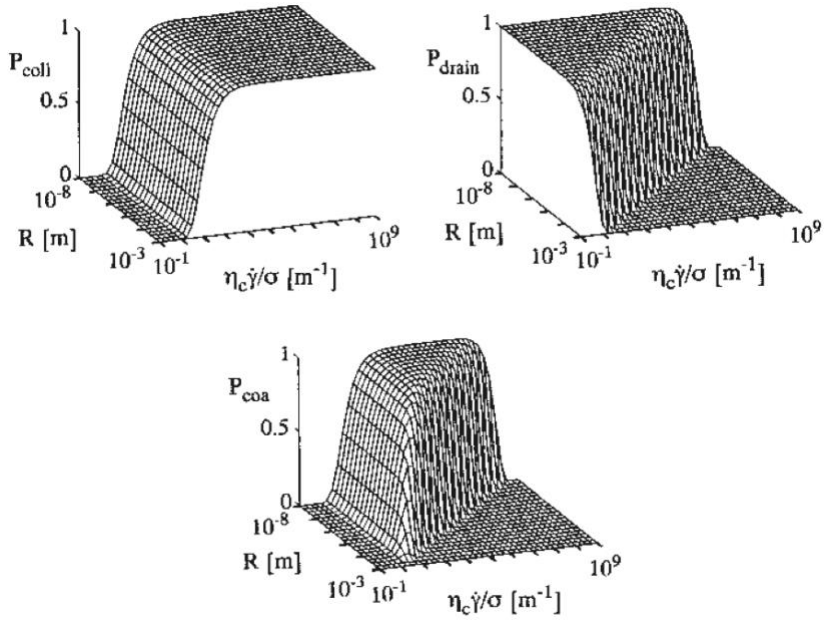

Fig. II.6 *Combination of collision and drainage probabilities under the following conditions: simple shear rate 0.01 s^{-1}; viscosities of dispersed phase and matrix equal to 1 Pa.s; γ_{AB}=10^{-2} N/m; $t_{proc} = 50s$; $h_{crit} = 10^{-9} m$; $\varphi = 0.1$.* [Meijer et al., 2009]

From Fig. II.6, it is obvious that at a similar volume fraction, small drop sizes are favourable for the coalescence process to occur. However, the limit of the shear rate is rather delicate: it should be large enough to press two drops together during the collision, but not too high to ensure enough interaction time of the two drops to allow the film drainage to take place.

II.2.1.3 Combination of breakup and coalescence

When considering the breakage and coalescence in a real polymer blend, the time should be taken into account. At the initial state of the blend, the polymer pellets melt, leading to sizes at the scale of millimetres which will lead to a large value of the capillary number. As a result, the distributive dispersion takes the dominant role in this first step of blending, decreasing the size of the inclusions. As the morphology becomes finer with the shear effect, the decreasing size of the dispersed phase results in a reduction of the capillary number and thus the dispersion mechanism changes into dispersive dispersion, which will lead to an even finer morphology. Because of the small inclusion size, the

coalescence is then more likely to happen at this stage of blending. At the end, breakup and coalescence are in a dynamical equilibrium state, and the average size of inclusions will not vary anymore.

The discussion here is to clarify the behaviour of drops near the dynamical equilibrium state. In the situation of a single drop, the competition between drop breakup and coalescence is described in Fig. II.7 with different models for coalescence, supposing that the viscosity ratio is equal to unity and the time is long enough for coalescence to take place [Meijer et al., 2009]. This idea was first introduced by Elmendorp [Elmendorp, 1986].

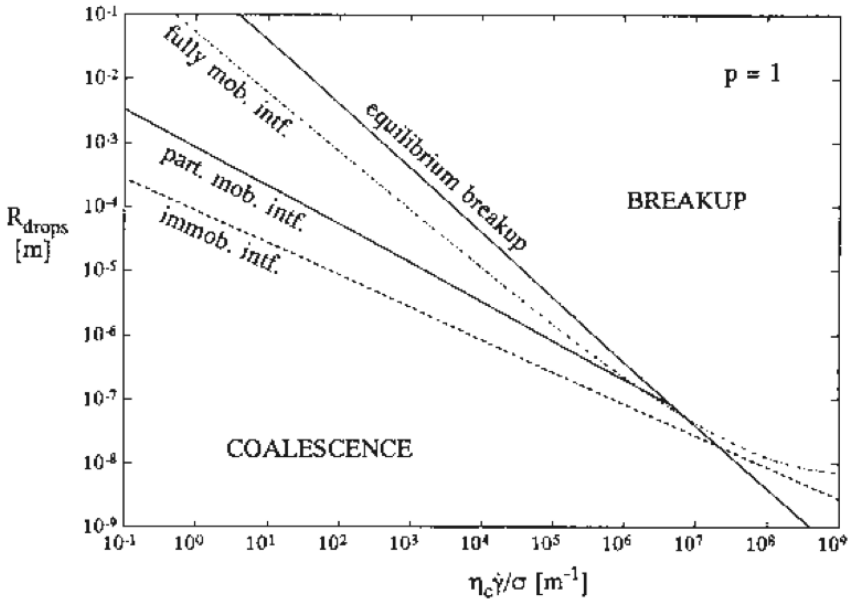

Fig. II.7 *Competition between breakage and coalescence under shear* [Meijer et al., 2009]

The solid line corresponds to equilibrium breakup and indicates the limit for shear-induced breaking. As discussed before, small drops are favourable for coalescence and breakage happens with large drops. The region between the equilibrium breakup line and the lines corresponding to coalescence is the region where drop sizes are stable. Yet this is still a too simple approach for a real polymer blend owing to the fact that both shear and elongational flow occur during a real blending process and the model of a single drop loses its validity when describing the integration of the whole blend. Aware of this issue, Wu [Wu, 1987] investigated the behaviour of the inclusion size of PA 6-6 and ethylene propylene rubber (EPR) blends with different polymer viscosities and a fixed volume fraction of dispersed phase equal to 15%. By studying the relationship

between the inclusion size and the shear rate, an "apparent critical capillary number" (Ca_{crit}^{app}) was introduced. The purpose of this new number is to simplify the breakup/coalescence (noting that breakup includes distributive and dispersive dispersion) competition into a simple shear-breaking model. If $Ca > Ca_{crit}^{app}$, drops are breaking up, otherwise they are coalescing. The relationship between Ca_{crit}^{app} and the viscosity ratio is shown in the following empirical equation:

$$Ca_{crit}^{app} = 4\left(\frac{\eta_d}{\eta_m}\right)^{\pm 0.84} \qquad \text{Eq. 7}$$

The exponent of the power law dependence takes a positive value if the viscosity ratio is larger than unity, otherwise it is negative. The great advantage of this model is that it can be used to estimate the average inclusion size in polymer blends. However, an obvious drawback of this model is that no coalescence due to the concentration of dispersed phase is taken into consideration since no term linked to it appears in the equation. Three years later, Serpe [Serpe et al., 1990] proposed a correction of Wu's equation by adding a term linked to the fraction of dispersed phase:

$$Ca_{crit}^{app} = 4\left(\frac{\eta_d}{\eta_m}\right)^{\pm 0.84} \Big/ \left[1-(4\varphi_m\varphi_d)^{0.8}\right] \qquad \text{Eq. 8}$$

where φ_m and φ_d refer to the volume fractions of matrix and dispersed phase respectively.

Although this equation is empirical, it is often used to estimate the average size of the included phase in the binary polymer blend.

II.2.2 Immiscible ternary polymer blends

Adding a third polymer gives a huge amount of morphological possibilities and the focal point of the study of ternary blends is quite different from that of binary blends. The theories predicting the morphology of immiscible ternary polymer blends were developed only 20 years ago, and it is still a new-born domain in polymer compounding, with few industrial applications. In the following discussion, the control of the morphology of ternary systems will be described.

II.2.2.1 Macroscopic and microscopic considerations

Macroscopic view

As for all systems in the world, the evolution of polymer blend morphology is towards a direction with lower free energy, in order to reach a more stable state. In a polymer blend, the expression of this parameter is written as:

$$G = \sum A_{ij}\gamma_{ij} + \sum n_i\mu_i \qquad \text{Eq. 9}$$

The first term refers to the interfacial contribution on the free energy, where A_{ij} stands for the interfacial area between phases, γ_{ij} for their interfacial tension. The second term is for the partial molar free energy which depends on the number of moles and on the chemical potential of each component. When discussing the possibility of obtaining different morphologies, it is not necessary to consider the term $\sum n_i\mu_i$ as the components of the blend do not vary. Only the interfacial contribution should be taken into account for the free energy. Guo et al. [Guo et al., 1997] were the first to apply this approach to predict the morphology of ternary blends. First, all the possible morphologies were drafted out. Then the term $\sum A_{ij}\gamma_{ij}$ of each possibility was calculated and compared. The morphology with the lowest free energy is the most probable to happen as it is the thermodynamically favourable state.

For instance, for two phases dispersing in a third one as matrix, three possible morphologies are drafted out as in Fig. II.8:

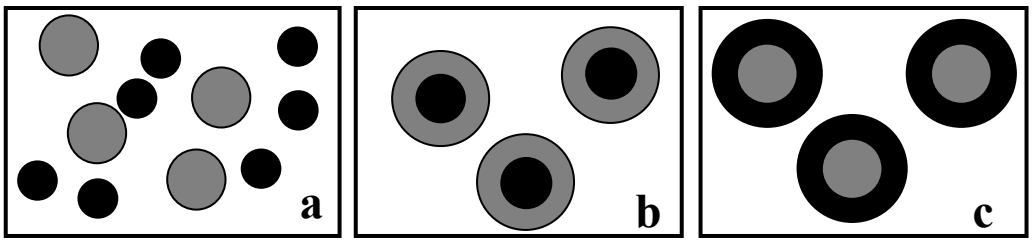

Fig. II.8 *Possible morphologies for a ternary blend*

The interfacial contributions to the free energy for morphologies a, b, and c in Fig. II.8 can be written as:

$$G_a = (4\pi N_g)^{1/3}(3\phi_g V)^{2/3}\gamma_{gw} + (4\pi N_b)^{1/3}(3\phi_b V)^{2/3}\gamma_{bw}$$

$$G_b = (4\pi N)^{1/3}(3\phi_b V)^{2/3}\left[\gamma_{gb} + (\frac{\phi_b + \phi_g}{\phi_b})^{2/3}\gamma_{gw}\right] \qquad \text{Eq. 10}$$

$$G_c = (4\pi N)^{1/3}(3\phi_g V)^{2/3}\left[\gamma_{gb} + (\frac{\phi_b + \phi_g}{\phi_g})^{2/3}\gamma_{bw}\right]$$

where G_a, G_b and G_c are the interfacial free energies of morphologies a, b and c, respectively. Subscripts *g*, *b* and *w* refer to the respective colour of the phase on the figure: grey, black and white. N is the number of drops, ϕ is the volume fraction, V is the total volume of the mixture and γ stands for the interfacial tension.

In Guo's paper [Guo et al., 1997], a rough approximation is used, stating that N_g, N_b and N are the same, which is obviously a suspicious hypothesis. This is the untoward part of this approach: to estimate the value of the total interfacial area in the blend is not a simple task as it means the sum of the surface area of millions of drops in the blends! One way to solve this question concerning the total interfacial area is to first use Wu or Serpe's equation (Eq. 7 or 8) to estimate the average inclusion size of the different dispersion phases, then to use it to calculate the average volume of the drops. As the total volume of the dispersed phase is a known factor when preparing the polymer blend, the number of drops can be deduced. Afterwards, it only needs to be combined with the average surface area of every drop to get the total value in the blend. Although this is a path to make the estimation, it is in practice very difficult to do due to the interplay of so many parameters. Error accumulates at each step of calculation and the result is not very reliable. Even more, when the morphology is complicated as in the case of semi-encapsulation, it just becomes inapplicable because there is still no theory that predicts the inclusion size of the semi-encapsulation situation. It is thus necessary to take a second approach into account.

Microscopic view

In this approach, the object of the study is no longer the whole blend but the local situation at the three polymer interfaces. A ternary polymer blend can be simply considered as a tri-phase deformable system, the interfacial preference determining what kind of structure will be formed locally. This "preference" is described by the interfacial force balance; the first study on this phenomenon was on the gas–liquid–solid system as shown in Fig. II.9:

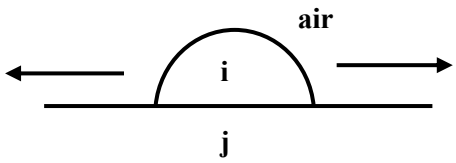

Fig. II.9 *Spreading of a liquid drop i on the substrate j in the air*

The condition for the liquid drop to cover the whole surface is that the spreading coefficient (λ_{ij}) defined in Harkins's equation [Harkins, 1941] is positive:

$$\lambda_{ij} = \gamma_j - \gamma_i - \gamma_{ij} > 0 \qquad \text{Eq. 11}$$

where γ_i and γ_j are the surface tension of liquid *i* and substrate *j*, γ_{ij} is the interfacial tension. Behind the mathematical expression of these phenomena, the mechanism is actually the interfacial preference: for instance, for an attracting surface with $\lambda_{ij} = \gamma_j - \gamma_i - \gamma_{ij} > 0$, it will lead to $\gamma_j > \gamma_i + \gamma_{ij}$. If surface tension γ_j is large, indicating a poor affinity between the solid phase and air, the area of the interface of these two phases has the tendency to decrease and this is exactly the motor for the liquid phase to spread, in order to minimize the solid–air interface area.

By extending the situation from gas–liquid–solid to three liquid phases, this theory can thus be applied to describe the morphology of ternary polymer blends [Hobbs et al., 1988]. The condition to have a full capsulation of phase *j* by phase *i* in the matrix of *k* is that the spreading coefficient is positive:

$$\lambda_{ij} = \gamma_{jk} - \gamma_{ik} - \gamma_{ij} > 0 \qquad \text{Eq. 12}$$

where γ_{ik} and γ_{jk} are the interfacial tensions instead of γ_j and γ_j. A schematised situation is shown in Fig. II.10:

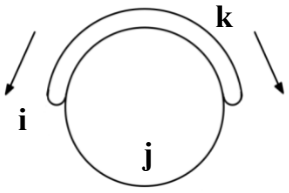

Fig. II.10 *Tendency of encapsulation of phase j by phase i in the matrix k*

Le Corroller and Favis [Le Corroller and Favis, 2009] developed this theory further by considering all the three spreading coefficients of the three phases:

$$\lambda_{B/A/C} = \gamma_{BC} - \gamma_{AB} - \gamma_{AC}$$
$$\lambda_{A/B/C} = \gamma_{AC} - \gamma_{AB} - \gamma_{BC} \qquad \text{Eq. 13}$$
$$\lambda_{A/C/B} = \gamma_{AB} - \gamma_{AC} - \gamma_{BC}$$

With different combinations of these three spreading coefficients, there are four possible morphologies, as shown in Fig. II.11:

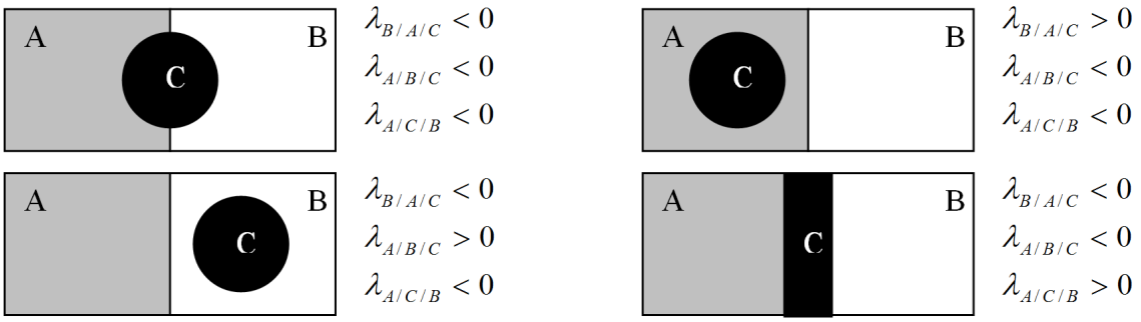

Fig. II.11 *Extension of spreading coefficient to ternary phases*

The advantage of this approach is that a study of the interfacial property is enough to predict the type of morphology. It has been used successfully to predict the morphology of ternary blends PET/PS/PEG [Kolahchi et al., 2014], HDPE/PA-6/EVOH [Rastin et al., 2014]. And thit is this method that will be applied in our study.

However, while it is known that the interfacial tension is the most important parameter controlling the morphology of ternary blends, other parameters like rheological effects should not be neglected.

Contribution of the viscosity

The models of Guo and Hobbs have successfully predicted the morphologies in ternary blends in most situations [Wilkinson et al., 2004] [Jazani et al., 2010] [Tchomakov, 2004] where the property of the interface with large values of spreading coefficients or high contrast of free energy is the main factor that determines the type of morphology. However, if the interfacial effect is weak, these models may no longer provide the correct prediction. The actual morphology depends on other parameters, as in the example below.

In a PP/liquid crystalline polymer (LCP)/polycarbonate (PC) blend [Nemirovski et al., 1995], the calculation of the spreading coefficient of the PC relatively to the LCP gives $\lambda_{PP/PC/LCP}$ =0.16. This means that in the PP matrix, the PC phase should form a shell around sub-inclusions of LCP, and the low value of $\lambda_{PP/PC/LCP}$ implies that the interfacial effect is rather weak for this blend. However, the obtained morphology is contrary to the prediction: LCP encapsulates the PC phase. The explanation for this phenomenon is that the viscosity of LCP is much lower than that of PC, so it is more difficult to deform the PC phase during the blend, which tends to remain in the shape of spheres. On the other hand, it is much easier for the LCP phase to form the shell despite the fact that this morphology is slightly unfavourable from the interfacial balance point of view.

II.2.2.2 Parameters controlling the microstructure

Parameters controlling the number of sub-inclusions

Ternary blends made of high density polyethylene (HDPE), polystyrene (PS) and poly(methyl methacrylate) (PMMA) can have a core–shell morphology with an encapsulation of PMMA by PS in an HDPE matrix, as shown by [Reignier and Favis, 2000]. In their work, the volume fraction (PS+PMMA)/HDPE was fixed at 20/80. A variation of the morphology of sub-inclusions was observed by changing the PS/PMMA volume ratio (Fig. II.12).

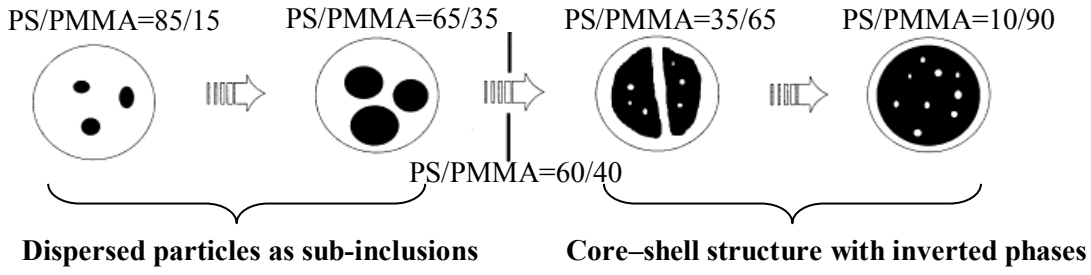

Fig. II.12 *Evolution of microstructure of composite drops in ternary (PS/PMMA)/HDPE blends on varying the PS/PMMA volume ratio* [Reignier and Favis, 2000].

As shown in Fig. II.12, at the point of phase inversion (PS/PMMA=60/40), a significant structural change occurs in the droplets: PMMA sub-inclusions (represented in black) change from dispersed spheres to a continuous phase, with PS becoming sub-inclusions. It can be noted that a layer of PS remains around the PMMA phase after phase inversion (last scheme in Fig. II.12). This is due to the large difference of the spreading

coefficient of the PS/PMMA blend. Similar phenomena on the phase inversion between inclusion and sub-inclusion were also found in PS/styrene-butadiene rubber (SBR)/PE blends [Luzinov et al., 1999].

Parameters controlling the size of dispersed phase

The size of dispersed phase in binary blends was well studied and described in the work of Wu [Wu, 1984] and Serpe et al. [Serpe et al., 1990]. Hemmati [Hemmati et al., 2001] succeeded in predicting the droplet size in a core–shell structure ternary blend considering the complex inclusion to be a homogeneous drop, with the viscosity being the weight average of the two dispersed phases and the interfacial tension equal to that between the shell and the matrix.

However, a study performed by Reignier and Favis [Reignier and Favis, 2000] in (PS/PMMA)/HDPE ternary and HDPE/PS, HDPE/PMMA binary blends gave a different picture. In all these three blends, HDPE served as matrix. Fig. II.13 shows the variation of the drop size versus the volume fraction of dispersed phase. The authors compared the droplet size in the ternary blend relative to the droplet size in the two binary blends obtained in similar conditions. They found that the average size of the droplets increases with the dispersed phase volume fraction for all blends. In the case where PS/PMMA=1/6 (Fig. II.13.a), the droplet size curve for the ternary blend is located between the curves for the binary blends. In the case of equal content of PS and PMMA (Fig. II.13.b), the droplet size curve in the ternary blend superimposes with the PS/HDPE blend curve when the dispersed phase is larger than 20%. This fact shows that the evolution of the dispersed phase size does not obey the composite viscosity effect in the entire composition range. The authors explained this superimposition with the influence of the shell thickness on the rheological behaviour of the composite drop, since the shell becomes thicker and thicker as the PS+PMMA content in the mixture increases. Once the shell thickness exceeds a threshold value, the matrix does not feel the effect of the sub-inclusions anymore, and the apparent rheological behaviour of the composite drop becomes identical to that of a pure PS drop. So the major factors dominating the droplet size of the dispersed phase are not only the composite effect of viscosity but also the influence of the shell thickness on the rheological behaviour of the composite drop.

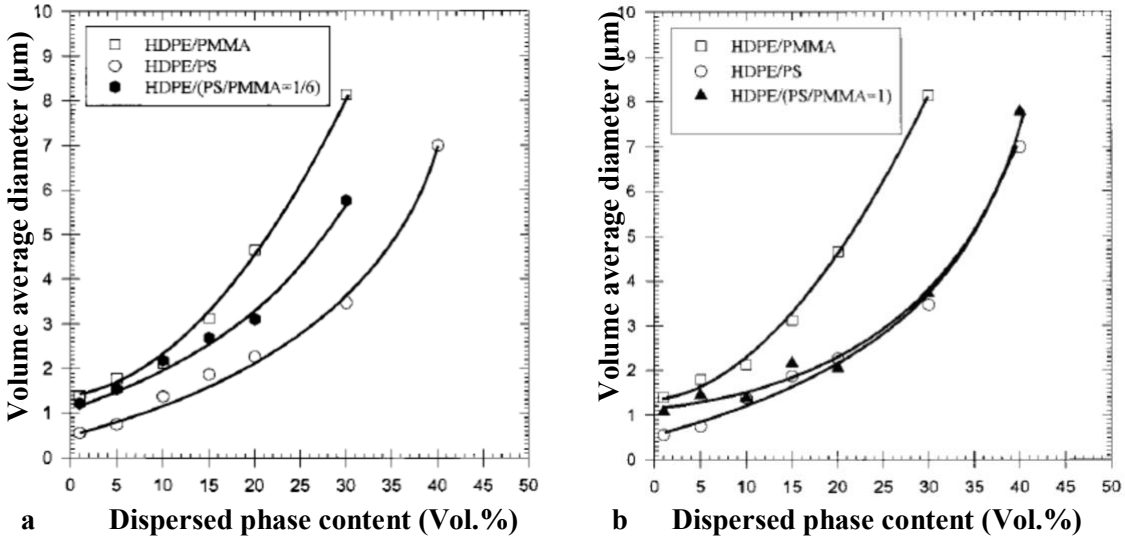

Fig. II.13 *Variation of the dispersed phase droplet size with volume ratio (PS+PMMA)/HDPE relative to the binary blends for two different volume ratios of PS/PMMA: a- PS/PMMA=1/6; b- PS/PMMA=1* [Reignier and Favis, 2000]

This explanation is validated when plotting the droplet size versus the PS content relative to the droplet phase volume instead of the total dispersed phase volume fraction (Fig. II.14). These measurements were performed at a fixed fraction of dispersed phase on the matrix ((PS+ PMMA)/HDPE=20/80). Increasing the PS volume fraction in the dispersed phase results in a decrease of the droplet size, as also shown in Fig. II.13 a and b. Fig. II.14 shows that the composite drop behaves as a pure PS drop after the PS volume fraction in the dispersed phase exceeds 50%. Correlating Fig. II.13b and Fig. II.14 provides further proof supporting the observation that when the thickness of the PS shell exceeds a certain value, an identical behaviour of pure PS and PS/PMMA complex inclusion takes place. The authors concluded that the critical shell thickness of PS is 0.2 µm relative to 1 µm radius of a composite drop. This explains also why, in Fig. II.13a, this phenomenon does not take place, as the thickness of the PS shell is never sufficient to erase the rheological contribution of PMMA sub-inclusions, and thus no superimposition of curves is observed here. A subsequent study confirming this interpretation was published by the same authors three years later [Reignier and Favis, 2003].

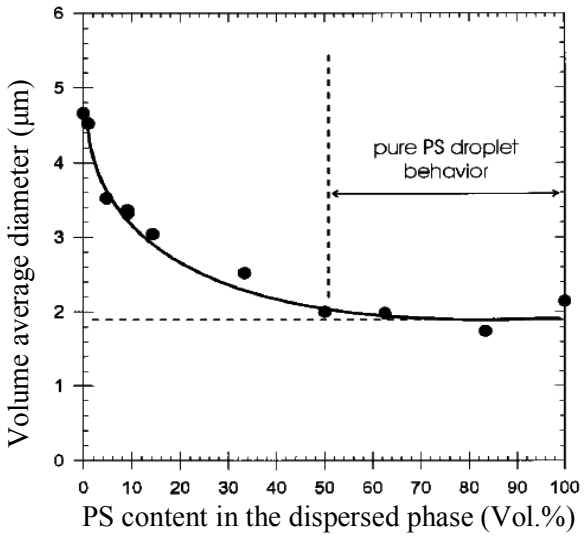

Fig. II.14 *Dispersed phase size as a function of PS content relative to the dispersed phase for a (PS+ PMMA)/HDPE=20/80 composition* [Reignier and Favis., 2000]

Influence of mixing parameters

- Mixing time:

Studies on both binary [Sundararaj et al., 1992] [Macosko et al., 1996] and ternary blends [Reignier and Favis, 2000] showed that both the morphology and the dispersed phase size become stable after a few minutes of blending. As mentioned in the section on thermodynamic interpretation, there will be no further evolution of the morphology once the thermodynamically stable state is reached.

- Mixing order:

Huang [Huang et al., 2006] reported that the order of mixing (simultaneous introduction of components or pre-mixed batch) does not have a significant influence on the type of morphology and the microstructure in PP/EOR/EOR-g-MAH blends. The same result was also found in HDPE/PS/PMMA [Tchomakov et al., 2004]. This can also be explained by the thermodynamic stability under kinetic conditions: if the composition and kinetic conditions are fixed, the existence of a thermodynamically stable state is unique and must be reached in all cases. Since the order of mixing changes neither the composition nor the mixing conditions, it only modifies the way to reach the unique stable state. Thus the final morphology should not depend on this parameter if the process is not kinetically limited.

- Mixing speed:

In ternary blends, the role of the blending speed is similar to binary blends. With a higher shear rate, the size of the dispersed phase becomes smaller [Jazani et al., 2010], but this parameter has no influence on the type of morphology [Shokoohi et al., 2009].

- Mixing temperature:

The effect of temperature can be considered as its contribution to the viscosities (main parameter) and interfacial tensions. However, the fact that the degradation of polymer is accelerated with higher temperature should not be neglected [Jazani et al., 2010].

II.3 Measurement of interfacial tensions between polymers

As discussed in the previous section, the interfacial tension plays a dominant role for controlling the morphology of ternary blends. Unlike parameters like the mechanical and rheological properties that have been studied extensively for a long time now, the modern methods of characterizing interfacial tension such as thread breaking and drop retraction were developed only around 20 years ago [Luciani et al., 1997] [Elemans et al., 1990], and some methods are still under development with in situ techniques [Velankar et al., 2004] [Yu et al., 2004]. There is no direct way to obtain experimentally the value of the interfacial tension between two molten polymers. It must be deduced by balancing interfacial tension with another force, mainly gravity and shear forces. The techniques to calculate or measure the interfacial tension between two molten polymers can be classified into three categories:

- Calculation from the intrinsic properties of each polymer;
- Calculation from the rheological response of a polymer blend;
- Local observation of a drop/fibre/disk embedded in between two polymeric molten layers and deformed.

II.3.1 Calculation of interfacial tension from intrinsic properties of each polymer

The interfacial tension between two molten polymers can be calculated from the knowledge of the surface tensions or solubility parameters of the two polymers. Antonoff [Antonoff, 1942] proposed a very straightforward way to estimate the interfacial tension between two polymers, as illustrated in the following equation:

$$\gamma_{ij} = \gamma_i - \gamma_j \qquad \text{Eq. 14}$$

γ_i and γ_j are the surface tension of two polymers, γ_{ij} is their interfacial tension.

Obviously, this can only yield a rough estimation. Afterwards, the dispersive term and polar term were taken into consideration of the surface tension as:

$$\gamma = \gamma^D + \gamma^P \qquad \text{Eq. 15}$$

This expression was employed in the harmonic average by Wu [Wu, 1982] to calculate the interfacial tension:

$$\gamma_{ij} = \gamma_i + \gamma_j - 4\left(\frac{\gamma_i^D \gamma_j^D}{\gamma_i^D + \gamma_j^D} + \frac{\gamma_i^P \gamma_j^P}{\gamma_i^P + \gamma_j^P}\right) \qquad \text{Eq. 16}$$

This is the most commonly used method to estimate the interfacial tension, thanks to the relatively easy procedure for the characterization of surface tension. A potential drawback of this method is that the values of surface tension are usually available at room temperature. Using these values to deduce the interfacial tension at temperatures above the melting point, very often at elevated temperatures, may introduce a considerable error in the final result. Moreover, even when using a temperature correlation to extrapolate the surface tension above the melting point, the influence of the phase transition from solid to liquid state on the surface property is neglected, although Lee et al. [Lee et al., 1970] established a model describing the correlation between interfacial tension and temperature with consideration of the phase transition. The numerous hypotheses of this model raise some doubts about it [Gaines, 1972].

Besides the surface tension, the interfacial tension between polymers can also be calculated from their solubility parameters. Similar to the composition of surface tension, there are three components in the expression of solubility parameters:

$$\delta^2 = \delta_d^2 + \delta_p^2 + \delta_h^2 \qquad \text{Eq. 17}$$

δ_d , δ_p and δ_h refer to the contribution of dispersion, polarity and hydrogen bond, respectively.

Hansen [Hansen, 1967] has used the following equation to estimate the compatibility of two polymers:

$$R^2 = \theta(\delta_{id} - \delta_{jd})^2 + (\delta_{ip} - \delta_{jp})^2 + (\delta_{ih} - \delta_{jh})^2 \qquad \text{Eq. 18}$$

A smaller value of R^2 refers to a better compatibility between the two polymers. Luciani et al. [Luciani et al., 1996] used this parameter and an empirical equation given below (Eq. 19) to predict the interfacial tension between two polymers *i* and *j*:

$$\gamma_{ij} = 0.881[(\delta_{id} - \delta_{jd})^2 + (\delta_{ip} - \delta_{jp})^2 + (\delta_{ih} - \delta_{jh})^2]^{0.422} \qquad \text{Eq. 19}$$

In brief, the advantage of this type of method is that information on the surface property of polymer is relatively easy to obtain. However, due to its poor reliability, it can only give a rough estimation of interfacial tensions [Biresaw et al., 2002].

II.3.2 Calculation from the rheological response of a polymer blend

Taylor [Taylor, 1932] was the first to describe the rheological response of a mixture of two viscoelastic phases from the intrinsic rheological properties of each component and their interfacial tension. Since then, several models have been developed, such as those of Choi et al. [Choi et al., 1975], Palierne [Palierne, 1990] and Bousmina [Bousmina, 1999], to determine the interfacial tension from the rheological properties of a polymer blend. Therefore, the interfacial tension can be deduced from the measurement of the rheological properties of the blend and of each component, knowing the size of inclusions and the volume fraction of dispersed phase. The main idea of this method is that the rheological response of a polymer blend is composed of the rheological contributions of the two components and of their interface. Here, the Palierne model is used as an example to illustrate this method.

The Palierne model was first published in 1990 [Palierne, 1990], it is a model derived by analogy with electric formalism aimed for predicting the rheological behaviour of a binary emulsion. To apply the Palierne model, the following hypotheses should be satisfied: The components of the blend should be incompressible viscoelastic fluids; the viscosity of the components should be high enough to neglect the effect of gravity and inertia; the morphology of the blend is globular; rheological measurements are performed in the linear viscoelastic domain where the stress is proportional to the strain, which indicates that the deformation of the drops under oscillatory strain is small. With all the aforementioned conditions satisfied, the Palierne model predicts that the complex modulus of the emulsion blend is a function of the complex modulus of the dispersed phase and the matrix, the interfacial tension between the two phases, the volume fraction and the particle size of the dispersed phase. In the original version of Palierne model, the interfacial tension was considered in a sophisticated way: Besides of the intrinsic interfacial tension between the dispersed phase and matrix, the effect of change of local interfacial area and shear modulus was also taken into consideration. When there is no compatilizer present between the matrix and the dispersed phase, these effects of local conditions are almost impossible to measure experimentally, related parameters are often set to zero [Graebling et al., 1993]. However in the presence of compatibilizer at the interface, the interfacial properties become dependent on the deformation (Marangoni effect) and the nonisotropic contribution to the interfacial stress also needs to be considered [Riemann et al., 1997]. In the present work, the Palierne

model was only used for non-compatibilized blends. By assuming the dispersed phase is monodispersed and using the volume average diameter to represent the particle size of the dispersed phase, the second version of Palierne model was published in 1993 [Graebling et al., 1993] as shown in Eq.20:

$$G^* = G_m^* \frac{1+3\phi H}{1-2\phi H} \qquad \text{Eq. 20}$$

where

$$H = \frac{\left[4\gamma_{AB}/R_v\left(2G_m^* + 5G_d^*\right)\right] + \left[\left(G_d^* - G_m^*\right)\left(16G_m^* + 19G_d^*\right)\right]}{\left[40\gamma_{AB}/R_v\left(G_m^* + G_d^*\right)\right] + \left[\left(2G_d^* + 3G_m^*\right)\left(16G_m^* + 19G_d^*\right)\right]} \qquad \text{Eq. 21}$$

In the equations above, G^* is the complex modulus, *d* and *m* refer to the dispersed phase and matrix, γ_{AB} is the interfacial tension, ϕ is the volume fraction of the dispersed phase. To use the monodisperse hypothesis is that the polydispersity of the blend cannot be too high: $R_v / R_n < 2$, where R_n is the number average radius, R_v is the volume average radius. Thanks to the simplicity of this version of Palierne model, it is much more widely used than the original version [Bousmina and Muller, 1993] [Carreau et al., 1994] [Lacroix et al. 1996] when dealing with polymer blends in absence of copolymer. The interfacial tension/over the drop size can be determined by fitting the experimental curve of the storage modulus of the blend by the model. A second method of using rheological behaviour of the polymer blend to calculate the interfacial tension was proposed by Gramespacher and Meissner [Gramespacher and Meissner, 1992]. In this case, information of *G'* and *G"* is used to plot weight relaxation spectrum $\tau H(\tau)$ in function of relaxation time $log\ \tau$ [Tschoegl, 1989]. The relaxation spectrum of the blend contains three peaks: Two of the peaks correspond to the blend components, the additional third peak usually observed at longer relaxation time corresponds to the characteristic time of droplet relaxation in the polymer blend. Then the interfacial tension can be calculated with this relaxation time, average size of the droplet and rheological properties of the blend components.

From a practical point of view, using this method to characterize interfacial tension requires the performance of three rheological tests: on the blend and on each of the two components, and a morphological observation to measure the average size of the inclusions. Although many steps are required in this method, all of them are easy to carry out. The potential risk of this method is that systematic errors in the final result may become quite substantial through the accumulation of small errors of each measurement,

especially during the characterization of the average size of inclusions. Another risk is that since the response of interfacial tension needs be measured in the low frequency region, the sensitivity of the rheometer may not be accurate enough to detect the contribution of the interface. Moreover, if the morphology of the blend is not perfectly globular, e.g. part of the dispersed phase is in form of ribbons instead of spherical drops, the model is no longer valid. A more detailed discussion of these aspects will be given in the experimental part.

II.3.3 Dynamic/static observations of a drop/fibre/disk in a polymer melt

Unlike the previous method which studies the rheological behaviour of the whole two-phase polymer blend, this class of methods considers only one drop or fibre or disk. The advantage of this type of method is that it is based on direct optical observation of local deformations, and the information obtained is more complete compared to the method based on the rheological properties of the blend. Three types of observations have been developed where a given polymer object is submitted to a deformation due to another force, i.e. gravity or flow.

II.3.3.1 Equilibrium situation for a drop deformed by the gravity

Pendant drop and sessile drop are classical methods to characterize surface tension between air and a liquid phase, or interfacial tension between liquids or polymers.

Pendant drop

In this method, a molten polymer drop is pendant in the other polymer, satisfying the condition that the system is at a mechanical equilibrium state and the density of the matrix is lower than that of the drop. Then the profile of this drop can be described by an equation established by Bashforth and Adams [Bashforth and Adams, 1883], which was originally developed for a gas–liquid system. It can, however, also be applied to two molten polymers as all hypotheses are valid in this case. Fig. II.15 shows the schema for this method.

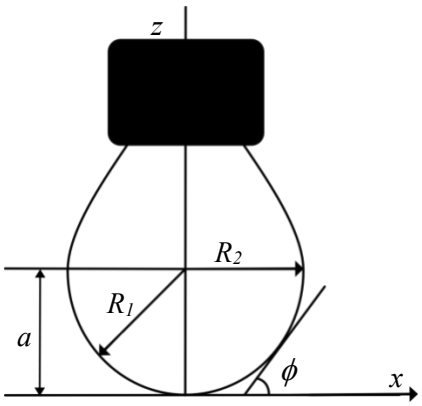

Fig. II.15 *Pendant drop geometry for an algebraic analysis*

A drop of polymer liquid is pendant on a syringe immersed in another polymer. Bashforth has used the following equation to describe the profile of this drop:

$$\frac{a}{R_1}+\frac{a\sin\phi}{x}=-B\frac{z}{a}+2 \qquad \text{Eq. 22}$$

where

$$B=\frac{a^2 g\Delta\rho}{\gamma} \qquad \text{Eq. 23}$$

In the equation above, a is the radius of the curvature at the lowest apex, g is the gravity constant, and $\Delta\rho$ is the difference of density between the two phases, γ refers to the interfacial tension. If x, z are the coordinates of a certain point on the profile, the expressions of R_1 and $\sin\phi$ are given as below:

$$R_1=\frac{ds}{d\phi}=\frac{[1+(\frac{dz}{dx})^2]^{3/2}}{\frac{d^2z}{dx^2}} \qquad \text{Eq. 24}$$

$$\sin\phi=\frac{\frac{dz}{dx}}{[1+(\frac{dz}{dx})^2]^{1/2}} \qquad \text{Eq. 25}$$

Later, several simplifications and improvements of this method were made by Andreas [Andreas, 1938], Anastasiadis et al. [Anastasiadis et al., 1986] and others. However, the main routine remains the analysis of the drop profile to calculate the value of interfacial tension.

Beside the limit that the density of the matrix should be lower than that of the drop, its transparency should also be ensured. There are other inconveniences, such as that the time to achieve the stable state is usually very long due to the high viscosities of the molten polymers and that the density of molten polymers can be difficult to measure.

Sessile drop

A drop of polymer liquid is put on the surface of a polymer liquid whose density is high enough to prevent the drop from sinking under the substrate's surface. The form of the drop is determined by the equilibrium of interfacial force, surface tensions of the two phase and gravity effect. Unlike the pendant drop method, it is difficult to describe the whole profile of the drop. The interfacial force balance along the horizontal axis is shown in Fig. II.16.

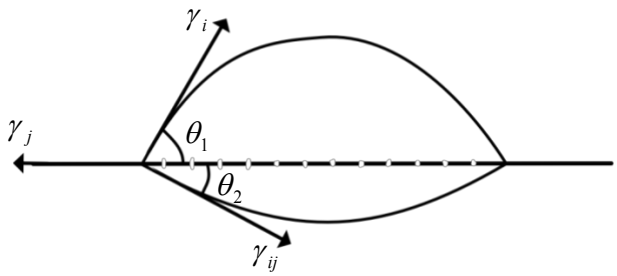

Fig. II.16 *Schema for a sessile drop*

The surface tension γ_j of a floating polymer drop should be balanced by the projection of γ_i and γ_{ij} on the horizontal vector. This relationship can be written as:

$$\gamma_j = \gamma_i \sin\theta_1 + \gamma_{ij} \sin\theta_2 \qquad \text{Eq. 26}$$

As mentioned before, in the pendant drop method the polymer used as matrix must be transparent to ensure the feasibility of observation. For a sessile drop, transparency of the polymers is not a restriction since the drop–substrate can be cooled down to solid state and cut from the middle of the drop to obtain the profile with a conventional optical observation.

By all means, the advantage of this set of methods is that few steps are required during the characterization. However, these methods are based on the shape of the interface at equilibrium. A possible complication, often difficult to assess, is the slow

process towards the equilibrated state, which can be as long as eight hours and thus may lead to the polymer degradation [Demarquette et al., 2003].

II.3.3.2 Relaxation to equilibrium after a deformation

In this set of methods, the observed object is a non-spherical piece of dispersed polymer embedded in another polymer in the form of a drop, fibre or even disk at a temperature above their melting point and which has been pre-deformed or deformed in a flow. Then the measurement of the relaxation kinetics from deformed to equilibrium shapes allows the interfacial tension to be deduced if the viscosities of the two polymers are known. This is the most commonly used experimental method for the characterization of interfacial tension between two polymers.

Drop retraction

A deformed Newtonian drop will relax to a spherical form with a given kinetics as illustrated in Fig. II.17:

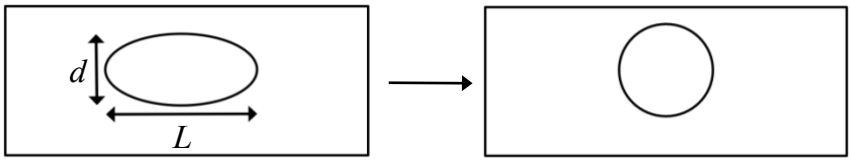

***Fig. II.17** Retraction of drop in the matrix*

During the relaxation, the deformation of the ellipsoid is defined as:

$$D_{ef} = \frac{L-d}{L+d} \qquad \text{Eq. 27}$$

If supposing that the only motor for the drop retraction is the interfacial tension, Taylor [Taylor, 1932] described the kinetics of decay of deformation by the following equation:

$$D_{ef} = D_{ef_0} \exp\left(-\frac{t}{\tau}\right) \qquad \text{Eq. 28}$$

$$\tau = \frac{(2p+3)(19p+16)}{40(p+1)} \frac{\eta_m R_0}{\gamma_{AB}} \qquad \text{Eq. 29}$$

In this equation, p is the viscosity ratio between the dispersed phase and the matrix, R_0 is the radius of the drop at the end of the relaxation procedure, η_m is the viscosity of the

matrix and γ_{AB} is the interfacial tension. This equation is only valid for slightly deformed droplets.

Thus the interfacial tension can be deduced by measuring the kinetics of the drop retraction. Although the theory was established in 1932, the first measurement of interfacial tension using this method was only performed more than 60 years later by Luciani et al. [Luciani et al., 1997]. As the deformed drop is often obtained by shear, there is an issue about the orientation of the long axis of the ellipsoid [Verhulst et al., 2009], which is not always easy to measure because of the optical observation method, inducing an error in the measurement of the length of the object. A detailed discussion on this point will be given in the experimental part.

Fibre retraction

As there is a competition between the interfacial effect tending to restore the drop to a spherical form and the growth of instability at the interface, there are two possible behaviours for the relaxation of a liquid fibre embedded in a polymer: retraction first to a dumbbell then finally to a sphere as in Fig. II.18, or breakage into droplets with a certain wave pattern. The parameter determining which behaviour will be active is the aspect ratio between the length and diameter of the fibre. If the aspect ratio is less than 10, it will retract to a drop as in Fig. II.18. Carriere et al. [Carriere et al., 1989] developed a model for this situation that is able to describe the kinetics of the retraction process of such short fibres passing through the dumbbell shape.

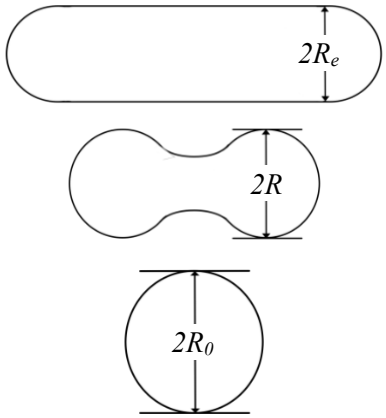

Fig. II.18 *Retraction of a fibre into a drop*

In this model, the time dependence of the radius R of the dumbbell is described by the following equation:

$$f(\frac{R}{R_0}) - f(\frac{R_e}{R_0}) = t\frac{\gamma_{12}}{R_0\eta_e} \qquad \text{Eq. 30}$$

$$f(x) = \frac{3}{2}\ln\frac{\sqrt{1+x+x^2}}{1-x} + \frac{3\sqrt{3}}{2}\arctan\frac{\sqrt{3}x}{2+x} - \frac{x}{2} - \frac{4}{x^2} \qquad \text{Eq. 31}$$

$$\eta_e = \frac{\eta_m + 1.7\eta_d}{2.7} \qquad \text{Eq. 32}$$

R_e and R_0 refer to the radius of the fibre before relaxation and of the sphere at the end of relaxation. η_m and η_d are the viscosities of the matrix and the dispersed phase. Thus the interfacial tension γ_{12} can be calculated with this equation from the measurement of the kinetics of the drop retraction.

The problem of this method is that preparing a straight fibre with a homogeneous diameter and immersing it perfectly horizontally in the matrix polymer is a delicate manipulation. The viscosity ratio between the dispersed phase and matrix should be lower than 103 to avoid long observation times [Xing et al., 2000].

Thread breakup

As mentioned before, the other possible relaxation behaviour of a fibre is a breakage into a series of droplets in the case of a long filament through the development of an instability (Fig. II.19). This phenomenon is often called “Rayleigh’s instability” since Rayleigh [Rayleigh, 1897] was the first to describe the breakage of a water stream in the air. Tomotika [Tomotika, 1935] extended this work to the case of two molten phases. The first measurement of interfacial tension by this method was realized by Chappelear [Chappelear, 1964], however with a considerable error in the result, since he used the viscosity data from a low shear rate region with a capillary viscometer as being the zero-shear rate viscosities. Finally, Elemans et al. [Elemans et al., 1990] developed a complete protocol which is used nowadays.

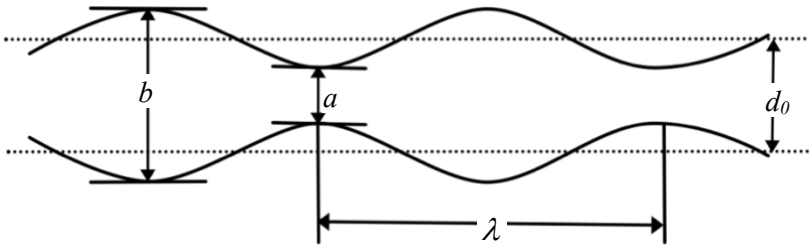

Fig. II.19 *Thread-breaking schema; the dotted line is the original form of the thread*

Fig. II.19 illustrates the two states during the relaxation, where the dotted line is the original form of the thread; the solid line stands for the development of the wave pattern instability which will develop further and lead to the breakage of the filament into a series of drops. The amplitude of the wave instability is defined as:

$$\alpha = \frac{b-a}{2d_0} \qquad \text{Eq. 33}$$

where b and a refer to the widest and narrowest diameter of the wave pattern, and d_0 is the initial diameter of the thread.

As in the case of drop retraction, the deformation evolves exponentially with time as:

$$\alpha = \alpha_0 e^{qt} \qquad \text{Eq. 34}$$

$$q = \frac{\gamma_{12}\Omega(x,p)}{\eta_m d_0} \qquad \text{Eq. 35}$$

where γ_{12} refers to the interfacial tension, η_m is the matrix's viscosity. $\Omega(x,p)$ depends on the wave number $x\,(=2\pi R_0/\lambda)$ and the viscosity ratio between the dispersed phase and matrix p. $\Omega(x,p)$ can thus be regarded as a constant in a given test. With this method, the interfacial tension can be calculated.

Disk retraction

This is similar to the fibre retraction method, but with a flat cylinder embedded in matrix with the whole system in a molten state. During the relaxation, the disk will first relax into the form of an oblate spheroid, then into a sphere. The relaxation process is used to deduce the interfacial tension. The retraction process is shown in Fig. II.20:

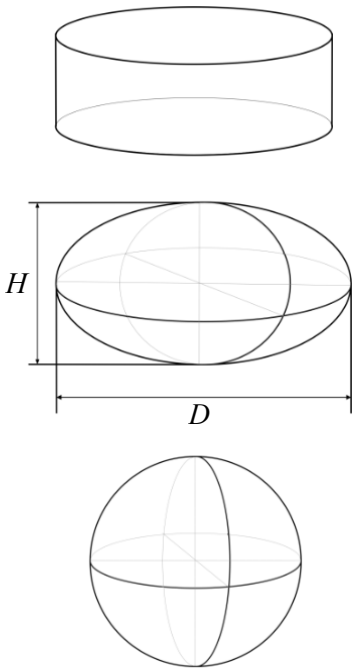

Fig. II.20 *Disk retraction: from a flat disk to a sphere*

During the retraction, the deformation of the oblate spheroid is defined as:

$$\alpha = \frac{D}{D_\infty} \qquad \text{Eq. 36}$$

where D is the length of the short axis of the oblate spheroid and D_∞ is the diameter of the sphere at the end of retraction.

The kinetics can be described by the following equations:

$$f(\alpha) - f(\alpha_0) = \frac{t}{\lambda} \qquad \text{Eq. 37}$$

$$f(x) = \ln\left(\frac{x^2+1}{x^2-1}\right) \qquad \text{Eq. 38}$$

$$\lambda = \frac{\chi \eta_e D_\infty}{4\gamma_{12}} \qquad \text{Eq. 39}$$

In Eq. 39 defining λ, γ_{12} is the interfacial tension, η_e is the effective viscosity with the following expression:

$$\eta_e = \eta_m \frac{(2p+3)(19p+16)}{40(p+1)} \qquad \text{Eq. 40}$$

The hydrodynamic coefficient χ takes a universal value of 1.33 [Rundqvist et al., 1996]. Thus the interfacial tension can be calculated using the equations above.

General comment

A shortcoming of the methods based on the kinetics of relaxation starting from a solid object in a solid matrix is that, due to the poor thermal conductivity of polymer, the thermal distribution will take some time to achieve a homogeneous state during heating. But during this equilibrium time, part of the fibre/disk may melt first and begin to relax while the rest is still melting. Considering the dependence of the viscosity on temperature, this partial melting effect may introduce a substantial error in the final result. Thus, the drop retraction method has a clear advantage as the observations can be performed after the distribution of temperature is stable when the deformed drop is obtained by applying a shear on the initially molten drop. On the other hand, using relaxation laws applicable only to Newtonian liquids while using polymers requires elastic terms to be neglected, which is a condition satisfied for the fibre/disk relaxation method, as during melting the elastic effects have mostly been relaxed. Elastic effects can be a source of error for the drop retraction method, if the observation is performed directly after stopping the shear. Indeed, observations of the relaxation process can be recorded after the polymer relaxation in order that the drop relaxation is only driven by the interfacial tension. Care should be taken that the drop relaxation time is large enough compared to the polymer relaxation time.

In all these methods based on the relaxation kinetics of drops of various initial shapes, the polymer matrix should be transparent to allow optical observation. In addition, the different models are based on the Newtonian liquid hypothesis. If the tested polymer is highly cross-linked [Xing et al., 2000] or has some internal structure, as in the case of a liquid crystalline polymer [Bousmina, 1999], the model cannot be applied and the determination of the interfacial tension is no longer valid. As mentioned above, care should be taken that the drop relaxation time is much larger than the longest relaxation time of the polymer. This can be tuned by observing very large drops in order to increase its relaxation time. In this case, attention should be paid to the drop size relatively to the gap in order to void any effect of confinement.

II.3.3.3 Equilibrium between interfacial tension and an imposed flow

In this method, the interfacial tension is measured from its equilibrium with a dynamic movement. Spinning drop is the typical experiment of this method.

A fluid drop is put in another fluid with a higher density in a container of a horizontally placed transparent tube. As the tube rotates around its long axis, the drop is stretched along this axis due to the centrifugal force, first into an ellipsoid then into a cylinder. For a given rotation speed, the drop deformation caused by centrifugal force will be counter-balanced by the contribution of the interfacial tension, as shown in Fig. II.21:

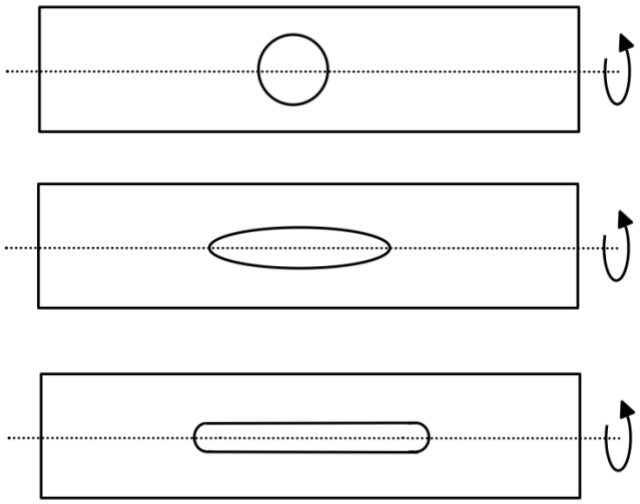

Fig. II.21 *Spinning drop method*

In the work of Vonnegut [Vonnegut, 1942], he proposed a theory predicting the interfacial tension as:

$$\gamma_{12} = \frac{\Delta\rho\omega^2 r^3}{4} \qquad \text{Eq. 41}$$

where $\Delta\rho$ is the difference between the densities of two phases, r is the radius of the cylinder at equilibrium and ω corresponds to the angular speed at this moment.

Princen et al. [Princen et al., 1967] extended this method to molten polymers and found that the time required to achieve equilibrium can easily reach hours with high viscosity polymers. A higher rotation speed can reduce this duration and Elmendorp [Elmendorp, 1986] constructed an apparatus which can rotate at 25000 rpm. However, such high rotation speeds also introduce great difficulties in controlling the temperature. The difficulty of performing observations under the vibrations caused by the rotation is another negative effect of using large rotation speeds.

II.3.4 Examples of interfacial tension measurements

The following table is a summary of some values of the interfacial tension between two polymers including PLA/PBAT reported in the literature. An obvious remark is that even if the same method at the same temperature is used, the value of interfacial tension can be very different depending on the authors (e.g. PP/PS at 200 °C, by thread breakup). This difference is even larger when considering results issued from different measuring methods. This is also true in the case of PLA/PBAT with values reported between 0.5 and 7 mN/m. We thus decided to measure ourselves the values of interfacial tension we needed. Considering the availability of apparatus and the feasibility, drop retraction and the rheological method based on the Palierne model were chosen in this study to measure the interfacial tensions between the polymers we used in our work.

Polymer pair	Interfacial tension (mN/m)	Method	Temperature (°C)	Reference
PMMA/PS	1.9-2.2	Choi-Schowalter	170	Gramespacher and Meissner, 1992
	2.08-3.1	Palierne	190	Friedrich et al., 1995
	0.9	Fibre retraction	190	Cohen and Carriere, 1989
	0.67-1.4	Fibre retraction	190	Carriere et al., 1989
	1	Drop retraction	200	Luciani et al., 1997
	1.8	Thread breaking	200	Luciani et al., 1997
	2.4	Thread breaking	200	Reignier et al., 2003
	2.09	Spinning drop	200	Joseph et al., 1992
	1.26	Spinning drop	200	Elmendorp, 1986
	0.94	Pendant drop	200	Elmendorp, 1986
	1.1	Disk retraction	210	Rundqvist et al., 1996
	1.33	Spinning drop	225	Joseph et al., 1992
	0.25	Spinning drop	250	Joseph et al., 1992
	0.39	Harmonic equation	270	Hobbs et al., 1988
PP/PS	5.25	Harmonic equation	185	Nemirovski et al., 1995
	3.3-3.7	Thread breaking	200	Le Corroller et al., 2011
	4.6		200	Ghodgaonkar et al., 1996
	7.83±0.57	Thread breaking	200	Demarquette et al., 2003

	6.25±0.87	Palierne	200	Demarquette et al., 2003
	7.82±0.43	Fibre retraction	200	Demarquette et al., 2003
	5.28±0.26	Pendant drop	200	Demarquette et al., 2003
	6.25±0.87	Palierne	200	Macaubas et al., 2001
	4.86	Harmonic equation	220	Nemirovski et al., 1995
	2.26	Harmonic equation	260	Omonov et al., 2005
	3.5±0.2	Thread breaking	200	Virgilio et al., 2010
PA6/PS	20	Thread breaking	230	Elemans et al., 1990
	7.63	Thread breaking	230	Son, 2001
	8.4±1.5	Thread breaking	230	Xing et al., 2000
	7.5±1.4	Fibre retraction	230	Xing et al., 2000
	7.2±2.0	Palierne	230	Xing et al., 2000
	6.8±1.8	Drop retraction	230	Xing et al., 2000
	7.2±0.1	Pendant drop	230	Xing et al., 2000
	7.3	Thread breaking	240	Cho et al., 1996
	13.72	Harmonic equation	260	Omonov et al., 2005
PLA/PBAT	0.5	Drop retraction	180	Al-Itry et al., 2015
	0.6	Palierne model	180	Jajali Dil et al., 2015
	7	Palierne model	180	Nofar et al., 2015

II.4 Conclusion

In this chapter, we presented the main features of PLA, an important bioplastic and the main polymer used in our work. The way to use polymer blend to improve its toughness was also described, as well as the parameters that control the morphology of a polymer blend. Since the key parameter controlling the morphology of ternary blends is the interfacial tension, we gave an overview of the methods that are able to measure this parameter. In the following part of this thesis, the methods presented in this chapter will be used to measure the interfacial tensions between the blend components, then these interfacial tensions will be used to predict the morphology of ternary blends. If the result morphology is not the one aimed for, interfacial tensions will be modified to realize the target morphology.

References

Al-Itry, R., Lamnawar, K. and Maazouz, A. (2014). Rheological, morphological, and interfacial properties of compatibilized PLA/PBAT blends. *Rheologica Acta* 53 501-17

Anastasiadis, S. H., Chen, J. K., Koberstein, J. T., Sohn, J. E. and Emerson, J. A. (1986). The determination of polymer interfacial tension by drop image processing: Comparison of theory and experiment for the pair, poly(dimethyl siloxane)/polybutadiene. *Polymer Engineering & Science*, *26*(20), 1410–1418.

Andreas, J. M. (1938). *Interfacial Tension by Pendant Drops*. Massachusetts Institute of Technology.

Antonoff, G. (1942). On the validity of Antonoff's rule. *The Journal of Physical Chemistry, 46*(4), 497–499.

Bashforth, F., & Adams, J. C. (1883). *An Attempt to Test the Theories of Capillary Action by Comparing the Theoretical and Measured Forms of Drops of Fluid*. University Press.

Biresaw, G., & Carriere, C. J. (2002). Interfacial tension of poly(lactic acid)/polystyrene blends. *Journal of Polymer Science Part B: Polymer Physics*, *40*(19), 2248–2258.

Bousmina, M. (1999). Rheology of polymer blends: linear model for viscoelastic emulsions. *Rheologica Acta*, *38*(1), 73–83.

Broz, M. E., VanderHart, D. L., & Washburn, N. R. (2003). Structure and mechanical properties of poly (d, l-lactic acid)/poly (ε-caprolactone) blends. *Biomaterials*, *24*(23), 4181–4190.

Carriere, C. J., Cohen, A., & Arends, C. B. (1989). Estimation of interfacial tension using shape evolution of short fibers. *Journal of Rheology*, *33*, 681-689.

Desbois, P., Warzelhan, V., Niessner, N., Deffieux, A., & Carlotti, S. (2006). Anionic high impact polystyrene: A new process for low residual and low cost HIPS. *Macromolecular Symposia, 240*(1), 194–205.

Jajali Dil, E., Carreau, P.J., Favis, B.D. (2015) Morphology, miscibility and continuity development in poly(lactic acid)/poly(butylene adipate-co-terephthalate) blends. *Polymer* 68, 202-2012.

Cho, K., Jeon, H. K., Park, C. E., Kim, J., & Kim, K. U. (1996). The effect of end-sulfonated polystyrene on the interfacial tension of nylon-6/polystyrene blends. *Polymer*, *37*(7), 1117–1122.

Cohen, A., & Carriere, C. J. (1989). Analysis of a retraction mechanism for imbedded polymeric fibers. *Rheologica Acta*, *28*(3), 223–232.

Demarquette, N. R., De Souza, A. M. C., Palmer, G., & Macaubas, P. H. P. (2003). Comparison between five experimental methods to evaluate interfacial tension between molten polymers. *Polymer Engineering & Science*, *43*(3), 670–683.

Elemans, P., Janssen, J., & Meijer, H. (1990). The measurement of interfacial tension in polymer/polymer systems: The breaking thread method. *Journal of Rheology*, *34(8)*, 1311-1325.

Elmendorp, J. J. (1986). *A Study on Polymer Blending Microrheology*. PhD thesis, Delft University of Technology, the Netherlands.

European Bioplastics (2012). Institute for Bioplastics and Biocomposites, www.european-bioplastics.org.

Friedrich, C., Gleinser, W., Korat, E., Maier, D., & Weese, J. (1995). Comparison of sphere-size distributions obtained from rheology and transmission electron microscopy in PMMA/PS blends. *Journal of Rheology*, *39*, 1411-1425.

Ghodgaonkar, P. G., & Sundararaj, U. (1996). Prediction of dispersed phase drop diameter in polymer blends: The effect of elasticity. *Polymer Engineering & Science*, *36*(12), 1656–1665.

Grace, H. P. (1982). Dispersion phenomena in high viscosity immiscible fluid systems and application of static mixers as dispersion devices in such systems. *Chemical Engineering Communications*, *14*(3-6), 225–277.

Gramespacher, H., & Meissner, J. (1992). Interfacial tension between polymer melts measured by shear oscillations of their blends. *Journal of Rheology*, *36*, 1127-1141.

Guo, H.-F., Packirisamy, S., Gvozdic, N. V., & Meier, D. J. (1997). Prediction and manipulation of the phase morphologies of multiphase polymer blends: 1. Ternary systems. *Polymer*, *38*(4), 785–794.

Harkins, W. D. (1941). A general thermodynamic theory of the spreading of liquids to form duplex films and of liquids or solids to form monolayers. *The Journal of Chemical Physics*, *9*, 552-568.

Halary, J. L., Laupretre F., & Monnerie, L. (2008). *Mécanique des Matériaux Polymères*. Editions Belin, Paris.

Hansen, C. M. (1967). *The Three-Dimensional Solubility Parameter and Solvent Diffusion Coefficient*. PhD thesis, Technical University of Denmark.

Harada, M., Ohya, T., Iida, K., Hayashi, H., Hirano, K., & Fukuda, H. (2007). Increased impact strength of biodegradable poly(lactic acid)/poly(butylene succinate) blend composites by using isocyanate as a reactive processing agent. *Journal of Applied Polymer Science*, *106*(3), 1813–1820.

Hemmati, M., Nazokdast, H., & Shariat Panahi, H. (2001). Study on morphology of ternary polymer blends. II. Effect of composition. *Journal of Applied Polymer Science*, *82*(5), 1138–1146.

Hinch, E. J., & Acrivos, A. (1979). Steady long slender droplets in two-dimensional straining motion. *Journal of Fluid Mechanics*, *91*(3), 401-414.

Hinch, E. J., & Acrivos, A. (1980). Long slender drops in a simple shear flow. *Journal of Fluid Mechanics*, *98*(2), 305–328.

Hobbs, S. Y., Dekkers, M., & Watkins, V. H. (1988). Effect of interfacial forces on polymer blend morphologies. *Polymer, 29*(9), 1598–1603.

Huang, J. J., Keskkula, H., & Paul, D. R. (2006). Elastomer particle morphology in ternary blends of maleated and non-maleated ethylene-based elastomers with polyamides: Role of elastomer phase miscibility. *Polymer*, *47*(2), 624–638.

Jazani, O. M., Arefazar, A., & Beheshty, M. H. (2010). Study on the effect of processing conditions on the mechanical properties of PP/PC/SEBS ternary blends using Taguchi experimental analysis. *E-polymer*, 1–14.

Jiang, L., Wolcott, M. P., & Zhang, J. (2006). Study of biodegradable polylactide/poly(butylene adipate-co-terephthalate) blends. *Biomacromolecules*, *7*(1), 199–207.

Joseph, D. D., Arney, M. S., Gillberg, G., Hu, H., Hultman, D., Verdier, C., & Vinagre, T. M. (1992). A spinning drop tensioextensometer. *Journal of Rheology*, *36*, 621-662.

Kolahchi, A. R., Ajji, A. and Carreau, P.J. (2014) Surface Morphology and Properties of Ternary Polymer Blends: Effect of the Migration of Minor Components. *The Journal of Physical Chemistry B* 118 (23), 6316-6323

Le Corroller, P., & Favis, B. D. (2011). Effect of viscosity in ternary polymer blends displaying partial wetting phenomena. *Polymer*, *52*(17), 3827–3834.

Luciani, A., Champagne, M. F., & Utracki, L. A. (1997). Interfacial tension coefficient from the retraction of ellipsoidal drops. *Journal of Polymer Science Part B: Polymer Physics*, *35*(9), 1393–1403.

Luzinov, I., Xi, K., Pagnoulle, C., Huynh-Ba, G., & Jerome, R. (1999). Composition effect on the core–shell morphology and mechanical properties of ternary polystyrene/styrene–butadiene rubber/polyethylene blends. *Polymer*, *40*(10), 2511–2520.

Macaubas, P., & Demarquette, N. R. (2001). Morphologies and interfacial tensions of immiscible polypropylene/polystyrene blends modified with triblock copolymers. *Polymer*, *42*(6), 2543–2554.

Macosko, C. W., Guégan, P., Khandpur, A. K., Nakayama, A., Marechal, P., & Inoue, T. (1996). Compatibilizers for melt blending: Premade block copolymers. *Macromolecules, 29(17),* 5590-5598.

Meijer, H. E. H., Janssen, J. M. H., Anderson, P. D. (2009). Mixing of immiscible liquids, in *Mixing and Compounding of Polymers* edited by Manas-Zloczower, I., Hanser Verlag, München.

Nemirovski, N., Siegmann, A., & Narkis, M. (1995). Morphology of ternary immiscible polymer blends. *Journal of Macromolecular Science, Part B: Physics*, *34*(4), 459–475.

Nofar, M., Maani, A., Sojoudi, H., Heuzey, M.C. & Carreau, P.J. (2015). Interfacial and rheological properties of PLA/PBAT and PLA/PBSA blends and their morphological stability under shear flow. *Journal of Rheology*, 59(2), 317-333.

Omonov, T. S., Harrats, C., & Groeninckx, G. (2005). Co-continuous and encapsulated three phase morphologies in uncompatibilized and reactively compatibilized polyamide 6/polypropylene/polystyrene ternary blends using two reactive precursors. *Polymer*, *46*(26), 12322–12336.

Palierne, J. F. (1990). Linear rheology of viscoelastic emulsions with interfacial tension. *Rheologica Acta*, *29*(3), 204–214.

Princen, H. M., Zia, I., & Mason, S. G. (1967). Measurement of interfacial tension from the shape of a rotating drop. *Journal of Colloid and Interface Science*, *23*(1), 99–107.

Rastin, H., Jafari, S.H., Saeb, M.R., Hossein Ali Khonakdar, Wagenknecht, U., and Heinrichde, G. (2014). On the reliability of existing theoretical models in anticipating type of morphology and domain size in HDPE/PA-6/EVOH ternary blends. *European Polymer Journal* 53, 1-12

Rayleigh, L. (1879). On the capillary phenomena of jets. *Proceedings of the Royal Society of London*, *29*(196-199), 71–97.

Reignier, J., & Favis, B. D. (2000). Control of the subinclusion microstructure in HDPE/PS/PMMA ternary blends. *Macromolecules*, *33*(19), 6998–7008.

Reignier, J., & Favis, B. D. (2003). Core–shell structure and segregation effects in composite droplet polymer blends. *AIChE Journal*, *49*(4), 1014–1023.

Reignier, J., Favis, B. D., & Heuzey, M.-C. (2003). Factors influencing encapsulation behavior in composite droplet-type polymer blends. *Polymer*, *44*(1), 49–59.

Riemann, R.-E., Cantow, H.-J. and Friedrich Chr. (1997). Interpretation of a new interface-governed relaxation process in compatibilized polymer blends. *Macromolecules* 30, 5476–5480.

Rundqvist, T., Cohen, A., & Klason, C. (1996). The imbedded disk retraction method for measurement of interfacial tension between polymer melts. *Rheologica Acta*, *35*(5), 458–469.

Serpe, G., Jarrin, J., & Dawans, F. (2004). Morphology-processing relationships in polyethylene-polyamide blends. *Polymer Engineering & Science*, *30*(9), 553–565.

Schirrer, R., Fond, C., & Lobbrecht, A. (1996). Volume change and light scattering during mechanical damage in polymethylmethacrylate toughened with core-shell rubber particles. *Journal of Materials Science*, *31*(24), 6409–6422.

Shen, L., Haufe, J., & Patel, M. K. (2009). Product overview and market projection of emerging bio-based plastics. PRO-BIP 2009. *EPNOE, European Bioplastics*, 1–243.

Shokoohi, S., & Arefazar, A. (2009). A review on ternary immiscible polymer blends: morphology and effective parameters. *Polymers for Advanced Technologies*, *20*(5), 433–447.

Son, Y. (2001). Measurement of interfacial tension between polyamide-6 and poly (styrene-co-acrylonitrile) by breaking thread method. *Polymer*, *42*(3), 1287–1291.

Stegeman, Y. W., Van De Vosse, F. N., & Meijer, H. E. (2002). On the applicability of the Grace curve in practical mixing operations. *The Canadian Journal of Chemical Engineering*, *80*(4), 1–6.

Sundararaj, U., Macosko, C. W., Rolando, R. J., & Chan, H. T. (1992). Morphology development in polymer blends. *Polymer Engineering & Science*, *32*(24), 1814–1823.

Taylor, G. I. (1932). The viscosity of a fluid containing small drops of another fluid. *Proceedings of the Royal Society A: Mathematical, Physical and Engineering Sciences*, *138*(834), 41–48.

Taylor, G. I. (1934). The formation of emulsions in definable fields of flow. *Proceedings of the Royal Society A: Mathematical, Physical and Engineering Sciences*, *146*(858), 501–523. doi:10.1098/rspa.1934.0169

Tchomakov, K. P., Favis, B. D., Huneault, M. A., Champagne, M. F., & Tofan, F. (2004). Composite droplets with core/shell morphologies prepared from HDPE/PS/PMMA ternary blends by twin-screw extrusion. *Polymer Engineering & Science*, *44*(4), 749–759.

Todo, M., Park, S. D., Takayama, T., & Arakawa, K. (2007). Fracture micromechanisms of bioabsorbable PLLA/PCL polymer blends. *Engineering Fracture Mechanics*, *74*(12), 1872–1883.

Tomotika, S. (1935). On the instability of a cylindrical thread of a viscous liquid surrounded by another viscous fluid. *Proceedings of the Royal Society A: Mathematical, Physical and Engineering Sciences*, *150*(870), 322–337.

Tschoegl, N. W. (1989) *The Phenomenological Theory of Linear Viscoelastic Behaviour* Springer, Berlin.

Utracki, L. A. (2003). *Polymer Blends Handbook*. Springer.

Velankar, S., Zhou, H., Jeon, H. K., & Macosko, C. W. (2004). CFD evaluation of drop retraction methods for the measurement of interfacial tension of surfactant-laden drops. *Journal of Colloid and Interface Science*, *272*(1), 172–185.

Verhulst, K., Cardinaels, R., Moldenaers, P., Afkhami, S., & Renardy, Y. (2009). Influence of viscoelasticity on drop deformation and orientation in shear flow. Part 2: Dynamics. *Journal of Non-Newtonian Fluid Mechanics*, *156*(1-2), 44–57.

Virgilio, N., Desjardins, P., Esperance, G. L., & Favis, B. D. (2010). Modified interfacial tensions measured in situ in ternary polymer blends demonstrating partial wetting. *Polymer*, *51*(6), 1472–1484.

Wang, R., Wang, S., Zhang, Y., Wan, C., & Ma, P. (2009). Toughening modification of PLLA/PBS blends via in situ compatibilization. *Polymer Engineering & Science*, *49*(1), 26–33.

Weiss, P. A. (1962). Renewable Resources: A Report to the Committee on Natural Resources of the National Academy of Sciences-National Research Council, 1. Washington, DC: The National Academies Press.

Wilkinson, A. N., Clemens, M. L., & Harding, V. M. (2004). The effects of SEBS-g-maleic anhydride reaction on the morphology and properties of polypropylene/PA6/SEBS ternary blends. *Polymer*, *45*(15), 5239–5249.

Wu, S. (1987). Formation of dispersed phase in incompatible polymer blends: Interfacial and rheological effects. *Polymer Engineering & Science*, *27*(5), 335–343.

Xing, P., Bousmina, M., Rodrigue, D., & Kamal, M. R. (2000). Critical experimental comparison between five techniques for the determination of interfacial tension in polymer blends: Model system of polystyrene/polyamide-6. *Macromolecules*, *33*(21), 8020–8034.

Yu, W., Bousmina, M., Zhou, C., & Tucker, C. L. (2004). Theory for drop deformation in viscoelastic systems. *Journal of Rheology*, *48*(2), 417.

Zhang, N., Wang, Q., Ren, J., & Wang, L. (2008). Preparation and properties of biodegradable poly(lactic acid)/poly(butylene adipate-co-terephthalate) blend with glycidyl methacrylate as reactive processing agent. *Journal of Materials Science*, *44*(1), 250–256.

Chapter III

Materials and experimental methods

III Materials and experimental methods

In this chapter, we describe the polymers which were chosen, and the apparatuses used for sample preparation and characterization. A detailed discussion will be given on the custom-built rheo-optical system.

III.1 Polymers

As described in the literature survey chapter, the purpose of this study was to realize a core–shell morphology which is potentially able to improve the mechanical properties of PLA. We chose the PLA 3051D grade from NatureWorks LLC. Although this grade of PLA is designed for injection moulding, its thermo-resistance is identical to PLA 2002D which is for extrusion use, but PLA 3051D has a lower resistance to rupture than PLA 2002D, which is a good case for trying to enhance ductility.

The second component chosen was PBAT Ecoflex® FBX 7011 from BASF. PBAT shows an excellent ductility with rupture deformation higher than 700% at room temperature. Its blend with PLA has shown promising mechanical improvement [Jiang et al., 2006][Jiang et al., 2009][Zhang et al., 2008]. Therefore the combination of these two polymers has drawn the attention not only of numerous academic researchers but also of the polymer industry. For instance, BASF has commercialized a product based on this blend under the trademark Ecovio®. In addition to the impressive mechanical improvement, another reason for the popularity of the PLA/PBAT blend is that the biodegradation feature is retained after blending, despite the fact that PBAT is fossil-based. PBAT exhibits a glass temperature around -30 °C and a melting temperature around 120 °C.

Two grades of PBAT were investigated. These grades differ in their molar mass. They are issued from the same reference but PBAT(2007) was stored for 4 years (storage in a closed bag, with no light and a relative constant temperature) and the second one, referred to as PBAT(2011), was used as received. PBAT is very sensitive to photo degradation but in the present case was also sensitive to degradation during storage. We took advantage of this fact to evaluate the effect of the viscosity level on the measurement of the interfacial tension. PBAT(2011) refers to the high viscosity polymer recently received: Newtonian viscosity at 180 °C of 3250 Pa.s (see Fig. III.1). PBAT(2007) refers to the low viscosity sample, low viscosity linked to a too long storage: Newtonian viscosity at 180 °C of 150 Pa.s (see Fig. III.1). In practice, the PBAT rheology was systematically measured and the viscosity value used was the one measured at the moment of the experiment. PBAT(2007) was only used in chapter IV in interfacial tension measurements and non-compatibilized blends.

The last component selected was a bio-based copolyamide (PA) with trade name Platamid® HX 2656 from Arkema. There were two main reasons for choosing this grade of PA: first it is derived from castor oil, which guarantees the eco-friendly feature of the whole blend; second it possesses a remarkably low melting temperature around 130 °C, an obligation in order to compound it with polyesters which easily degrade under high temperatures.

The polymers were chosen for their respective immiscibility and to guarantee the eco-friendly character of the whole blend.

The rheological behaviour of the three polymers is depicted in Fig. III.1.

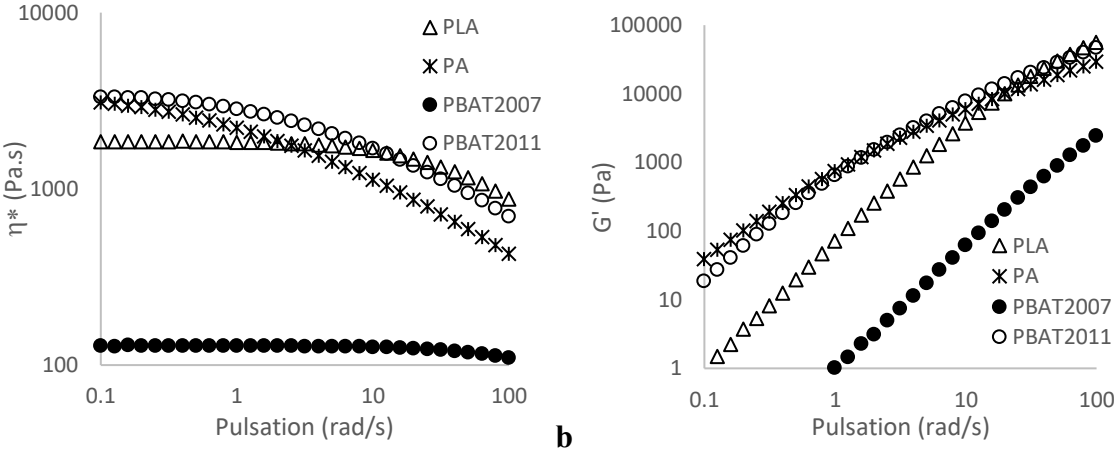

Fig. III.1 *Complex viscosity (**a**) and G' (**b**)curves for the three polymers at 180°C*

PLA, PBAT(2011) and PA have quite close viscosities. As expected, PBAT(2007) shows a much smaller viscosity.

The three polymers being sensitive to humidity, the different polymers were dried at 80°C in a vacuum oven for at least 4h prior to any use of the polymers in the molten state (compounding, compression moulding and rheometry). This also true for the blends.

III.2 Experimental Methods

III.2.1 Blend preparation

Two compounders were used in this study:

- an internal mixer, ThermoFisher Scientific Rheomix 600p with roller rotors,
- a micro-compounder, Haake MiniLab micro compounder from ThermoFisher Scientific.

There are two main differences between these two compounders:

The first one is their volume capacity. The available volume for mixing in the chamber of the internal mixer is 69 cm^3. The filling ratio must be fixed at around 70%. The volume of blend prepared by internal mixer was thus about 48 cm^3. The mixing volume is only 7 cm^3 in the micro-compounder.

The second difference is the mixing structure of the two pieces of equipment. The micro-compounder contains two different zones: a conical section which contains the two counter-rotating screws and a rectangular reservoir zone. Fig. III.2 shows a schematic representation of the micro-compounder. The arrows depict the direction of circulation of the material. The twin screw zone corresponds to a zone of high shear rate which is efficient for dispersion. The reservoir zone corresponds to a zone of low shear with two singular zones at the entrance, with a diverging flow giving rise to an elongational flow perpendicular to the flow direction and a converging zone at the exit which is characterized by a high elongational flow parallel to the flow direction. A bypass valve allows the material to be recirculated through both zones in order to fix a chosen mixing time.

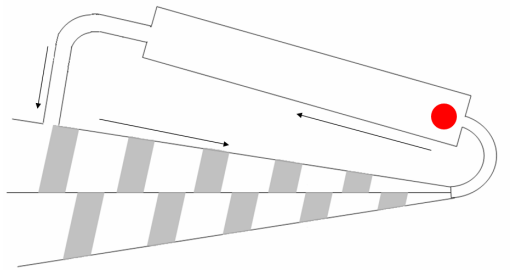

Fig. III.2 *Schema of micro-compounder*

Compared to the micro-compounder, the structure of the internal mixer is much simpler, as shown in Fig. III.3. The blended material remains in the same chamber without any exterior circulation.

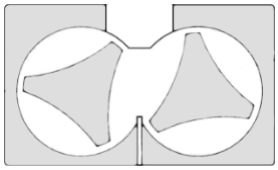

Fig. III.3 *Schema of internal mixer*

A calibration of the internal mixer was performed in a previous work [Lertwimolnun, 2006] in order to estimate the mean shear rate and the stress during the compounding. The approach proposed by Bousmina et al. [1999] was used to determine the correspondence between the shear stress τ (rheological measurement) and the torque M (data from the mixer) on the one hand and between the shear rate $\bar{\dot{\gamma}}$ (rheological data) and the rotation speed N on the other. In this approach, the rotors are represented as cylinders and the mixing chamber as a double Couette cell. Data were obtained on a polypropylene at 180 °C and a filling rate of 80% for the mixer. It was determined that:

$$\bar{\dot{\gamma}} = 0.72\ N$$

$$\tau = 6290\ M$$

In this work, we only used the estimation of the shear rate in the mixer.

Since the thermo-mechanical history in both compounders is very different, it was not possible to properly compare the obtained morphologies.

The use of the micro-compounder was restricted to preliminary experiments in order to limit the quantity of materials used. This was important in particular when compatibilized blends were prepared, since the limiting factor was the amount of the synthesized block copolymers.

III.2.2 Compression moulding

The product prepared in the internal mixer was ground (Hellweg M50/80 grinder) for further forming.

Compression moulding and injection moulding are two widely used forming methods. Since the outcome of rheological/mechanical measurements highly depends on the microscopic morphology of the sample, it is preferable that the forming method has little or no influence on the morphology in particular in the case of polymer blends. Since injection moulding implies high shear conditions, compression moulding was preferred to prepare the samples, even though some coalescence of droplets may happen in the non compatibilized blends during the annealing of compression moulding.

The mould used to prepare the sample for rheological test was an aluminium plate of dimensions 200×200×1mm with empty cylindrical shapes with 25mm diameter. The ground material was filled in the mould then the mould was cover by Teflon® sheets on both sides.

The heating plates of the compression machine (Carver 3853-0) were preheated at 190 °C prior introduction of the filled mould. The mould was left at atmospheric pressure for 5min in order to ensure the melting of the material and then submitted to 6 tons pressure for 2 min. The whole system was next cooled down to room temperature by water circulation and disk shape samples were demoulded. As the material was filled in excess in the mould to avoid bubble formation during compression moulding, the disk sample obtained at the end often had burrs at edge. These burrs were carefully removed by a scalpel.

Samples prepared in the same conditions were characterized in parallel by SEM and rheometry in order to be sure to probe the same morphology of the blend (see paragraph IV.1.1).

III.2.3 Rheometer

Rheological measurements were performed with the ARES (Advanced Rheometric Expansion System) rheometer from TA Instruments. It consists of an oven wherein a cone and plate geometry with 25 mm diameter and a cone angle of 0.04 rad is placed. The upper tool is connected to a torque sensor to measure the shear stress when applying a deformation, the test range of the sensor is 2.10^{-6} to 0.2 N.m. The temperature for all rheological measurements was fixed at 180 °C. Since bio-based polyesters like PLA can easily degrade at high temperature in presence of humidity, all the samples for rheological study were dried in a vacuum oven at 80 °C for at least 4 hrs before testing. The oven of the rheometer was preheated at 180 °C until temperature stabilization. The disk sample was placed on the bottom plate for 1 min to melt. The gap was set down to 0.85 mm to ensure no air bubble was present in the sample and then set to its operational value. The material in excess squeezed out of the geometry was then carefully removed by a scalpel. Measurements were performed at 180°C under a nitrogen environment in order to minimize the polymer degradation.

The linear domain was determined for the different polymers and blends. 10% strain, being well in the linear domain, was chosen for the frequency sweeps. Frequency sweeps were run from 100 down to 0.1 rad/s. Since the test in the low frequency region takes much longer time than the one in the high frequency, the frequency sweep was started at 100 rad/s and decrease in order to probe the morphology of interest and detect any potential evolution during the duration of the test.

III.2.4 Scanning electronic microscopy (SEM) and image analysis

III.2.4.1 SEM machines and observation modes

Two SEMs were employed in the study, Philips XL 30 ESEM LaB6 and Zeiss Supra 40. The difference between these two SEMs is that the power of the electron beam used by Philips XL 30 is around 15 eV while Supra 40 can work with a tension as low as 3 eV to obtain a clear image. This feature was quite useful when performing observations at high magnification, as PLA easily degrades under the electron beam. A lower working tension significantly reduces the degradation effect.

There are two working modes of SEM machines: Secondary electrons (SE) mode and back-scattered electrons (BSE) mode. The SE mode provides a detailed topography down to a few tens of nanometers. Pictures obtained under BSE mode include information not only on topography but also on the surface composition. The image contrast is created mainly by the differences in hydrogen atomic density. Recording images in the BSE mode on a perfectly flat surface (after polishing of the surface) is a way to observe a blend morphology if the polymers present differences in atomic numbers. These two modes were applied in the study for different purposes. During this study, the Philips XL 30 ESEM LaB6 was used in both modes for blends with a coarse morphology (drops with a size larger than 10 μm), while the

Zeiss Supra 40 was only used in SE mode for blends with a fine morphology (around the micron size).

III.2.4.2 Sample preparation and image analysis

Samples for SEM observations were prepared in two ways: mechanical polishing and cryofracture. The choice of method depended wholly on the objective of observation. For instance, one of the SEM observation objectives was to obtain the average inclusion size of the polymer blend. As this is a statistical value which requires a considerable amount of data, this process could hardly be done manually. Visilog® image analysis software was used for this purpose. After binarization of the image, the software determines the area of each drop by counting the number of pixels it occupies. The diameter of every drop is then calculated from this area assuming a circular shape. This automatic image analysis was performed on images obtained in the BSE mode on polished samples.

The polishing process was performed on the polishing machine Presi Mecatech 334. Samples were first embedded in a thermosetting resin (Presi cold mounting resin KM-V and KM-U blended at room temperature with volume ratio U/V=1/2). Pads were then mounted on the machine and polished with successive abrasive papers with decreasing grain sizes (ranging from 125 to 8.4 µm grain sizes, 5 min polishing per grain size) and water as lubricant. In order to maximize the smoothness of the sample surface, the last polishing step was performed using a glossy carpet and an aqueous suspension containing 0.03 µm diamond fragments. The limits of the mechanical polishing are linked to the fact that material fragments are removed by abrasive friction which can induce a local self-heating, and to the size of the abrasive grains relative to the characteristic size of the morphology. Therefore the method should be used with caution in the case of polymers with a glass transition temperature close to room temperature, and it is not applicable to samples with too small inclusions (micron size).

To compensate this shortcoming of polishing, cryofracture was applied to observe samples with micron size morphologies. Samples were first immersed into liquid nitrogen for 5 min and then broken with a steel hammer. The creation of a surface by a sudden rupture at -200 °C ensures that all the morphological details were retained during the preparation of the sample. A platinum layer of 70 nm was then cast on the fracture surface to ensure its conductivity for SE mode observations.

Selective dissolution of the different phases would have been a very efficient way to probe the blend morphology. However, in this study, as both PLA and PBAT are polyesters and share the same solvent, i.e. acetone, it was not possible to dissolve one phase selectively. We did not use this method.

III.2.5 Rheo-optical observations

A transparent counter-rotating shear cell coupled with an optical microscope and a digital CCD camera was used to record the relaxation process of deformed drops embedded in a polymer matrix in the molten state. Fig. III.4 shows a schematic representation of the rheo-optical device developed and constructed in CEMEF. The transparent shear cell is constituted by two glass plates rotating in opposite directions in order to fix the drop location relative to the laboratory framework. The velocities of the two glass plates are controlled independently. The relaxation is recorded after the shear is stopped.

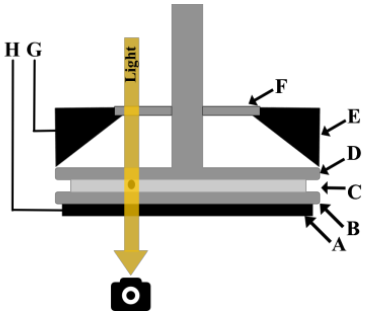

Fig. III.4 *Schematic front section of the shear cell and the heating parts*

Temperature control

The heating and temperature control of the lower glass plate (part B) is ensured by the direct contact with a fixed metallic part (part B) containing a thermal resistance. The shape of this metallic part is shown in Fig. III.5. The U-shape hole in this circular metallic plate allows the transmission of light to the objective of the microscope. The heating and temperature control of the upper glass plate (part D) is done by radiant heating via an annular chamber constituted by two half-ovens (part E) equipped with apparent resistances on the inner surface. Two thin glass plates (part F) ensure a relative confinement of the heat and permit transmission of the light beam. This open structure allows direct observation of the sample in the cell (part C). The two heating components are controlled separately by the control panel (G, H). Particular attention was paid during the conception of the heating parts to ensure a good temperature control of the glass plates containing the sample but also a good thermal insulation of the heating parts relative to other parts of the machine in order to limit heat transmission by conduction to these parts. For example, the upper glass plate is plugged and fixed by a thermosetting resin into a metal support. Due to the thermal resistance of these resins, the temperature of the heating parts should not exceed 220 °C. The temperature control of the heating parts is based on the feedback from thermocouples fixed directly on metal parts (A and E). So the set temperature (G, H) of the machine is not the true temperature of the sample.

To calibrate the correlation between set and sample temperatures, four thin thermocouples (diameter 125 µm) were set between two films of PLA with thickness of 0.6 mm. This allows local measurement of the real temperature inside the melt polymer and

comparison with the set temperature imposed on the machine. Local temperatures were measured via the hot junction of thermocouple T thin wires.

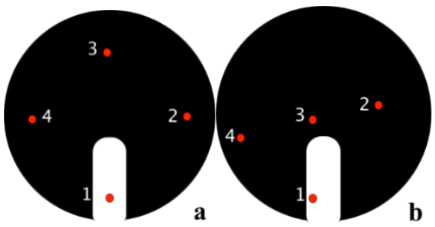

Fig. III.5 *Top view of the thermocouples' position on the heating lower part:* ***a*** *Initial position;* ***b*** *Final position after setting the gap*

A careful procedure was defined for the preparation of the PLA-thermocouple-PLA sandwich in order not to squeeze the welding point and also to keep the thermocouples in the middle of the PLA thickness. The same gap (1 mm) was used as during the rheo-optical tests in order to mimic the real thermal conditions. The difficulty of this calibration work was that the location of the thermocouples changed during the setting of the gap due to the squeezing flow of the molten PLA, as shown in Fig. III.4 b. However, the exact thermocouple location was easily controlled by looking from above. To establish the calibration, the temperature of the thermocouples was only noted 10 min after the change of the set temperature in order to ensure that the temperature inside the sample was stable. The relationship between the set temperatures and those of thermocouples is shown in Table III.1.

Set temperature (°C)	Annular oven (part E)	200	205	210	215	220
	Heating part below (part A)	190	190	200	190	188
Measured temperature (°C)	Thermocouple 1	176	177	186	179	178
	Thermocouple 2	186	187	195	187	185
	Thermocouple 3	182	183	192	184	183
	Thermocouple 4	181	182	192	183	182

Table III.1 *Correspondence between the set temperature and measured temperatures inside the polymer*

It was decided to determine the interfacial tension at 180 °C. The temperature of thermocouple 1 was always lower than the other ones. This is due to the fact that there is no lower heating part at that location. The influence of the annular oven on the temperature of the sample is quite limited. No matter how the two set temperatures were fixed, there was always a distribution of temperature in the sample along the horizontal direction. However, a higher annular chamber temperature tended to limit this temperature difference. An annular oven temperature set at 220 °C with 188 °C set for the lower heating part resulted in an average sample temperature close to 180 °C. These conditions were chosen for the rheo-

optical experiments. The application of a shear during the rheo-optical test also decreased the temperature differences in the horizontal plane. The temperature gradient along the vertical axis could not be checked.

Experimental procedure

Samples for the drop retraction experiment were prepared in the following way. The lower heating part temperature was first set at 188 °C. A polymer film (matrix component) was laid on the lower glass plate. 10 min were waited in order to ensure the polymer melting. During that time, small fragments of the polymer serving as dispersed phase were cut and put on the molten polymer matrix. A second film of matrix was then deposited. 10 min were left to ensure the full melting of both phases so that the shape of the dispersed phase changed from fragments droplets and the homogenization of the temperature before setting the gap at 1 mm. Care was taken not to introduce air bubbles around the dispersed phase. Different sequences of shear and relaxation were applied in order to have droplets in the right order of size. Care was taken to observe isolated droplets. After localization of a drop, shear was applied until the drop was deformed to an amount below 15%. The flow was then stopped and the kinetics of the drop deformation relaxation was monitored.

Angle correction

A Newtonian drop suspended in a Newtonian matrix under a constant shear flow (at low capillary number) deforms into an ellipsoid oriented at 45° relative to the flow direction [Taylor, 1932]. Taylor obtained this result by making a first order calculation and assuming a viscosity ratio between the dispersed phase and the matrix equal to unity. In recent years, studies on the drop deformation behavior in shear flow revealed that the tilt angle between shear and drop deformation direction varies from 45° to 0° depending on the Ca value and the viscoelastic character of the blend component [Verhulst et al., 2009][Chung et al., 2007]. If the tilt angle does not seem to be modified during the relaxation step in the case of two Newtonian components [Assighaou and Benyahia, 2010], this is different when one of the components presents a viscoelastic character [Verhulst et al., 2009]. In the present work both extremities of the tilt angle (0 and 45°) were considered upon calculating the drop deformation, the interfacial tensions calculated from these two deformations were also compared.

The relationship between drop deformation at 45° and 0° are deduced as following: Suppose the tilt angle is 45° as illustrated in Fig. III.5, the present set-up only allows us to measure the dimensions of the projection of the deformed drop. Assuming that the ellipsoid is an ellipsoid of revolution, the minor axis determined from the projection of the drop should correspond to the real minor axis of the ellipsoid (*b* axis marked in blue in Fig. III.6). However, this is not the case for the major axis, where there is an obvious difference between the true length (*a* represented in red) and the projected length (*c* represented in green).

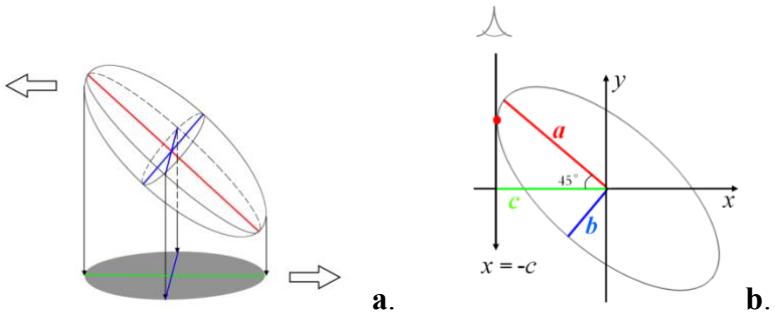

Fig. III.6 *Drop orientation under shear:* ***a****. Drop dimensions measured in the vorticity-flow plane,* ***b****. Drop dimensions in the gradient-flow plane.*

The next question turned out to be how to use the observed length of the minor axis b and the projection length c to determine the major axis length a. An ellipse is described by the following equation:

$$\frac{x^2}{a^2}+\frac{y^2}{b^2}=1$$

where a and b are the long and short axes of the ellipse when this is oriented along the x axis.

Considering the case of Fig. III.6 where the ellipse is tilted by 45° relative to the x, y reference, the equation to describe the ellipse becomes:

$$\frac{(\cos 45°x-\sin 45°y)^2}{a^2}+\frac{(\cos 45°y+\sin 45°x)^2}{b^2}=1$$

The coordinates of the red point (the point whose projection corresponds to the long axis of the projected ellipse) in Fig. III.6 also satisfy the equation above. The x-coordinate of this point corresponds to $-c$:

$$x=-c$$

The y-coordinate of the red point thus satisfies the following equation:

$$(a^2+b^2)y^2+2c(b^2-a^2)y+(a^2+b^2)c^2-2a^2b^2=0$$

which can be simplified by setting $m=a^2+b^2$, $n=2c(b^2-a^2)$ and $p=(a^2+b^2)c^2-2a^2b^2$

$$my^2+ny+p=0$$

The condition to ensure the uniqueness of the red point is that

$$n^2-4mp=0$$

Replacing the coefficients m, n, and p by their correlation with a, b and c finally leads to the following relationship:

$$a=\sqrt{2c^2-b^2}$$

a can then be calculated from the measured parameters b and c and used to determine the drop deformation at 45° tilt angle.

When the tilt angle is 0° the length of long axis from the observation is the true length of the ellipsoid, no further correction is needed. The influence of the drop rotation angle correction on the result of the interfacial tension will be discussed in the next chapter.

III.2.6 Tensile and impact test

Similar as samples for rheological characterization, samples for both tensile and impact tests were prepared by compression moulding in a Carver 3853-0 manual press. But since the sample for mechanical evaluation is substantially thicker than the sample for rheological test, a different protocol was used for forming:

- Preheat the mould at 205 °C for 15 min;
- Put polymer pellets in the mould and heat for another 15 min without pressure;
- Apply two tons pressure for 1 min;
- Apply four tons pressure for 2 min;
- Water cooling to room temperature and opening of the mould.

Tensile tests were performed on a Zwicky tensile machine with 2 kN force sensor and equipped with an extensometer at room temperature. The thickness of the sample is 2.5 mm, and other detailed dimensions of the sample are shown in Fig. III.7 (Unit of the dimensions is mm):

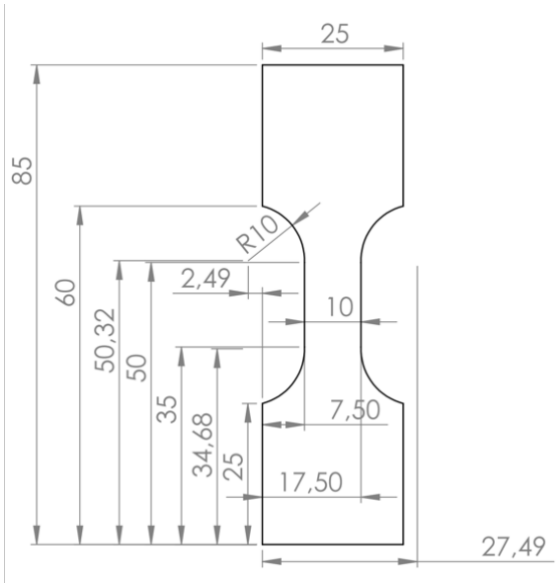

Fig. III.7 *Dimensions of tensile test sample*

With the hypothesis that, during the tensile test, the deformation is localized in the centre part (15 mm), the traction speed of the machine is set at 9 mm/min to have a deformation speed of 10^{-2} s^{-1}. Strain measurements in order to check the volume evolution inside the sample during tension were carried out using VIC3D.

The impact test was performed in a Ceast 9050 Charpy test machine. The shape of the sample follows ISO 179 80x10x4 mm, and they were notched.

III.2.7 DSC

To perform differential scanning calorimetry (DSC) measurements, a Perkin Elmer DSC 8500 was employed in this work. The sample mass is in the range of 5 to 8 mg and the material to be tested was placed in aluminium capsules for testing. The testing protocol was heating the sample up to 200 °C at a heating rate of 10 °C/min, isothermal stay for 5 min, then cooling down to -40 °C at the cooling rate of 10 °C/min.

III.2.8 X-ray diffraction

X-ray diffraction was performed on a PANalytical X'Pert Pro diffractometer. The X-ray generator is a Kα monochromatic copper anticathode with wavelength 1.5406 Å. The sensor is a ScanPixcel ultra-fast detector.

III.2.9 Molecular analysis

All the molecular analyses were performed by Marion Rollet at the Institut de Chimie Radicalaire of Aix-Marseille University.

^{1}H NMR analyses were performed on a Bruker Advance 400 spectrometer in $CDCl_3$. Polymer molecular weights and dispersities were determined by size exclusion chromatography (SEC). The system used was an EcoSEC (Tosoh, Japan) equipped with a PL Resipore Precolumn (4.6 x 50 mm, Agilent) and two linear M columns (4.6 x 250 mm, Agilent) with a gel particle diameter of 3 μm. These columns were thermostated at 40 °C. Detection was done using an UV/visible detector operated at λ = 254 nm, a dual flow differential refractive index detector, both from Tosoh, and a viscometer ETA2010 from PSS. Measurements were performed in THF at a flow rate of 0.3 mL min^{-1}. Calibration was based on polystyrene standards (ranging from 370 g/mol to 371 100 g/mol).

Liquid Chromatography at Limiting Conditions of Desorption (LC-LCD) was used in order to characterize the block copolymer PLA-*b*-PBAT. This was performed on a system equipped with a Waters 600E pump and a controller, a Waters 717 autosampler, a 7725i rheodyne valve, a Croco-cil column oven at 25 °C and a PL-2100 ELS detector (nebulization temp.: 30 °C; evaporation temp.: 70 °C; nitrogen flow rate: 1.2 mL min^{-1}). The chromatographic conditions for the separation of PLA, PBAT-*b*-PLA and PBAT were developed by D. Berek in an unpublished work. The stationary phase was a column (300x7.5mm) packed by D. Berek with Kromasil bulk silica 60 Å – 10 μm. The eluent was a

mixture of THF, toluene and methylene chloride (28 / 12 / 60 wt%), filtered through Alltech PTFE membranes (0.2 μm). The flow rate was 1 mL min^{-1}. The barriers 1 and 2 are mixtures of THF, toluene and methylene chloride in the following ratios: 7 / 3 / 90 wt% for Barrier 1; and 14 / 46 / 40 wt% for Barrier 2. These solvents were chosen because THF is a desorli for PBAT and PLA, while toluene is a strong adsorli for PBAT and PLA but it is not a good solvent; this is why methylene chloride, a weak adsorli but a good solvent for PBAT and PLA, was added.

The barriers were injected manually by using the 7725i rheodyne valve, equipped with a 1000 μL injection loop. The samples were solubilized in the eluent mixture at 0.25 wt% and filtered through a Sodipro PTFE syringe filter (0.2 μm). Samples were injected by the autosampler with an injection volume of 50 μL. Injection delays were 0 – 3 – 5, which means Barrier 1 was injected at 0 minutes, Barrier 2 was injected at 3 minutes and the sample was injected at 5 minutes. Data recording started with the sample injection.

References

Assighaou, S., Pavy-Le Du, G., Benyahia, L. (2007). Dispositif d'observation de gouttes sous déformation: développement et validation. *Rhéologie*, 11, 45-56.

Bousmina, M., Ait-Kadi, A., Faisant, J. B. (1999). Determination of shear rate and viscosity from batch mixer. *Journal of Rheology*, 43, 415-433

Jiang, L., Wolcott, M. P., & Zhang, J. (2006). Study of biodegradable polylactide/poly(butylene adipate-co-terephthalate) blends. *Biomacromolecules*, 7(1), 199–207.

Jiang, L., Liu, B., & Zhang, J. (2009). Properties of poly(lactic acid)/poly(butylene adipate-co-terephthalate)/nanoparticle ternary composites. *Industrial & Engineering Chemistry Research*, 48(16), 7594–7602.

Lertwinmolnun, W. (2006). Réalisation de nanocomposites polypropylene/argile par extrusion bivis. Thèse de doctorat, Ecole des Mines de Paris, Sophia Antipolis.

Lim, L. T., Auras, R., & Rubino, M. (2008). Processing technologies for poly(lactic acid). *Progress in Polymer Science*, 33(8), 820–852.

Taylor, G. I. (1932). The viscosity of a fluid containing small drops of another fluid. *Proceedings of the Royal Society a: Mathematical, Physical and Engineering Sciences*, 138(834), 41–48.

Zhang, N., Wang, Q., Ren, J., & Wang, L. (2008). Preparation and properties of biodegradable poly(lactic acid)/poly(butylene adipate-co-terephthalate) blend with glycidyl methacrylate as reactive processing agent. *Journal of Materials Science*, 44(1), 250–256.

Chapter IV

Measurement of interfacial tension and morphologies of non-compatibilized ternary blends

IV Measurement of interfacial tension and morphologies of non-compatibilized ternary blends

Once the studied polymers were fixed as PLA, PBAT and PA, the objective of this work became to prepare a core–shell morphology with PA encapsulated by PBAT in PLA matrix. As introduced in the literature survey, the most important parameter controlling the morphology of ternary blends is the interfacial tension between the compounded components. Thus, this chapter explains in detail the characterization of the interfacial tension between PLA, PBAT and PA with two methods, one based on rheological measurements and the Palierne model and the other on the kinetics of drop retraction.

Afterwards, the measured interfacial tensions were used in the models based on interfacial force balance and thermodynamics to predict the morphology of ternary blends. The validity of the theoretical prediction was checked by observation of the morphology of several blends with an alternated matrix (PA and PBAT instead of PLA). The effect of various blending conditions on the morphology was also investigated.

IV.1 Measurement of interfacial tension by Palierne model

The theoretical basis of interfacial tension characterization based on the Palierne model was presented in the literature survey. In the present chapter, more attention is paid to the experimental aspects of this method, introduced in two parts: a working flow chart including detailed manipulation steps, and an example of measurement.

IV.1.1 Working flow chart of characterization of interfacial tension by the Palierne model

All the experimental steps needed to measure the interfacial tension by the Palierne model are listed in Fig. IV.1. Since most of these steps follow the protocols introduced in Chapter III, only some specific explanations will be given here.

The Palierne model uses the rheological data of pure polymers to calculate the rheological curve of the polymer blend. These calculated data are then compared with the experimental data measured on the polymer blend. This blend was prepared by an internal mixer. There is a risk that degradation of the polymers (with a decrease of molecular weight and viscosity) may take place during the mixing time. In order to overcome this difficulty, pure polymers serving as dispersed phase and matrix were also subjected to the same mixing procedure and compression moulding operation as the polymer blend in order to mimic the thermomechanical conditions arising during blending and thus to use the correct viscosities.

Another precaution that was taken is that during the preparation of polymer blend samples for rheological tests, besides the samples needed for the rheological characterization, more disks were prepared under the same conditions for the morphological observations. The reason for not directly using the blend product to observe its morphology is that, during compression moulding, the morphology of a polymer blend with no compatibilizer (which is the case here) may coarsen due to coalescence. By preparing the samples for rheological tests and SEM observations at the same time, it was ensured that the observed morphology of the polymer blend was identical to the one probed during the rheological test.

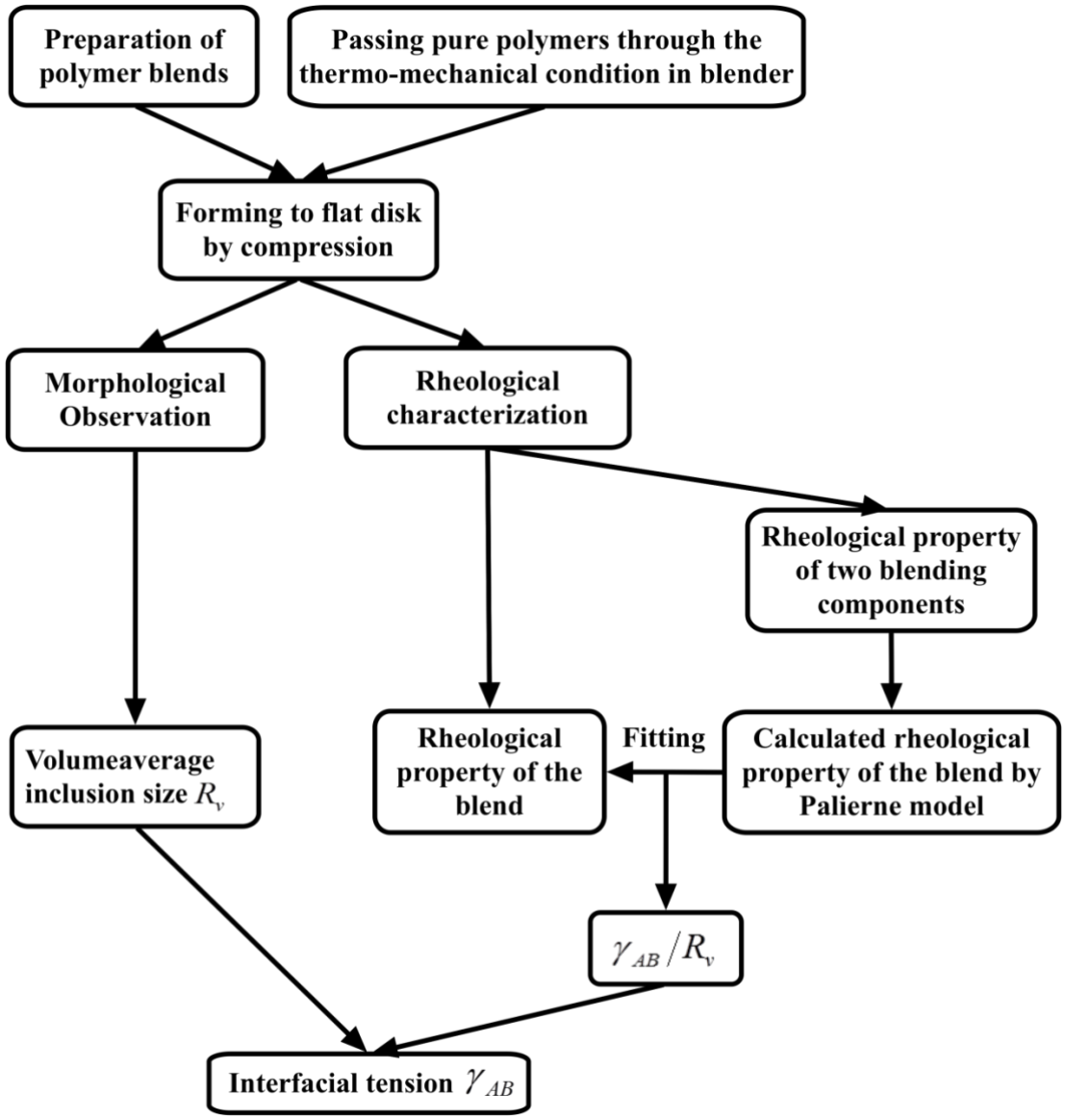

Fig. IV.1 *Working flow chart using the Palierne model to characterize the interfacial tension*

The blend apparatus used was the internal mixer. The polymers were introduced simultaneously and mixed for 12 min at 50 rpm and 180 °C. Three binary blends were prepared: 20PBAT/80PLA, 20PBAT/80PA and 20PA/80PBAT, where the numbers indicate

the weight fraction in percentage of individual components. In the following part, the PLA/PBAT couple is used as an example to illustrate the methodology we followed.

IV.1.2 PBAT/PLA as an example

When using the Palierne model to model the rheological curves of the two components and the polymer blend, Vinckier et al. [Vinckier et al., 1996] reported that the interfacial contribution is nearly invisible on the curve of loss modulus, and thus only the storage modulus was used.

As illustrated in Fig. IV.2, at high frequencies, the *G'* curve of the blend is situated between those of PLA and PBAT, which is in good agreement with the blending law proposed by Kerner [Kerner, 1956]. At lower frequencies, where droplets have time to relax, a shoulder shows up linked to the relaxation time of the droplets. The plotted frequency range is from 1 to 100 rad/s because the *G'* signal for PBAT was too low from 0.1 to 1 rad/s. The Palierne model enables us to calculate the $G'_{calculated}$ of the blend (Eq. 20) from discrete rheological data measured on the dispersed phase and the matrix, the volume fraction of dispersed phase and an assumed γ_{AB}/R_v. Then the experimental data of the polymer blend are fitted by the calculated ones by a least squares method using the Microsoft Excel solver, where the fitting parameter is γ_{AB}/R_v. A value of γ_{AB}/R_v is obtained ensuring a minimum value of $\sum_i \left(\frac{G'_{blend} - G'_{calculated}}{G'_{blend}}\right)^2$ by the least squares method. From the graph, it can be seen that these two curves superimpose perfectly in all the regions of pulsation, allowing the determination of γ_{AB}/R_v, being 2530 N/m^2.

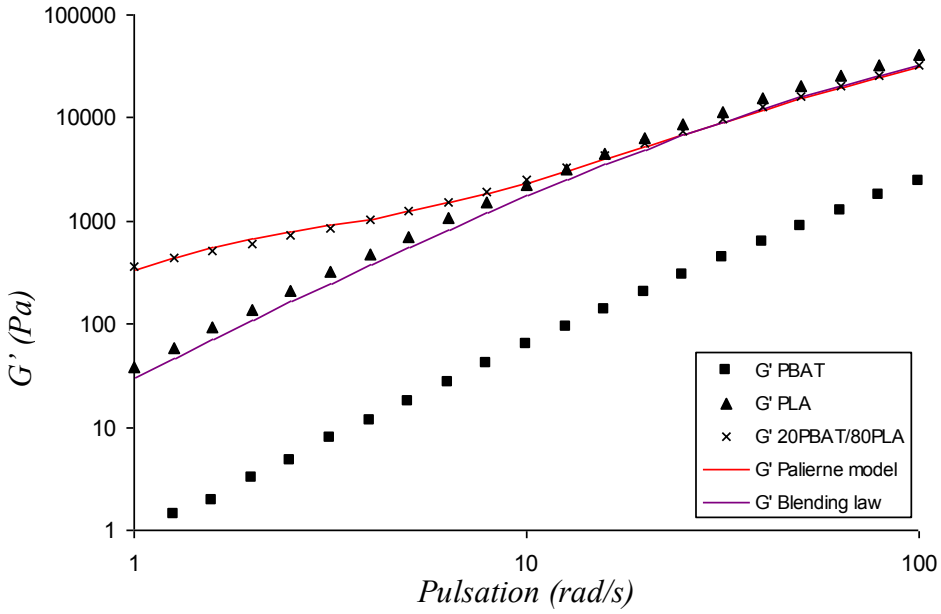

Fig. IV.2 *G' curves of pure PLA, PBAT, blend 20PBAT/80PLA, blending law and result of Palierne fit*

The next task was to measure the average inclusion size of the blend. From the SEM photos on the morphology of the cryofractured sample, it is observed that, besides the inclusion size, a lot of information on the topography of the surface is also included, as in the example shown in Fig. IV.3.a:

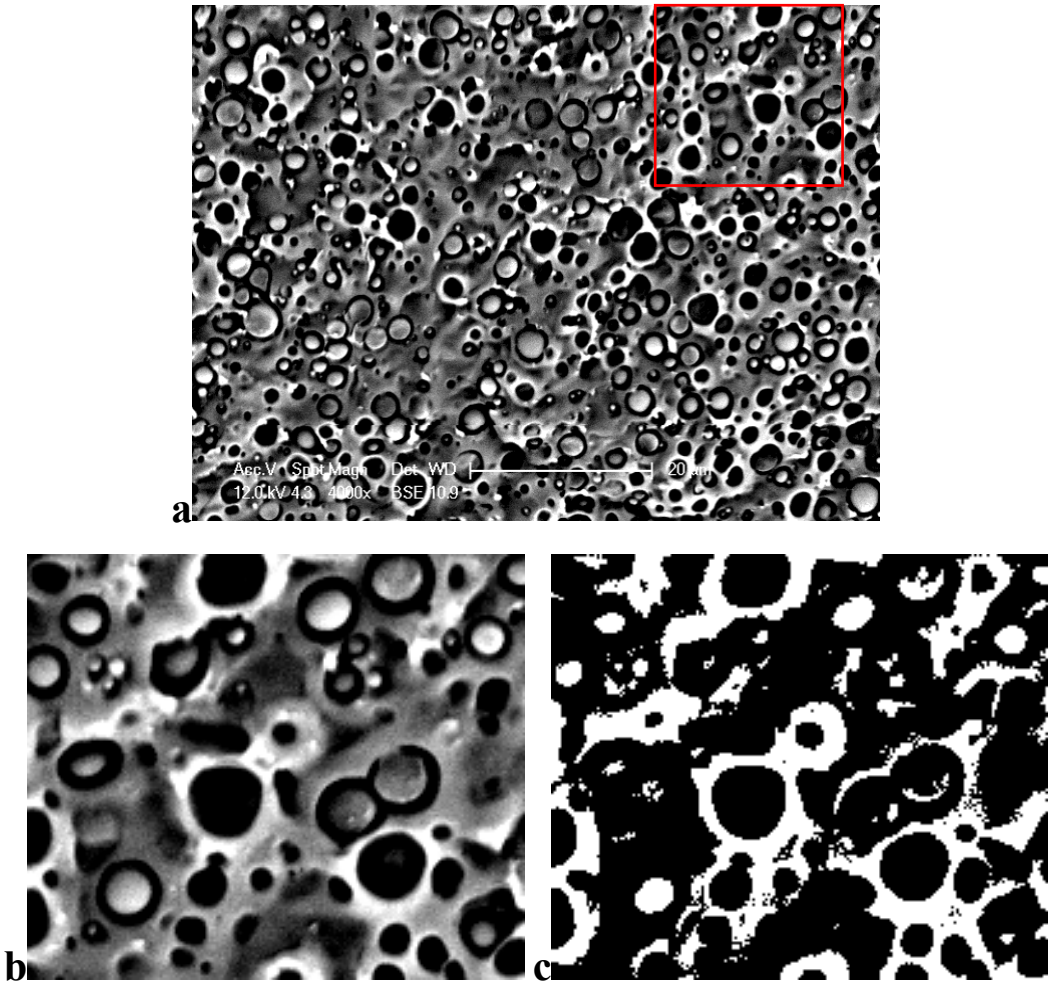

Fig. IV.3 a *SEM photo of blend 20PBAT/80PLA;* ***b*** *is a zoom of cropped square in* ***a;*** ***c*** *is a binarized result of photo* ***b***

Influenced by the geometry on the surface randomly created during the fracture, the presence of inclusions in the photo is revealed by empty holes and spheres under unidirectional light with both high light and low light parts. Since some of these low light parts are actually darker than the matrix, it is not possible to separate the dispersed phase and the matrix by a simple binarization over the image. For instance, in Fig. IV.3.c, the matrix at the geometric edge part is highlighted, so it also appears as a "white" part which is the same as inclusions during the binarization of the image. This fact would, of course, lead to the failure of the image analysis process.

To overcome this difficulty, the use of photos issued from the BSE mode to perform the image analysis was considered, since as mentioned, the SEM observation conducted

under BSE mode not only reveals the geometric information of the surface but also distinguishes zones with different densities of hydrogen atoms. Inspired by this feature of BSE mode observation, polishing was considered as a possible way to prepare the sample for the image analysis treatment, since it produces plane surfaces without any topographical characteristics. As shown in Fig. IV.4.a, geometric information such as a "basin" or "highland" on the surface was eliminated, leaving the inclusions with a colour significantly different from that of the matrix. In this way, the binarization treatment became quite convincing, as shown in Fig. IV.4.b using Visilog® software. It should be noticed that there is a loss of information resulting from the polished-image treatment process concerning small inclusions. During the polishing, the surface is created by friction to take away the materials. Although the final step of polishing is performed with micron scale rugosity abrasive papers, it is still a destructive way to obtain the flat surface. The drawback of this process is a loss of information on morphology details like small inclusions. Moreover, the image treatment software is not able to retain all the information after the binarization. From the comparison of Fig. IV.4.a and b, it is obvious that drops with a small size disappeared after the numerical treatment.

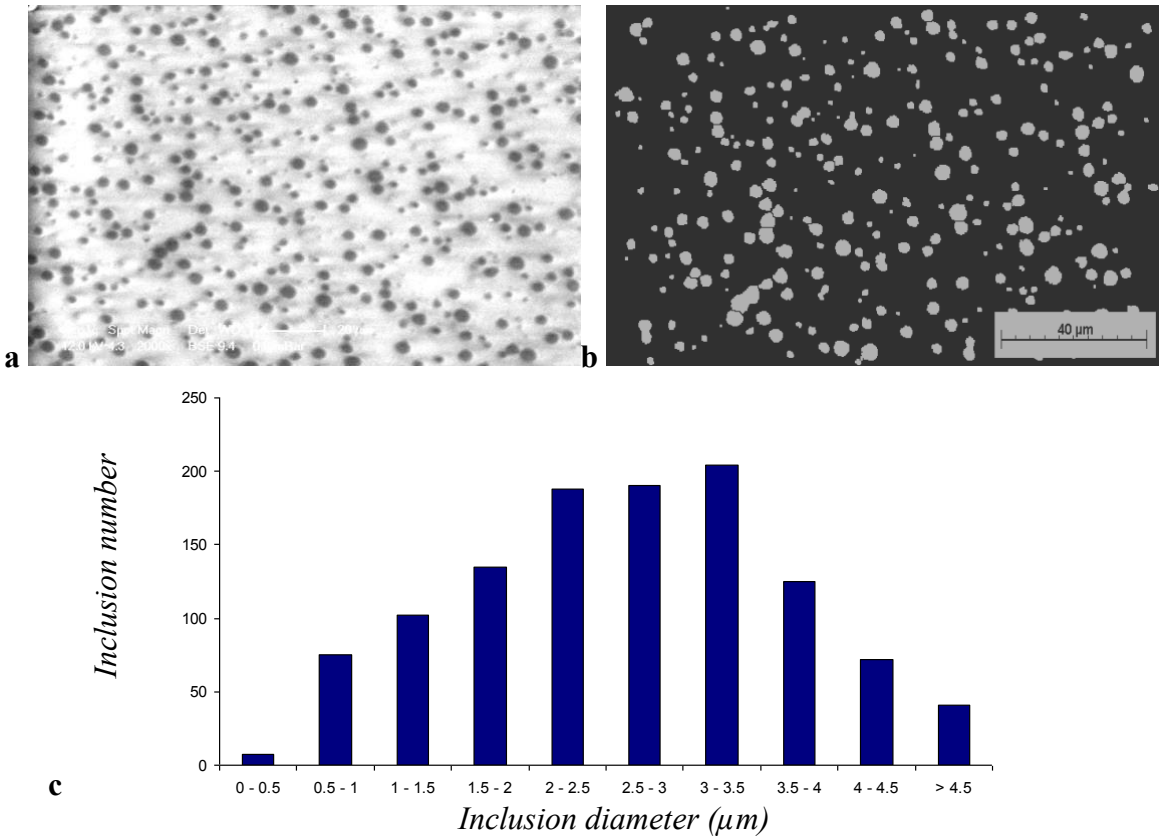

Fig. IV.4 a *Polished sample of 20PBAT/80PLA;* ***b*** *Treated image after binarization;* ***c*** *Size distribution of inclusions.*

However, since the volume average radius is defined as $R_v = \sum_i R_i^4 / \sum_i R_i^3$, the contribution of the droplets with a small radius becomes quite limited after the quartic and cubic calculations. For this reason, the influence of the lost information on the small size fraction is negligible. Using the size distribution shown in Fig. IV.4.c, the value of R_v was calculated to be 1.82 µm and R_n is 1.32 µm. The polydispersity index condition (R_v/R_v<2) to apply the Palierne model was satisfied.

With the results above, the interfacial tension for PLA and PBAT is calculated as being 3.8 mN/m. The same measurements were performed on the 20PBAT/80PA and 20PA/80PLA blends, the G' curves of these two blends are reported in Fig. IV.5:

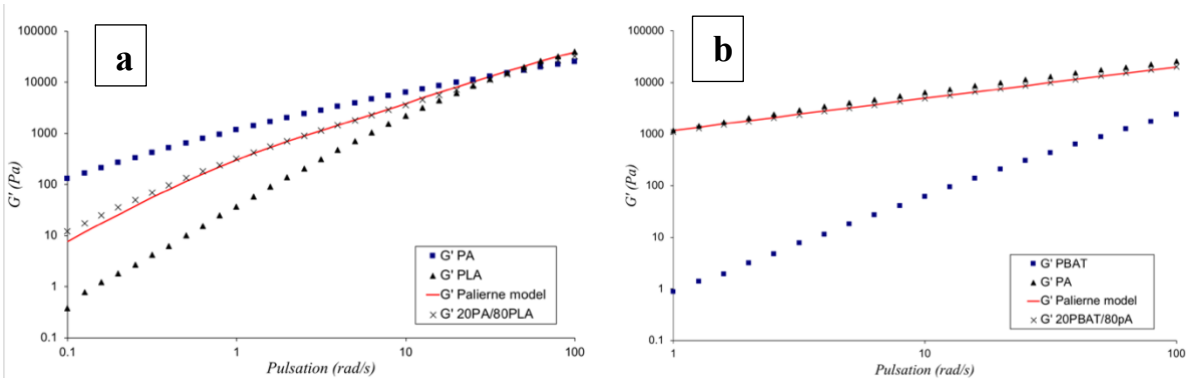

Fig. IV. 5 a *G' curves of PA, PLA, blend of 20PA/80PLA and fit result to Palierne model;* ***b*** *G' curves of PBAT, PA, blend 20PBAT/80PA and fit result to Palierne model.*

As observed in Fig. IV.5, the fit curves of Paliene model almost superimpose with the experimental data except for the low frequency range of 20PA/80PBAT. With R_v of this blend calculated as 1.26 µm, the Palierne model curve is already the most optimal algebraic solution to fit to the experimental curve leading to the result of interfacial tension between PA and PLA being 5.2 mN/m. Using the same method, the interfacial tension between PBAT and PA is calculated as 2 mN/m.

These results will be compared with those obtained by the drop retraction method at the end of this chapter.

IV.2 Measurement of interfacial tension by drop retraction

In this part, the manipulation steps for performing the drop retraction method are drafted in a work flow chart. An example of the use of this method to measure the interfacial tension between PLA and PBAT will also be presented. We also investigated the influence of polymer molecular weight on the interfacial tension. The different deformation direction

versus shear direction of PA drops in PBAT, and the influence of drop tilt angle correction on the result of interfacial tension will also be discussed.

IV.2.1 Working flow chart of drop retraction

The second method employed to characterize the interfacial tension is based on the kinetics of the retraction of a slightly deformed drop. The principle of the method has also been introduced in Chapter II. The experimental steps to apply this method are shown in Fig. IV.6.

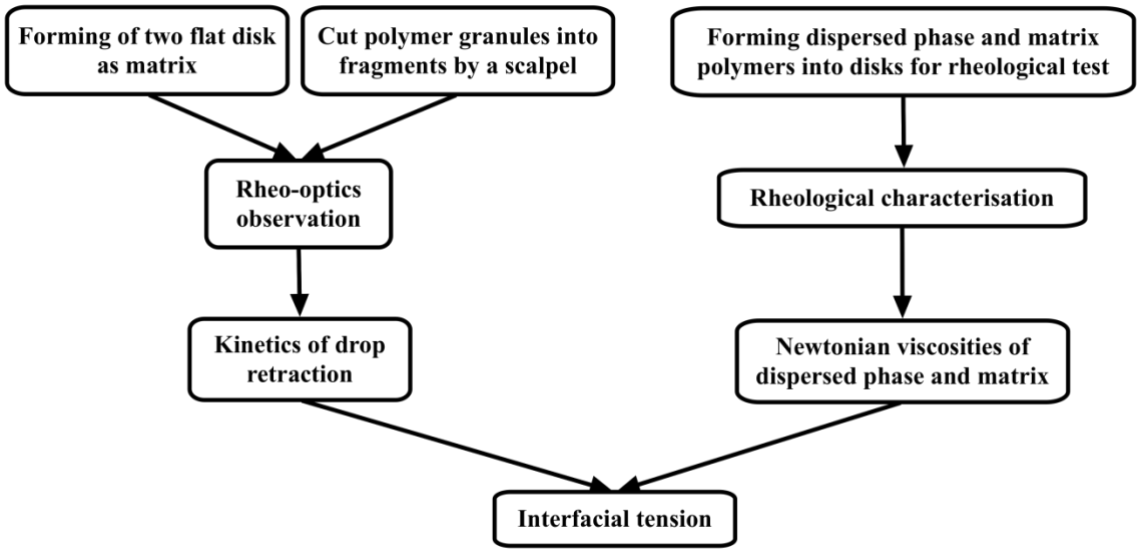

Fig. IV.6 *Working flow chart for drop retraction*

Since knowledge of the rheological properties of the polymers is also mandatory to implement this method to characterize the interfacial tension, it was also necessary to assess the potential decrease of polymer viscosities during the test. Unlike the severe thermomechanical conditions in the mixer, the observation conditions in rheo-optics are quite gentle. Therefore, the polymers were used as received, considering that they do not suffer degradation during the rheo-optical test.

As for the samples for rheo-optical observations, the matrix was shaped as a flat disk with thickness 0.6 mm and diameter 25 mm. The size of fragments serving as dispersed phase was 10 to 100 μm. Then, the observation was conducted following the protocol introduced in Chapter III.

IV.2.2 Retraction of PBAT drop in PLA as example

The retraction of a PBAT drop in the matrix of PLA after stopping shear is taken as an example in Fig. IV.7:

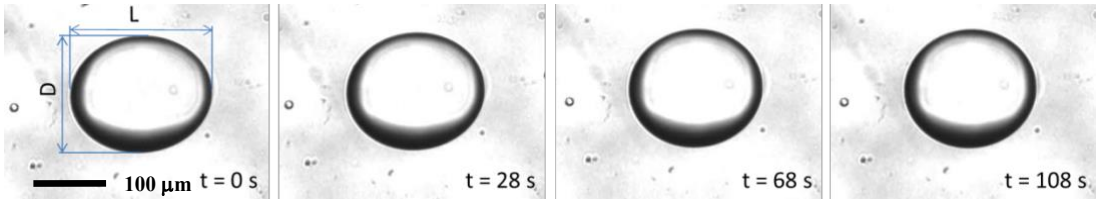

Fig. IV.7 *Retraction of PBAT drop in PLA after shear cessation*

The evolution of the drop deformation versus time during relaxation is plotted in a semi-logarithmic scale in Fig. IV.8. Using the equation given by Taylor [Taylor, 1934] (Eq. 28) to fit the data, a value of interfacial tension of 3 mN/m is obtained in the case of PLA/PBAT. Measurements were systematically performed on five droplets in order to have an average value. The measurement results by this method are summarized in Table IV.2.

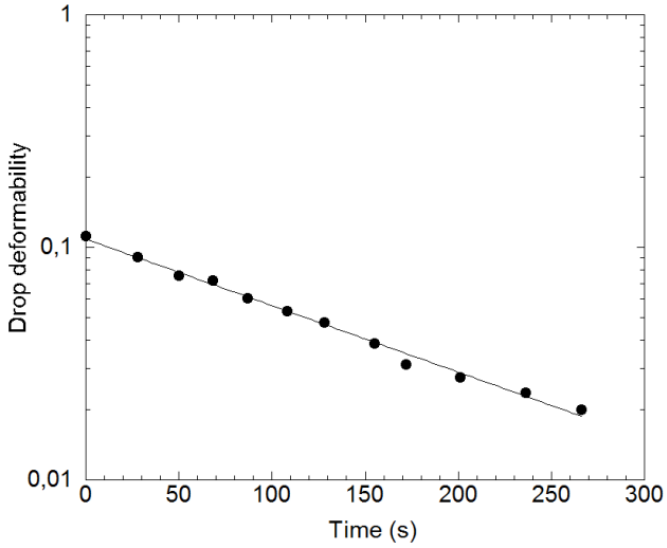

Fig. IV.8 *Deformation versus time during the retraction of PBAT drop in PLA*

IV.2.3 Influence of molecular weight and inversed matrix on interfacial tensions on PLA/PBAT

We took advantage of the degradation of PBAT with time (see paragraph III.1) to study the effect of the PBAT molecular weight on interfacial tension. To examine this effect, four series of drop retraction tests were conducted on the pairs PLA/PBAT: PBAT 2011 and PBAT 2007 respectively dispersed in PLA, and PLA dispersed in two matrices PBAT 2011 and PBAT 2007. The results of interfacial tensions are shown in Table IV.1:

PBAT 2007 in PLA	3 ± 0.4 mN/m
PBAT 2011 in PLA	3.3 ± 0.7 mN/m
PLA in PBAT 2007	3.6 ± 0.8 mN/m
PLA in PBAT 2011	3.4 ± 0.8 mN/m

Table IV.1 *Interfacial tensions between PLA and the batches of PBAT*

Although some literature [Anastasiadis et al., 1988] claimed that lower molecular weight leads to a lower interfacial tension, the results in Table IV.1 indicate that there is almost no effect from this parameter on the value of interfacial tensions.

To avoid any possible confusion in this chapter, "PBAT" mentioned without an indication of batch refers to PBAT 2007.

IV.2.4 Drop deformation along the vorticity axis of PA in PBAT

During the characterization of interfacial tension between PA and PBAT when the drop retraction test was conducted with a PA drop in the PBAT matrix, an unexpected phenomenon was observed while imposing the deformation of PA drops: In Fig. IV.9, under a shear in horizontal direction as indicated in the figure, the direction of drop deformation was observed to be perpendicular to the direction of shear.

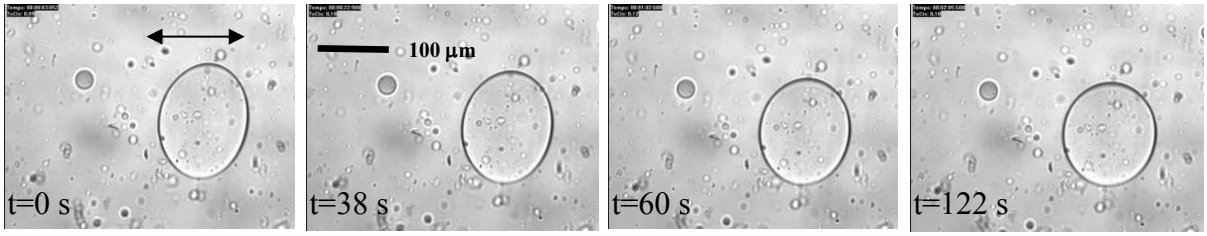

Fig. IV.9 *Drop retraction of a PA drop in PBAT, drop deformed along the vorticity axis. The arrow indicates the shear direction*

Mighri et al. [Mighri et al., 2002, 2005] conducted an extensive study on the phenomena and concluded that this vorticity deformation takes place when the elasticity of the dispersed phase is two times larger than that of the matrix at high shear rates with a quasi-Newtonian rheological behaviour of the matrix. From the rheological curves of PBAT(2007) and PA (Fig. III.1), it is found that both conditions are satisfied since the elastic modulus of PA is higher than that of PBAT over a large frequency range, and the viscosity of PBAT is constant and around 200 Pa.s over the whole frequency range.

IV.2.5 Influence of angle correction on the result of interfacial tension

As mentioned in the experimental part, during the characterization of interfacial tension using the drop retraction after a shear, the direction of the major axis of the drop has a 45° deviation from the shear direction. Under this circumstance, the observed length of the major axis is not the true long axis. Then it is interesting to know how large the difference between the observed length and the true length is, since it can affect the calculated interfacial tension (see Fig. III.6). The measurement of retraction of PBAT drops in the PLA matrix was taken as an example here to show the difference with and without correction in the following table:

	Interfacial tension without angle correction (mN/m)	Interfacial tension with angle correction (mN/m)
Drop 1	2.7	2.6
Drop 2	2.8	2.6
Drop 3	3.3	3
Drop 4	3.2	3.1
Drop 5	3.7	3.4
Average value	3.1	3

Table IV.2 *Interfacial tensions between PLA and PBAT with and without the angle correction*

From Table IV.2, the interfacial tension obtained with correction is always slightly smaller than the case without correction, although the difference between them is not very significant. It is understandable that both measurements give close results since the drop deformation is very small.

IV.3 Summary of interfacial tension measurement

The interfacial tensions between PLA, PBAT and PA were measured by the two methods. The results of these two measurements are given in the following table:

	Palierne model (mN/m)	Drop retraction (mN/m)
PBAT/PLA	3.8	3.3 ± 0.4
PA/PLA	5.2	5.6 ± 0.3
PA/PBAT	2	3 ± 0.4

Table IV.3 *Interfacial tensions measured by Palierne model and drop retraction*

The difference between the results issued from the two methods is most probably due to the large distribution of drop size obtained by mixing the two polymers when applying the Palierne model. The comparison of the working flow charts of the two methods (Fig. IV.1 and Fig. IV.5) shows that there are more experimental steps in the method of Palierne, which indicates that the accumulation of systematic error could be significant in this case. Moreover, since the results of at least five droplets were taken into account in the method based on the drop retraction, the values obtained by this method should be more reliable. In the following part, only the values from the drop retraction were used to predict the morphology of ternary blends.

IV.4 Prediction and validation of ternary blend morphology

IV.4.1 Prediction of the morphology based on interfacial force balance

Two theories predicting the morphology of ternary blends were described in Chapter II. One is based on the interfacial force balance and the other on calculation of blend free energy. Both approaches will be discussed in the following part.

First, the theory of interfacial force balance is used to predict the morphology of ternary blends PLA/PBAT/PA. The interfacial force balance is expressed by the spreading coefficients calculated below:

$$\lambda_{PBAT/PA/PLA} = \gamma_{PBAT/PLA} - \gamma_{PA/PBAT} - \gamma_{PA/PLA} < -5\ mN/m$$
$$\lambda_{PA/PBAT/PLA} = \gamma_{PA/PLA} - \gamma_{PBAT/PLA} - \gamma_{PA/PBAT} = -0.5 \pm 1\ mN/m$$
$$\lambda_{PA/PLA/PBAT} = \gamma_{PA/PBAT} - \gamma_{PBAT/PLA} - \gamma_{PA/PLA} < -5\ mN/m$$

$\lambda_{PA/PBAT/PLA}$ is about zero, while the other two spreading coefficients $\lambda_{PBAT/PA/PLA}$ and $\lambda_{PA/PLA/PBAT}$ are negative. According to the model, there are two possible morphologies as illustrated in Fig. IV.10.a: PA could either be encapsulated by PBAT or located at the interface between the PLA and PBAT phases. To check which morphology is really obtained, a ternary blend with the composition 60PLA/20PBAT/20PA was prepared and examined by SEM. The blend was prepared by introducing the three components at the same time in the

internal mixer at 180 °C and then mixing for 12 min at 50 rpm. The morphology is shown in Fig. IV.10.b. The black phase standing for the phase PA is mostly encapsulated by the grey phase (PBAT), sharing part of the interface with the white PLA phase, which is exactly in the middle of the situations shown in the two schemas in Fig. IV.10.a.

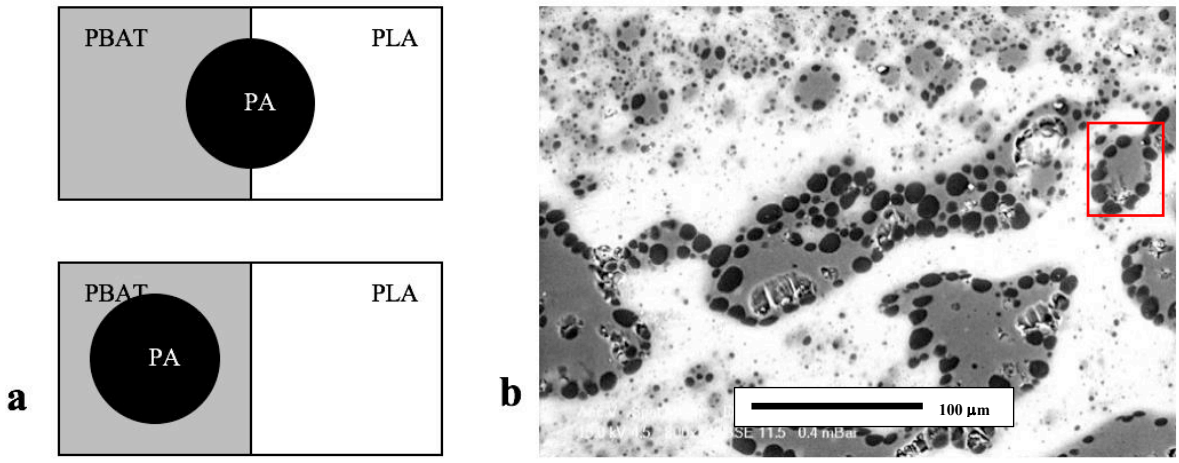

Fig. IV.10.a *Two possible morphologies according to the theoretical prediction;* ***b*** *Experimental morphology of blend 60PLA/20PBAT/20PA in internal mixer 180 °C, 50 rpm for 12 min*

To further confirm the morphology of the theoretical predictions, blends where the polymer matrix was changed were prepared in the same conditions and their morphologies were compared with the theoretical prediction, shown in Fig. IV.11: The situations of Fig. IV.11.d and f are vice versa. Hence in Fig. IV.11.f, since PA is the matrix, PLA should mostly be embedded in the PBAT phase to minimize its interface with PA; while in Fig. IV.11.e, when PBAT is the continuous phase, due to the poor affinity between PA and PLA, they should not form any kind of encapsulation.

To check the validity of those predictions, three blends with PA, PBAT and PLA matrices with composition 60/20/20 were prepared in the internal mixer. Their morphology demonstrates that whatever was the polymer matrix, the experimental results correspond perfectly with the theoretical prediction as shown in Fig. IV.11.

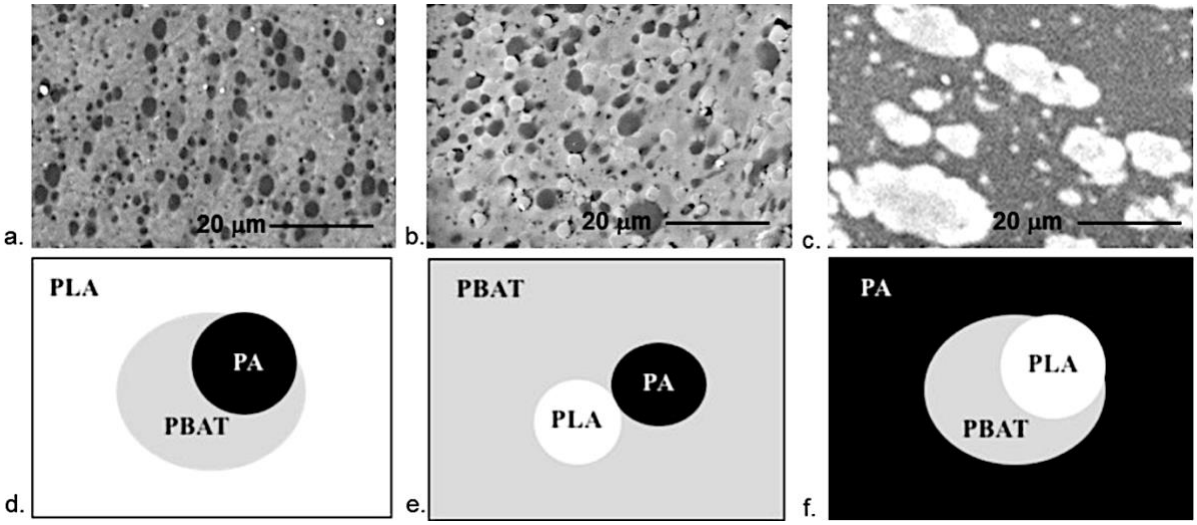

Fig. IV.11 *Morphologies of the three blends:* ***a*** *60PLA/20PBAT(2011)/20PA;* ***b*** *60PBAT(2011)/20PA/20PLA and* ***c*** *60PA/20PLA/20PBAT(2011) as seen by SEM and their respective model predictions (**d** to **f**). Experimental blends were prepared in the internal mixer at 180 °C, 80 rpm for 12 min.*

We observe a partial encapsulation morphology, which has also been reported by Le Corroller et al. (Le Corroller et al., 2011) in a HDPE/PP/PC system, where the volume fraction was 45HDPE/45PP/10PC. Similar to PA situated at the interface of PLA and PBAT, PC was located at the border of PP and PE. Interestingly, the interfacial balance condition for HDPE/PP/PC was slightly different from the PLA/PBAT/PA blends:

$$\lambda_{PC/PP/HDPE} = -1.9 \pm 1.7 mN/m$$
$$\lambda_{PP/PC/HDPE} = -19.3 \pm 1.7 mN/m$$
$$\lambda_{PP/HDPE/PC} = -1.3 \pm 1.7 mN/m$$

For PLA/PBAT/PA, two spreading coefficients are strongly negative, while for HDPE/PP/PC only one of them is strongly negative. The explanation for the similarity of the morphology is that despite the difference in the exact values of the spreading coefficients, all of them are negative or zero. Weakly or strongly negative spreading coefficients do not have a significant impact on the final morphology. They all lead to the same morphology.

IV.4.2 Interpretation of morphology from thermodynamic aspect

As introduced in the literature survey, the morphology of ternary blends can also be predicted by the calculation of the free energy of all the possible morphologies, the morphology with the lowest free energy being the favourable one from this thermodynamic approach. The difficulty in applying this method is that during the calculation of free energy,

information on the size of the different phases is needed, which is very difficult in the case of bi-continuous morphology. However, this method is especially efficient when used to examine similar morphologies. In the morphology of the ternary blend 60PLA/20PBAT/20PA(Fig. IV.9.b), a small PBAT-PA complex inclusion is selected as the study object as shown in the small red circle. The reason to select this particle is that it is relatively spherical so that it can be schematized as Fig. IV.12.a, where PA forms spherical droplets located at the interface between the PLA and PBAT. However, one can wonder why partial encapsulation is obtained instead of the full encapsulation as shown in Fig. IV.12.b? Calculation of the free energy of both morphologies in Fig. IV.12 was carried out to try to answer this question.

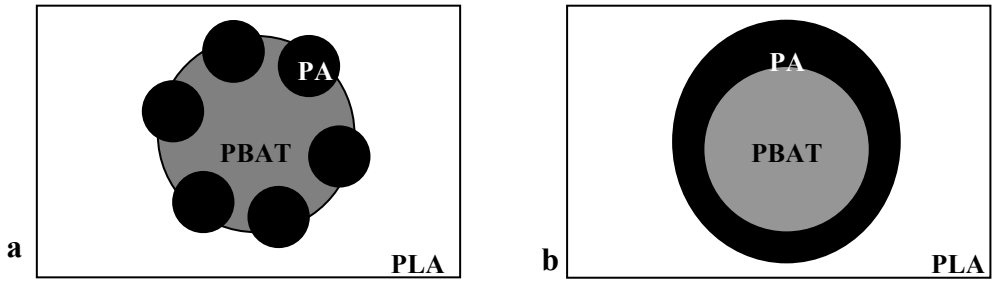

Fig. IV.12 *Schematic drawings representing:* ***a*** *Partial encapsulation morphology;* ***b*** *Full encapsulation morphology*

Using the method presented in Guo's work [Guo et al., 1997], the expressions of free energy of the morphologies in Fig. IV.12.a and b are calculated as below:

$$E_A = 4\pi R_{PBAT}^2\left(\left(\frac{k+2}{2}\right)^{\frac{2}{3}}\gamma_{PLA/PBAT} + \frac{1}{4}k^{\frac{2}{3}}n^{\frac{1}{3}}\left(2\gamma_{PA/PBAT} + 2\gamma_{PA/PLA} - \gamma_{PLA/PBAT}\right)\right)$$

$$E_B = 4\pi R_{PBAT}^2\left(\gamma_{PA/PBAT} + (k+1)^{\frac{2}{3}}\gamma_{PA/PLA}\right)$$

where R_{PBAT} is the radius of PBAT in both cases, γ refers to the interfacial tension, n is the number of PBAT drops in Fig. IV.12.a, and k is the volume ratio between the PA and PBAT.

According to the observation on the red square in Fig. IV.10.b, around a spherical PBAT drop the n value is approximately 10, therefore the relative values of E_A and E_B are given as:

$$E_A = 8.5 \times 4\pi R_{PBAT}^2$$

$$E_B = 10.5 \times 4\pi R_{PBAT}^2$$

This result indicates that the free energy of morphology A is lower than that of B, thus from the thermodynamic point of view, A is the more favourable morphology.

From the interpretation above, the spreading theory was first applied to predict the morphology in general. Then the calculation of free energy provided a clear distinction between the two possible morphologies. It also shows its advantage compared to the spreading model by examining the local difference of these two similar morphologies, since in this case, the influence of the size and number of drops of PA was not necessary for the calculation.

IV.4.3 Mechanism to form this morphology

In this part we tried to understand how the partial encapsulation morphology is formed during the blending operation. For this purpose, a 60PLA/20PBAT(2011)/20PA blend was prepared in the micro-compounder at 180 °C, 80 rpm, 12 min. Fig. IV.13 shows two photos of the sample taken at the entrance of the reservoir in the mini extruder. At this point, the shear rate decreases significantly since the material arrives from the high shear rate region of the twin screw into the low shear rate reservoir. The tree-like pattern at the entrance of the reservoir corresponds to the PBAT/PA inclusions elongated along the flow direction. A close look at this morphology shows that PBAT and PA threads compose every branch of this tree-like pattern. This can be interpreted considering the affinity between the phases: In the complex flow in these regions, once a PA inclusion approaches a PBAT inclusion, they are not likely to separate again, as $\gamma_{PA/PLA}$ is higher than $\gamma_{PA/PBAT}$, which means that the affinity between PA and PBAT is greater than that between PLA and PA. Then the kinetics to form this semi-encapsulated morphology can be understood as coming through two steps. In the high shear rate flow, dispersed phases are sheared and stretched into long threads. Then in the low shear part, due to the large interfacial tension with both the other phases, the PA thread breaks faster by the instability of interface. That is the reason why PA drops are attached around the PBAT phase as shown in Fig. IV.13.b.

a

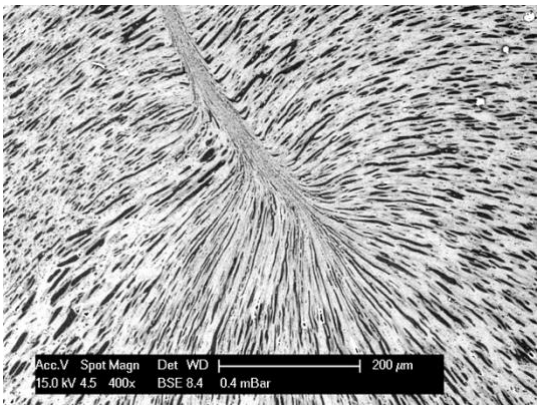

b

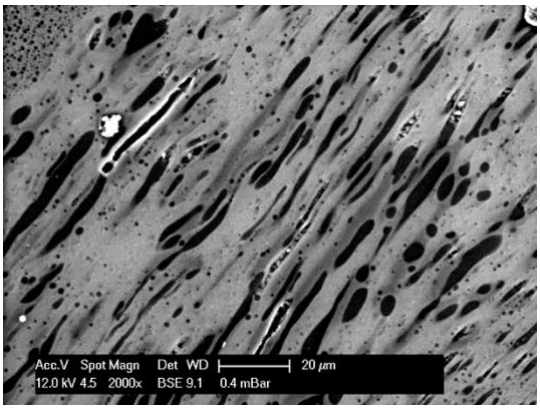

Fig. IV.13 a *Tree-like morphology at the entrance of reservoir;* ***b*** *Detail of the high shear part*

IV.5 Influence of blend condition on the morphology of the ternary blend

After having studied the development of the morphology, the effect of mixing conditions on the morphology was investigated by varying the rotation speed, the temperature and the duration of mixing. The composition was fixed at 60PLA/20PBAT(2011)/20PA. The standard blend condition was 180 °C, 12 min, 80 rpm in the micro-compounder.

Rotation speed

The two compounds shown in Fig. IV.14 were prepared under different rotation speeds but at the same temperature and duration. The comparison clearly shows that a higher rotation speed (or shear rate) leads to a finer dispersion of both PA and PBAT(2011). If the morphology is formed through the formation and rupture of long attached threads of PA and PBAT, the application of a higher rotation speed should lead to a smaller diameter of both phase threads resulting in smaller droplets after rupture.

a 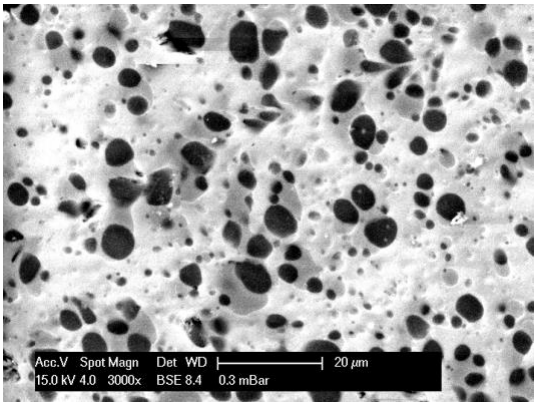

b 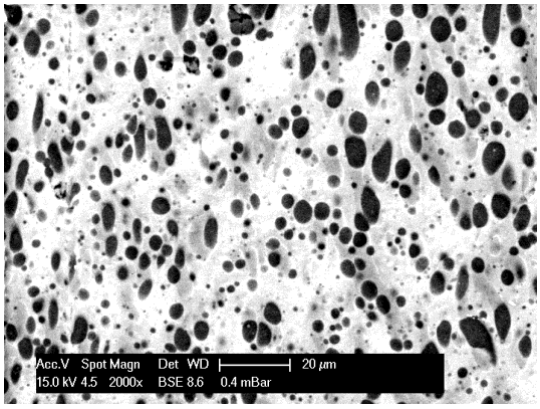

Fig. IV.14 *Morphology of the compound 60PLA/20PBAT(2011)/20PA at 180 °C, 12 min:* ***a*** *50 rpm,* ***b*** *100 rpm*

Temperature

The effect of temperature on the blend morphology is shown in Fig. IV.15:

a 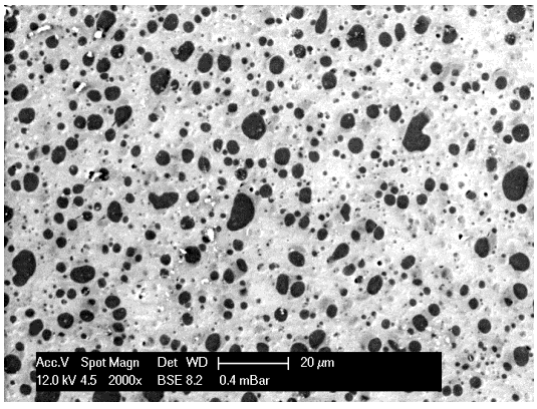

b 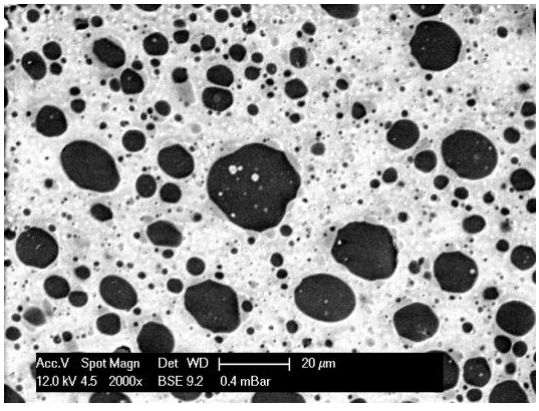

Fig. IV.15 *Morphology of the compound 60PLA/20PBAT(2011)/20PA at 80 rpm, 12 min:* ***a*** *170 °C,* ***b*** *190 °C*

The size of the PA inclusions significantly increases at a higher temperature. The size of the PBAT inclusions becomes smaller and they are attached to the surface of the PA. The PBAT and PA phases stick to each other and are dispersed in the matrix. The difference is that in Fig. IV.15.a, broken PA droplets are at the interface between the PLA and PBAT phases, and vice versa in Fig. IV.15.b, PBAT droplets are at the interface between the PLA and PA phases. The explanation for this phenomenon lies in the change of rheological properties during the rise of temperature.

Jordhamo et al. [Jordhamo et al., 1986] reported that in a binary blend, the fact that one phase is dispersed in another or vice versa depends on the viscosity ratio and volume fraction ratio between the two phases:

$$\text{If } \frac{\phi_A \eta_B}{\phi_B \eta_A} < 1, \text{ then phase A is dispersed in phase B}$$

$$\text{If } \frac{\phi_A \eta_B}{\phi_B \eta_A} > 1, \text{ then phase B is dispersed in phase A}$$

As the composition of this compound is PLA/PBAT/PA=60/20/20, the volume ratio between the PBAT and PA is always 1:1, hence the PA/PBAT structure only depends on the viscosity ratio. At 170 °C, above 1 rad/s, the viscosity ratio between the PA and PBAT decreases far below 1 (Fig. IV.16), indicating that the PA has a greater tendency to form the continuous phase. The viscosity ratio is even lower when the temperature is increased. This is the reason why the coalescence of PA is more noticeable at high temperature.

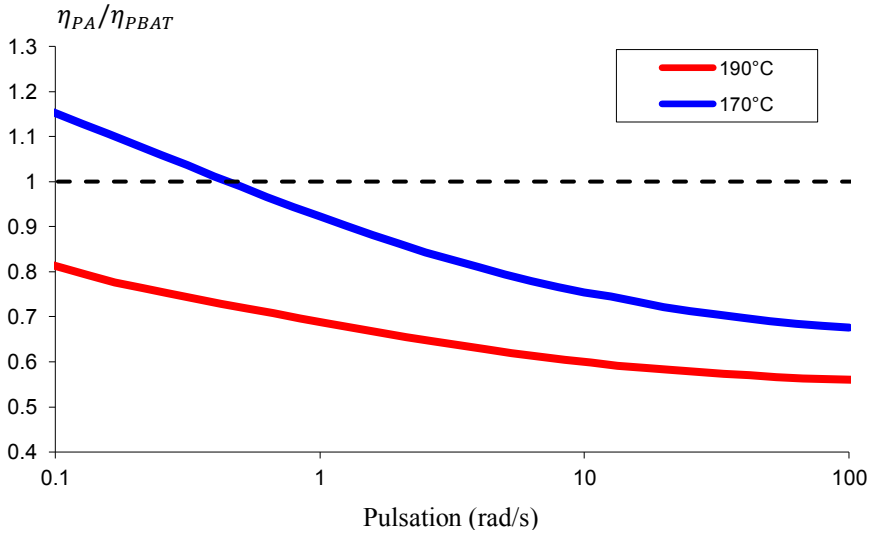

Fig. IV.16 *Viscosity ratio between PA and PBAT(2011) at different temperature*

Duration

Fig. IV.17 shows that complex inclusions of PA/PBAT seem to become slightly finer after a 20 min compounding compared to a 12 min one. The possible explanation for this outcome is that 12 min is not enough for the blend to reach its thermodynamic stable state. This could be confirmed by checking the torque curve from the machine. It was, however, not possible to measure it with the micro-compounder. In this apparatus the piston is manually forced to introduce the pellets in the hopper and the torque varies with the force to maintain the piston, so the torque value is not reliable.

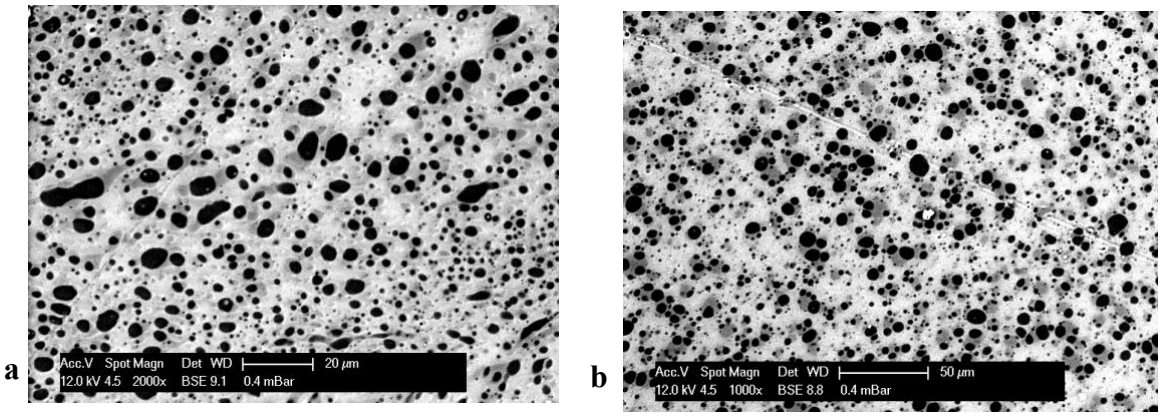

Fig. IV.17 *The morphology of compound 60PLA/20PBAT(2011)/20PA at 80 rpm, 180 °C:* ***a*** *12 min,* ***b*** *20 min*

IV.6 Conclusion

After measuring the interfacial tension between PLA/PBAT/PA by the Palierne model and drop retraction, the morphology of the ternary blends was predicted and confirmed experimentally on the blends. The influence of mixing conditions on the morphology was also investigated. However, the morphology obtained was different from the one aimed for: partial encapsulation relative to full encapsulation. To change the morphology of ternary blends, the values of interfacial tension must be changed. The most common way to modify the interfacial tension is by adding a compatibilizer. This work will be presented in the next chapter.

References

Assighaou, S. and Benyahia, L. (2010). Scaling law behaviour of the retraction of a Newtonian droplet after a strain jump in a Newtonian matrix. *Rheologica Acta* 49(6), 677-686.

Anastasiadis, S. H., Gancarz, I., Koberstein, J. T. (1988). Interfacial tension of immiscible polymer blends: temperature and molecular weight dependence. *Macromolecules*, 21(10), 2980-2987.

Jordhamo, G. M., Manson, J. A., Sperling, L. H. (1986). Phase continuity and inversion in polymer blends and simultaneous interpenetrating networks. *Polymer Engineering & Science*, 26, 517-524.

Kerner, E. H. (1956). The elastic and thermo-elastic properties of composite media. *Proceedings of the Physical Society. Section B*, 69(8), 808-813.

Le Corroller, P., & Favis, B. D. (2011). Effect of viscosity in ternary polymer blends displaying partial wetting phenomena. *Polymer*, 52(17), 3827–3834.

Mighri, F., & Huneault, M. A. (2002). Drop deformation and breakup mechanisms in viscoelastic model fluid systems and polymer blends. *The Canadian Journal of Chemical Engineering*, 80(6), 1028–1035.

Mighri, F., & Huneault, M. A. (2005). In situ visualization of drop deformation, erosion, and breakup in high viscosity ratio polymeric systems under high shearing stress conditions. *Journal of Applied Polymer Science*, 100(4), 2582–2591.

Taylor, G. I. (1934). The formation of emulsions in definable fields of flow. *Proceedings of the Royal Society a: Mathematical, Physical and Engineering Sciences*, 146(858), 501–523.

Vinckier, I., Moldenaers, P., & Mewis, J. (1996). Relationship between rheology and morphology of model blends in steady shear flow. *Journal of Rheology*, 40, 613-631.

Chapter V

Compatibilized ternary blends

V Compatibilized ternary blends

In the previous chapter, it was found that in the ternary blend PLA/PBAT/PA, the PA phase is located at the interface of PLA and PBAT phase (Fig. V.1a) due to the interfacial condition in the ternary blend:

$$\lambda_{PBAT/PA/PLA} = \gamma_{PBAT/PLA} - \gamma_{PA/PBAT} - \gamma_{PA/PLA} < -5\ mN/m$$
$$\lambda_{PA/PBAT/PLA} = \gamma_{PA/PLA} - \gamma_{PBAT/PLA} - \gamma_{PA/PBAT} = -0.5 \pm 1\ mN/m$$
$$\lambda_{PA/PLA/PBAT} = \gamma_{PA/PBAT} - \gamma_{PBAT/PLA} - \gamma_{PA/PLA} < -5\ mN/m$$

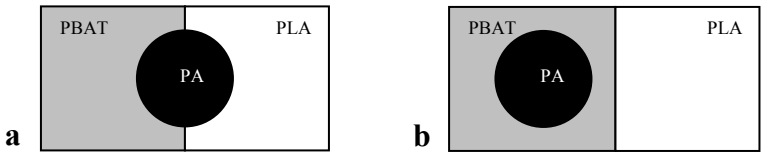

***Fig. V.1 a**. Morphology of uncompatibilized ternary blend PLA/PBAT/PA; **b**. Aimed for core–shell morphology when PA is fully encapsulated in PBAT.*

According to the model proposed by Le Corroller and Favis [Le Corroller and Favis, 2011], the interfacial condition to achieve the core–shell morphology shown in Fig V.1.a should be:

$$\lambda_{PBAT/PA/PLA} = \gamma_{PBAT/PLA} - \gamma_{PA/PBAT} - \gamma_{PA/PLA} < 0 mN/m$$
$$\lambda_{PA/PBAT/PLA} = \gamma_{PA/PLA} - \gamma_{PBAT/PLA} - \gamma_{PA/PBAT} > 0\ mN/m$$
$$\lambda_{PA/PLA/PBAT} = \gamma_{PA/PBAT} - \gamma_{PBAT/PLA} - \gamma_{PA/PLA} < 0\ mN/m$$

To increase $\lambda_{PA/PBAT/PLA}$ from negative to positive, there are two options:

1. To increase the value of $\gamma_{PLA/PA}$
2. To reduce the values of $\gamma_{PBAT/PLA}$ and $\gamma_{PA/PBAT}$.

From the practical point of view, the latter option is easier to implement, as the interfacial tension can be reduced by adding a compatibilizer in the binary blend. Ideally, the compatibilizer should be a selective one which would only reduce the interfacial tension of the PBAT/PLA and PA/PBAT blends, but not that of the PA/PLA blend.

Based on this approach, a first test was carried out with a commercial compatibilizer Lotader. Although not successful, this solution is described in the first part of this chapter. In the second part, the possibility of having a selective compatibilization using block copolymers was investigated. PBAT-*b*-PLA and PA-*b*-PBAT block copolymers were synthesized and characterized. After checking their compatibilization effect, a strategy to achieve the core–shell morphology was designed and realized. The mechanical performance of ternary blends was also evaluated.

V.1 Compatibilization with a commercial compatibilizer

Lotader AX8900 is a tercopolymer from Arkema built with ethylene, acrylic ester and glycidyl methacrylate blocks. Zhang et al. [Zhang et al., 2008] showed its compatibilization effect between PLA and PBAT. However, it can also compatibilize PA with the other polymers since its functional group is able to react with the different functional groups of the blend components PLA, PBAT and PA (Fig. V.2). It is thus a potential choice to decrease the interfacial tension and hence to modify the interfacial condition in order to achieve the targeted core–shell morphology.

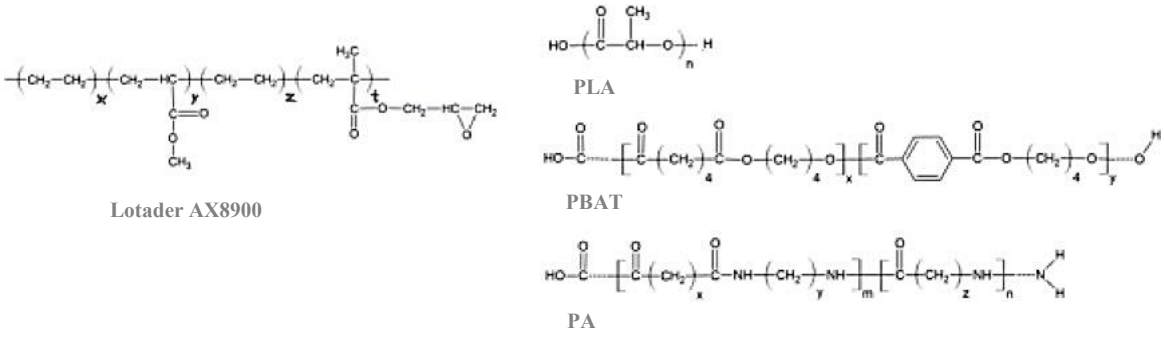

Fig. V.2 *Molecular structure of Lotader AX8900, PLA, PBAT and PA. The red circles indicate the functional groups that can react together*

A preliminary operation was to check the compatibilization effect of Lotader between PLA and PBAT. Several binary blends of PLA/PBAT were prepared with different concentrations of Lotader. Their morphology (polished surface of compression moulded samples) was observed by SEM as shown in Fig. V.3.

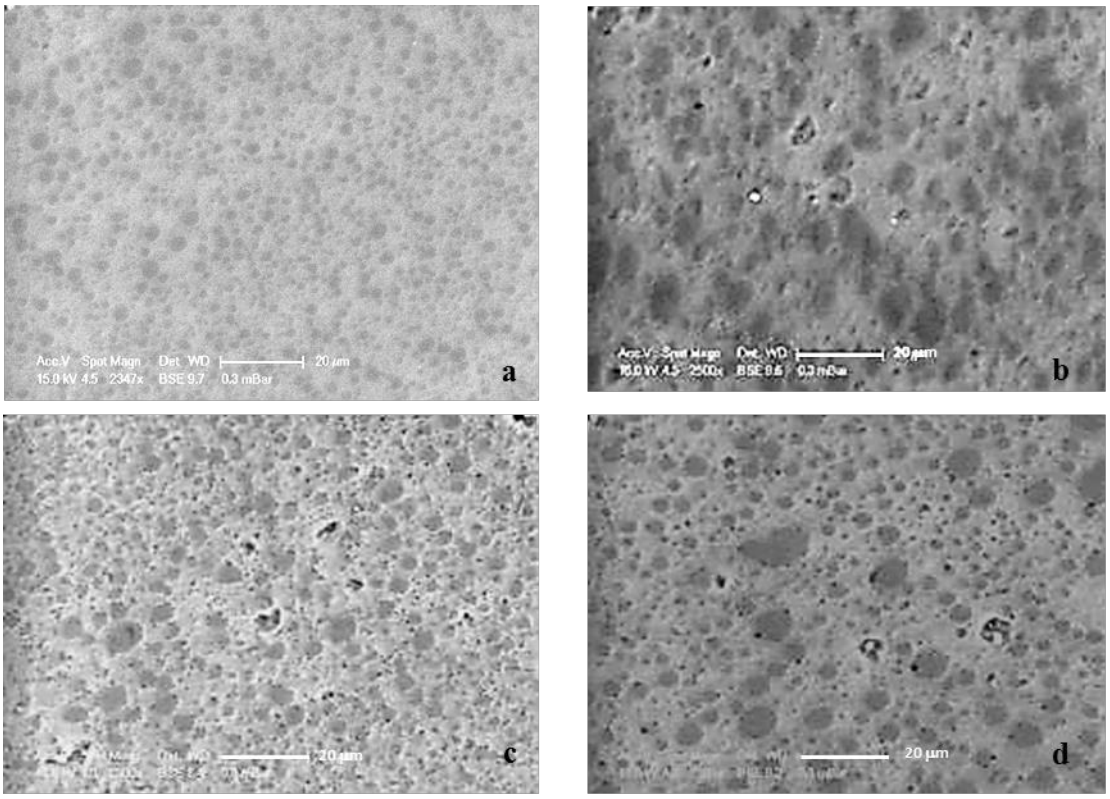

Fig. V.3 *Composition of the blends including the Lotader as compatibilizer:* ***a****. PLA/PBAT=65/35,* ***b****. PLA/PBAT/Lotader=63.4/34.2/2.4,* ***c****. PLA/PBAT/Lotader=61.9/33.3/4.8,* ***d****. PLA/PBAT/Lotader=61.9/33.3/4.8 but with a two-step order of introduction of components, at first introduction of PLA and PBAT and 3 min before the end of mixing, addition of Lotader. All blends were prepared in the micro-compounder at 50 rpm, 180 ºC for 12 min*

An effective compatibilizer should decrease the particle size since it decreases the interfacial tension and prevents the coalescence [Gramespacher et al., 1992][Serpe et al., 1990]. This is not the case with PLA/PBAT compatibilized by Lotader AX8900. The presence of 2.4% Lotader in the blend did not induce any decrease of particle size (Fig. V.3. a and b). When the quantity of Lotader is doubled (Fig. V.3.c), a lot of small black dots appear inside the PLA matrix and also at the PLA/PBAT interface. This may imply that the Lotader is not a good compatibilizer or that the amount is too large. The case where the Lotader was added 3 min before the end of mixing (Fig. V.3.d) is interesting. The picture shows that the Lotader tends to stay at the interface between the PLA and PBAT. However, this does not mean that it is an efficient compatibilizer, since it is forming particles at the interface instead of covering the surface of PBAT particles in a homogeneous way.

To further investigate the compatibilization effect of Lotader in the PLA/PBAT blend, samples were also prepared by cryofracture for SEM observation. The SEM pictures reveal a more complete picture of the influence of this compatibilizer. The comparison between Fig. V.4.a and b confirms that there is no decrease of the particle size in the presence of Lotader. The presence of neat holes at the surface of the fracture (Fig. V.4.a) indicates a poor adhesion between neat PLA and PBAT. In Fig. V.3.b, in the presence of Lotader, some of the holes on the fractured surface contain part of the broken PBAT particles. This tends to show that the affinity between the matrix and the dispersed phase will be stronger in the presence of Lotader. A closer look (red insert in Fig. V.4.b) indicates that Lotader is indeed located at the surface of the PBAT particles. This conclusion is deduced from the rough surface of the PBAT particles. When the quantity of PBAT is doubled (Fig. V.4.c), a better adhesion between PBAT and PLA is observed, since almost all the PBAT particles are broken within the matrix. In Fig. V.4.d, a bimodal distribution is observed, where large particles corresponding to the PBAT phase are surrounded by small particles of Lotader.

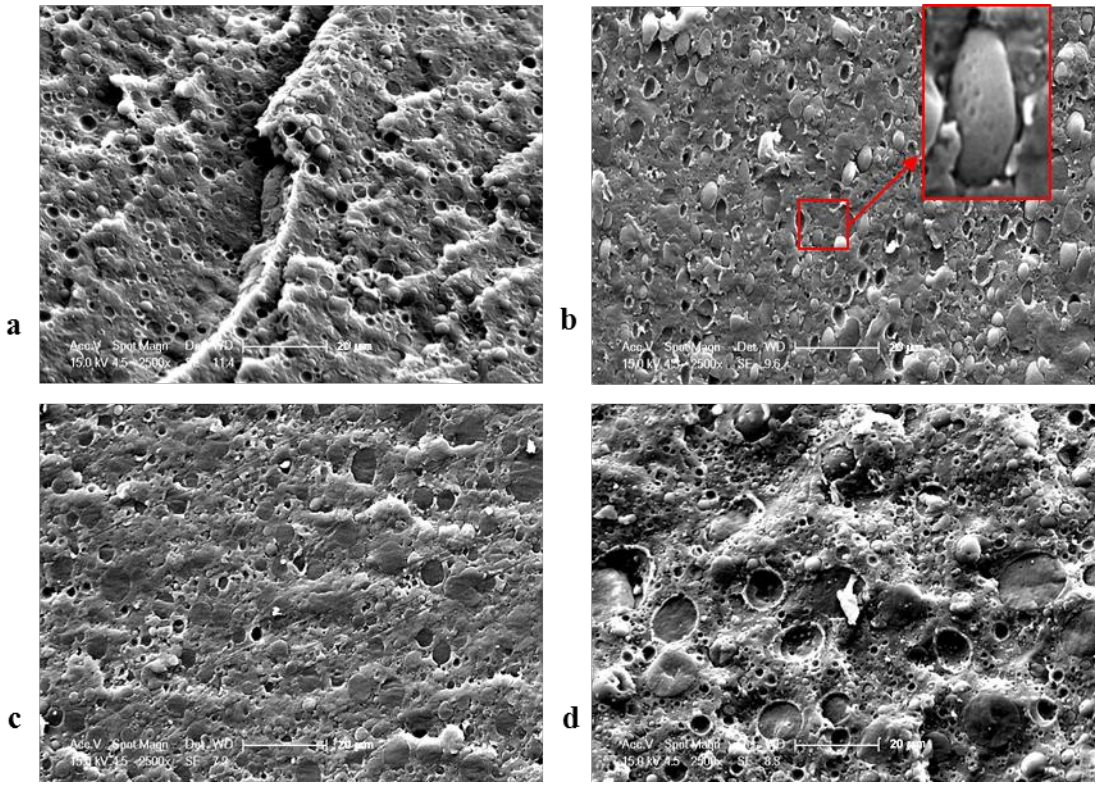

Fig. V.4 *Same samples as in Fig. V.3 prepared by cryofracture and observed by SEM:* ***a****. PLA/PBAT=65/35,* ***b****. PLA/PBAT/Lotader=63.4/34.2/2.4,* ***c****. PLA/PBAT/Lotader=61.9/33.3/4.8,* ***d****. PLA/PBAT/Lotader=63.4/34.2/2.4, with a two-step introduction - at first, introduction of PLA and PBAT, and 3 min before the end of mixing, addition of 2.4 wt% Lotader*

Rheo-optical observations were performed on Lotader fragments embedded in the PLA matrix. The Lotader looked as if it was still in the solid state inside the flowing PLA. This might be due to the experimental procedure of the rheo-optical observations. After positioning the samples in the solid state in the heated chamber, at least 15 min of conditioning is needed to make sure that the temperature is homogeneous and the polymers are fully molten before closing the chamber and performing observations. Since Lotader is able to crosslink at high temperature, 15 min of heating at 180 °C may be long enough for this phenomenon to occur. This could also explain why the Lotader appears as a separate phase between the PLA and PBAT in the blends after 12 min of mixing.

The next test was to use Lotader as a compatibilizer for the ternary blend PLA/PBAT/PA. It is obvious that if Lotader is added simultaneously with the other blend components, it may not modify the interfacial condition. $\lambda_{PA/PBAT/PLA}$ may remain negative, even if it may decrease all the interfacial tensions. For this purpose, different introduction sequences of Lotader were considered (Fig. V.5).

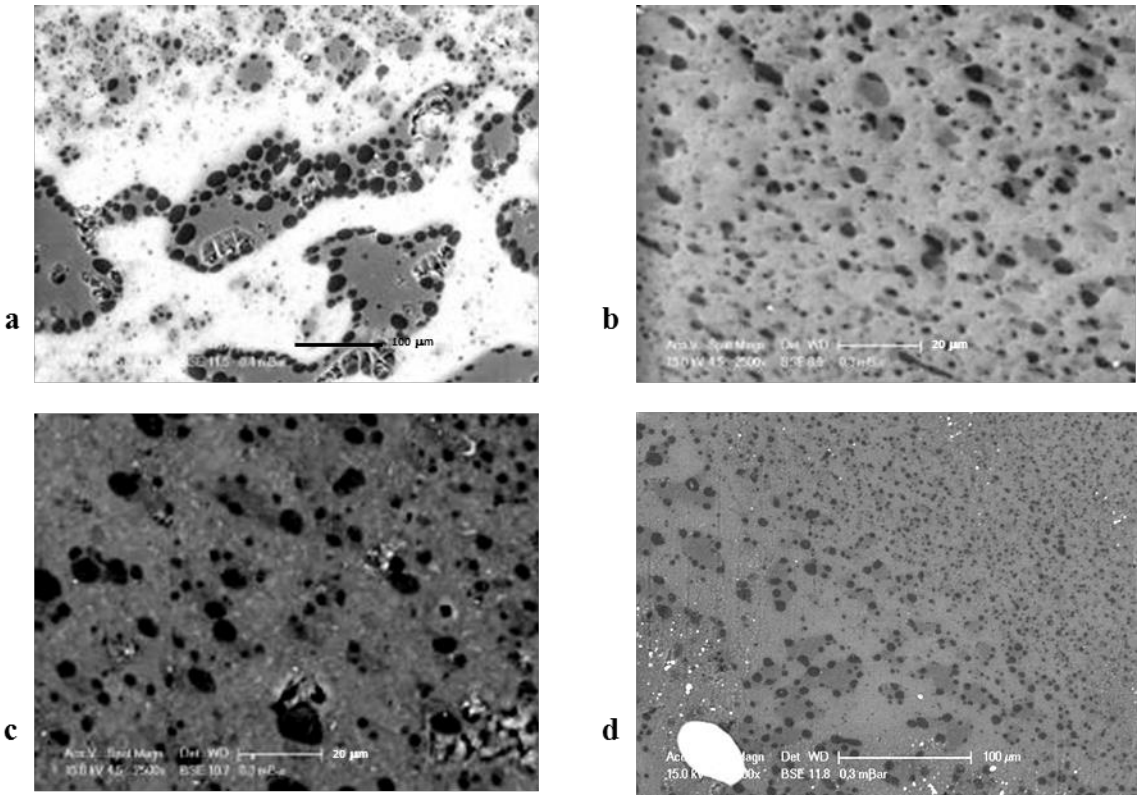

Fig. V.5 *Ternary blends including Lotader phase. All blends prepared in the micro-compounder at 50 rpm, 180 ºC for 12 min.* ***a****. PLA/PBAT/PA=60/27/13;* ***b****. first blending of PLA/PBAT/Lotader=63.4/24.2/2.4 and introduction of 13% PA 3 min before the end of mixing;* ***c****. first blending of 60% PLA, 24% PBAT and 2% Lotader, introduction of 13%*

PA after 6 min of mixing and addition of another 1% Lotader 3 min before the end; ***d****. Blending of 24% PBAT, 13% PA and 1% Lotader, introduction of 60% PLA after 6 min and addition of another 2% Lotader 3 min before the end of blending*

Since the purpose of investigating different introduction sequences was to compatibilize only two polymers (in the present case PLA and PBAT), the strategy was to first introduce PLA and PBAT and Lotader, wait until all the Lotader molecules have reacted and then add the third polymer. But this strategy was not able to produce the morphology which was aimed at since the PA phase (visualized as black in Fig. V.5) was always located at the interface of the PLA and PBAT. Hence, to achieve a core–shell morphology in PLA/PBAT/PA, selective compatibilizers are needed.

V.2 Synthesis and characterization of PBAT-*b*-PLA and PA-*b*-PBAT block copolymers

Compared to commercial compatibilizers which are often not very selective, the advantage of tailored block copolymers is that the compatibilization effect is well targeted on the pair of polymers composing the diblock. PBAT-*b*-PLA and PA-*b*-PBAT diblock copolymers were synthesized during the internship of Elena Dolci at the Institut de Chimie Radicalaire of Aix-Marseille University under the supervision of Trang Phan and Didier Gigmes.

V.2.1 Synthesis of block copolymers PBAT-*b*-PLA and PA-*b*-PBAT

V.2.1.1 PBAT-*b*-PLA

The synthesis of the PLA block is done by ring-opening polymerization (ROP) of lactide, catalyzed by tin octanoate and initiated by the hydroxyl functions of PBAT. This function enables us to initiate the polymerization of the PLA block. The PLA block grows directly on the PBAT block. The polymerization scheme is illustrated in Fig. V.6:

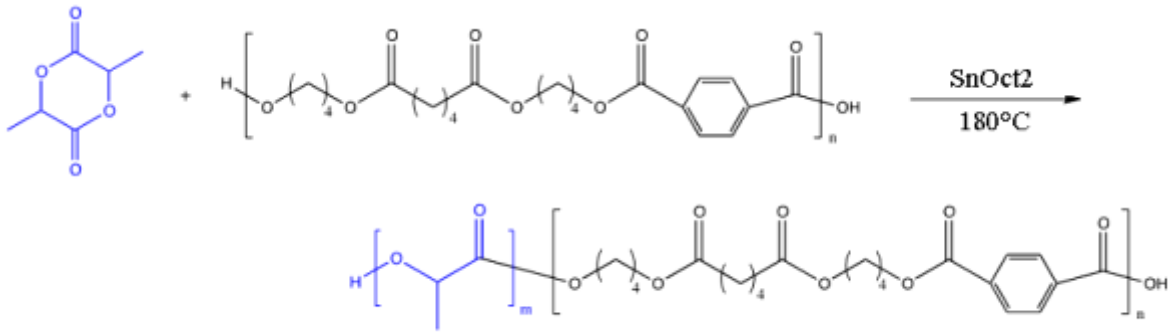

Fig. V.6 *Polymerization of diblock copolymer PBAT-b-PLA*

Tin octanoate has the advantage of being widely studied in the literature, and proved to be very effective for the ROP of lactide. It is used at an industrial scale for the synthesis of PLA by Cargill company. Its structure is given in Fig. V.7.

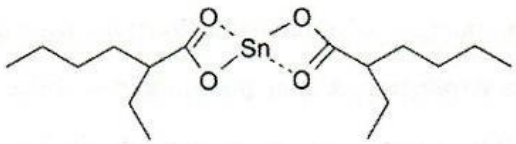

Fig. V.7 *Chemical structure of tin octanoate*

The ROP of PLA can be initiated by any alcohol function, in particular by water. Therefore the lactide should be handled carefully under clean and anhydrous conditions.

During the operation, the glassware used was washed with THF and then with acetone, and dried in an oven for at least 8 hours. The PBAT was dried under vacuum at 180 °C for 5 h with stirring. D-lactide was vacuum-dried at 40 °C for 3 h. $SnOct_2$, the catalyst, was dried under vacuum for 2 h at room temperature. The stoichiometric ratios were the following:

	PBAT	D-lactide	$SnOct_2$
Stoichiometry	1	275	2

The PBAT and D-lactide were put at 150 °C under an argon stream. Their mixture was well homogenized before adding the catalyst. Since the D-lactide degrades very

quickly, $SnOct_2$ was added dropwise using a syringe previously purged with argon, and the reaction was left to occur for 2 h at 150 °C while stirring the medium well. During the course of the reaction, the molten lactide reduced the viscosity of the medium. By incorporating it into the phase of molten PBAT, it decreased the viscosity of the whole medium, and the diffusion of the reactants was improved.

It is considered that the majority of PBAT chains have reacted and been extended with a PLA block. Purification focused on the separation of chains of homo-PLA and copolymers. Methanol is a non-solvent of PBAT and PLA. Acetone is a non-solvent of PBAT and a solvent of PLA. In acetone, the synthesized PBAT-*b*-PLA is slightly soluble. Therefore a mixture of these two solvents was used to reach a compromise between the dissolution of the homo-PLA, and precipitation of PBAT-*b*-PLA. The separation was realized by selective precipitation, by dissolving the synthesized product in a small amount of chloroform, and precipitating PBAT-*b*-PLA at 0 °C in an acetone/methanol mixture 2/1.25. The residue was filtered and dried under vacuum.

V.2.1.2 PA-*b*-PBAT

A first strategy was to prepare the PA-*b*-PBAT diblock copolymer by a coupling reaction between the two extremities of the PA block and PBAT block, but this was not possible because the PA copolymer was not miscible with PBAT and no common solvent was found.

A two-step strategy was thus chosen. Since PBAT is a random aliphatic copolyester of polybutylene terephthalate (PBT) and polybutylene adipate (PBA), a first step was to synthesize the PBT oligomers. Then the PBT oligomers were mixed together with adipic acid (AcAd) and 1,4-butanediol (condensation of which results in PBA oligomers) and PA chains leading to the polycondensation of PBT oligomers with AcAd and 1,4-butanediol from the chain-ends of the PA.

The synthesis of the PBT oligomer was realized by polycondensation of dimethyl terephthalate (DMT) with the 1,4-butanediol using titanium (IV) isopropoxide (TIP) as catalyst (Fig. V.8).

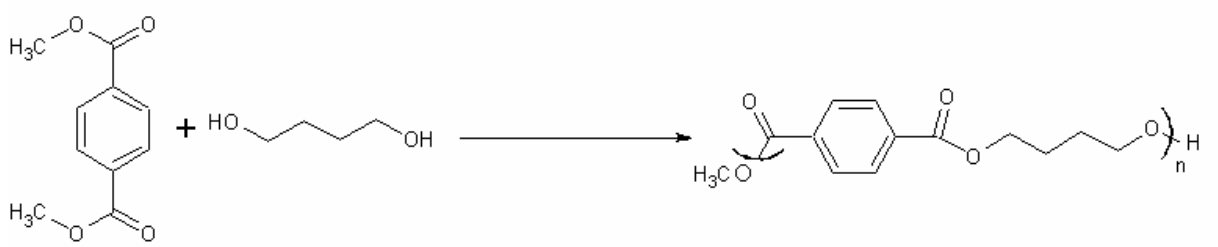

Fig. V.8 *Synthesis of the PBT oligomer*

DMT and 1,4-butanediol were placed in a 50 mL round-bottomed flask. The mixture was purged with an argon stream (needle directly immersed in the reagents) for 30 min at 180 °C with mechanical stirring. Then TIP was added dropwise by the syringe. The reaction lasted for 4 h at 195 °C under argon stream. The stoichiometric ratios were the following:

	DMT	1,4-butanediol	TIP
Stoichiometry	1.0	2.2	0.013

During the reaction, to promote the consumption of DMT [Le Hellaye, 2006], 1,4-butanediol was first put in excess, TIP being added at 0.2 wt%. 1,4-butanediol was then extracted at half the complete reaction time in order to prevent the equilibrium of the reaction forming PBT oligomers. The boiling temperature of DMT being 230 °C at atmospheric pressure, after an initial phase of esterification, the mixer was heated at 230 °C under reduced pressure to remove the excess 1,4-butanediol and to allow the formation of longer oligomers.

All the reactions of the second step leading to the formation of the PA-*b*-PBAT block copolymer are esterification reactions catalyzed by TIP and are presented in Fig. V.9.

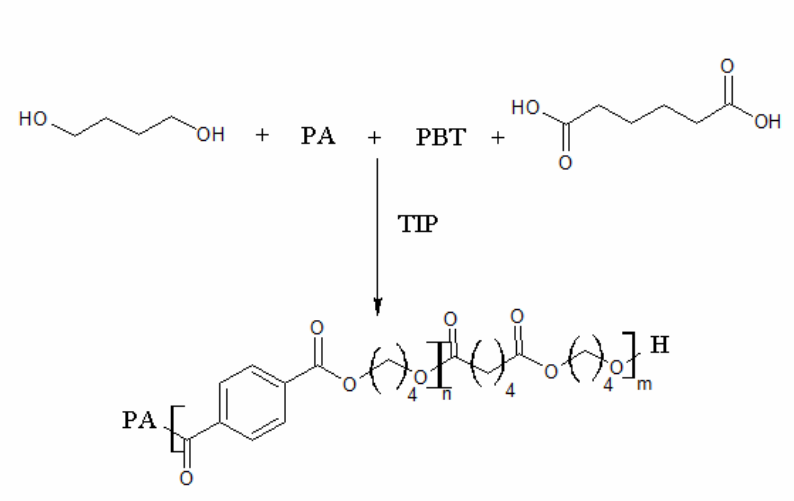

Fig. V.9 *Synthesis of PA-b-PBAT*

Then, PBT oligomer, AcAd, 1,4-butanediol and PA were put at 200 °C under argon and the mixture was homogenized. TIP was added up to 0.2 wt% using a syringe previously purged with argon. The whole system was held at 230 °C under vacuum for 3 h. The stoichiometric ratios were the following:

	PBT	PA	1,4-butanediol	AcAd	TIP
Stoichiometry	1	0.070	1.4	2.4	0.05

The final product was insoluble in the usual solvents: acetone, chloroform, THF, DMSO, ether, ethanol ... This posed great difficulties for the characterization and purification of the product.

V.2.2 Characterization of the PBAT-*b*-PLA and PA-*b*-PBAT block copolymers

V.2.2.1 Molecular analysis

As the synthesized product PA-*b*-PBAT was not soluble in the usual solvents, this prevented a molecular analysis of this copolymer since it requires the product to be soluble. We will thus only focus on the characterization of PBAT-*b*-PLA.

Bulk polymerization of lactide in the conditions we used reached a high conversion within 2h (>95%, determined by ^{1}H NMR). Fig. V.10 shows ^{1}H NMR spectra in $CDCl_3$ of the synthesized copolymer, and of the pure PBAT and PLA used to prepare it for comparison.

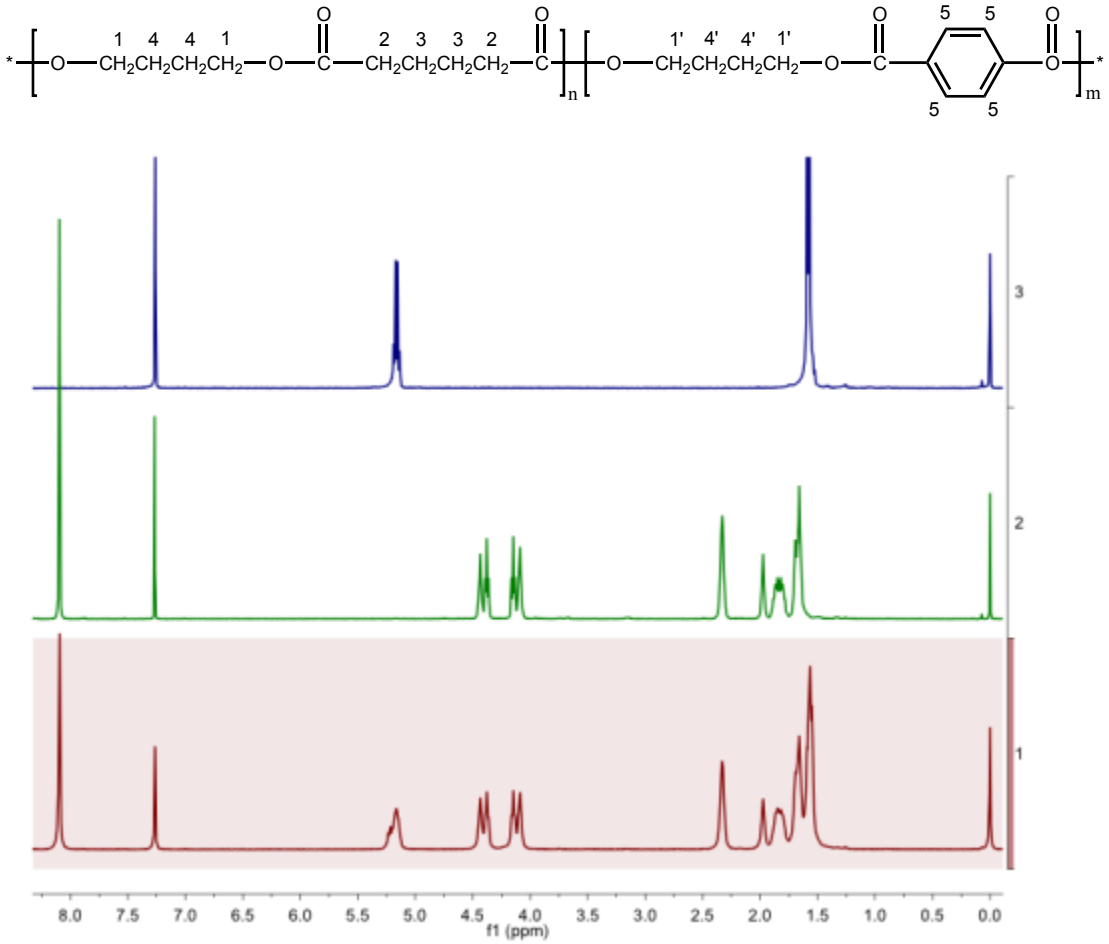

Fig. V.10 *PBAT structure and ^1H NMR spectra in $CDCl_3$ of (1) synthesized PBAT-b-PLA block copolymer, (2) PBAT and (3) PLA*

The analysis of the PBAT spectrum indicates that the signals occurring at 4.11–4.09, 2.33, 1.69, and 1.66 ppm can be assigned to the methylene protons H1, H2, H4, and H3 respectively. The ratio of the integrated peak area of H1:H2:(H4+H3) is 1:1:2, corresponding to those of butylene-adipate (BA) unit in equimolar ratio. The chemical shifts at 4.43 – 4.38 ppm for $–OCH_2$ – (H2), and 8.10 ppm for protons adjacent to aromatic carbon (H5) are attributed to those of butylene-terephthalate (BT) unit. No COOH resonance signal could be detected due to the instrumental detection limit. These data indicate that linear PBA chains are terminated by hydroxyl functional end groups. The ratio of the integrated peak intensities of H2 protons and H5 protons is 1.08:1, indicating that the content of BA unit is 51.9 mol%. These ^1H NMR data indicate that the molecular structure of the PBAT mostly consists of hydroxyl functional end groups, which were used to initiate the lactide polymerization. Analyzing the ^1H NMR spectrum of synthesized copolymer, we note that the characteristic signals of PBAT and PLA are present. Outside the PBAT signals as shown above, we identify two signals of PLA at

5.16 and 1.57 ppm corresponding to -CH-O- and CH_3 respectively. The molar and weight compositions of copolymer can easily be calculated from the ratio of the integrated peak intensities of H5 aromatic protons of PBAT and -CH-O- protons of PLA. The synthesized copolymer consists of 40 wt% of PLA, this data being calculated with the molar mass of BAT unit of 420 g/mol and the molar mass of lactide unit of 72 g/mol.

One of the most commonly employed techniques to characterize the polymer molar mass and molar mass distribution is Size Exclusion Chromatography (SEC). PBAT-*b*-PLA synthesized block copolymer and its macro-initiator (PBAT) were first analyzed by SEC using tetrahydrofuran as eluent; the obtained chromatograms are shown in Fig. V.11. To our surprise, the chromatogram of the synthesized copolymer was identical to that of the starting PBAT. For a composition of 40 wt% of PLA in the copolymer, we expected a chromatogram shifted to a lower elution volume (high molar mass). Other chromatographic conditions were applied by changing either the mobile phase or the stationary phase. For example, with the styrene-divinylbenzene columns, THF+0.2%TFA, $CHCl_3$ or DMF+0.01MLiBr were used as the mobile phase; for the PSS PFG columns, $CHCl_3$, $CHCl_3$+10%TFE or TFE + 10 $g.L^{-1}$ of potassium trifluoroacetate were used as the mobile phase. The same results were obtained with all these SEC conditions. PBAT and PBAT-*b*-PLA were eluted at the same elution volume, with the same peak shape as shown in Fig. V.11.

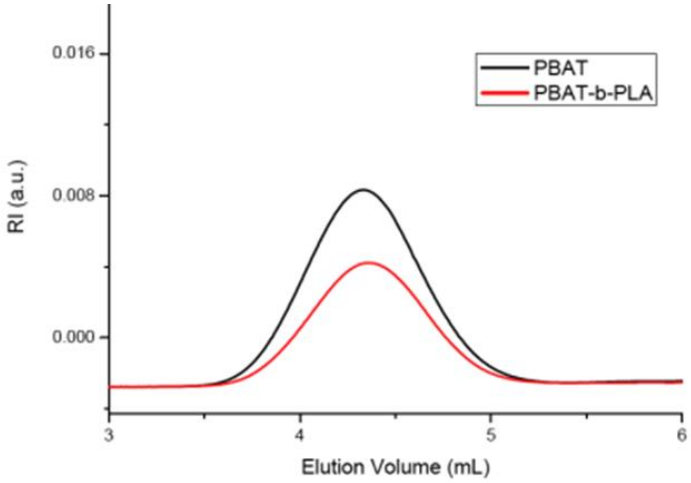

Fig. V.11 *SEC chromatograms of PBAT (black line) and PBAT-b-PLA (red line). Columns: PL Resipore 250x4.6 mm + guard column 50x4.6 mm at 40 °C; Eluent: THF at 0.3 mL.min^{-1}; RI detector*

It is well known that SEC does not have a sufficient resolution to separate a block copolymer from its parent homopolymers [Park et al., 2004]. Most of the block copolymers chromatograms obtained by SEC show multi-modal distributions because of the presence of parent homopolymers or secondary produced block copolymers. This is

not the case here. The PBAT-*b*-PLA chromatogram is almost identical to the PBAT chromatogram. Indeed, we were expecting a shift in elution volume from the PBAT to the PBAT-*b*-PLA block copolymer because of the increase in molar mass due to the PLA block. To explain these SEC results, we can assume that the block copolymer was retained on the stationary phase (synergy of interactivity) and only PBAT and/or PLA parent homopolymers were (co-)eluted.

Recently, D. Berek introduced a new liquid chromatography technique named Liquid Chromatography at the Limiting Conditions (LC-LC) [Berek, 2008]. This separation technique is based on the difference of the elution rate between macromolecules and organic molecules like solvent. According to the retention mechanism, different techniques can be distinguished. For example:

- Liquid Chromatography at Limiting Conditions of Enthalpic Interaction (LC-LCA);
- Liquid Chromatography at Limiting Conditions of Unpartition (LC-LCU);
- Liquid Chromatography at Limiting Conditions of Desorption (LC-LCD), which shows very good sample recovery.

According to Berek, Liquid Chromatography at Limiting Conditions of Desorption (LC-LCD) is the most promising technique because of its robustness, the high sample recovery and the high sample capacity [Berek, 2008]. Moreover, it is a technique that is easy to set up and to use [Berek, 2008].

LC-LCD has already been used to separate numerous block copolymers from their parent homopolymers [Berek, 2010]. Recently, poly(ethylene terephthalate) (PET), PBT, PLA and PBA were separated by LC-LCD [Siskova et al., 2012]. Moreover, Berek separated PBAT, PBAT-*b*-PLA and PLA by LC-LCD in an unpublished work. LC-LCD was applied with the same chromatographic conditions developed by Berek for those polymers. The separation of PBAT-*b*-PLA from its parent homopolymers is evidenced in Fig. V.12.

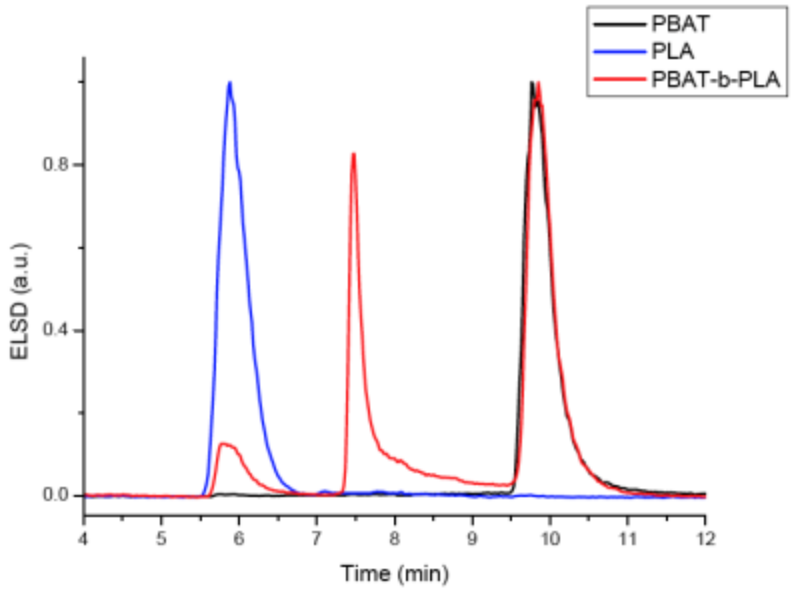

Fig. V.12 *LC-LCD chromatograms of PBAT (black line), PLA (red line) and PBAT-b-PLA (blue line). See experimental part for the chromatographic conditions.*

PLA is not retained by any of the barriers and it is eluted in SEC at about 6 min. PBAT is retained by Barrier 2 (B2) and it is accumulated against B2. It is eluted just after B2 as a narrow focused peak at about 10 mins. PBAT-*b*-PLA is not retained by B2 but it is retained by Barrier 1 (B1), which is more efficient than B2. PBAT-*b*-PLA is accumulated against B1 and it is eluted as a narrow focused peak at about 7.8 min.

This chromatogram confirmed the presence of block copolymer in the sample but also showed the presence of homopolymers of PLA and PBAT. The synthesis procedure allowed us to produce PBAT-*b*-PLA, but it would need to be optimized to decrease the amount of PBAT and PLA homopolymers.

It is interesting to point out the reproducibility and the robustness of LC-LCD. Indeed, by applying the same chromatographic conditions that Berek did, we obtained the same efficiency for the separation.

V.2.2.2 DSC

The PBAT-*b*-PLA block copolymer was also characterized by DSC. The result of the DSC test is shown in Fig. V.13. The T_g of PLA and PBAT, and T_f of PBAT can be found on the red curve representing the synthesized product, this phenomenon indicating the presence of PLA and PBAT blocks. However, a simple blend of PLA and PBAT

could give a similar result. Moreover, in the introduction of the protocol of synthesis, it is mentioned that water can also initiate the polymerization of lactide, thus separate PLA oligomers could be formed. As a result, the information supplied by DSC cannot indicate whether the PLA and PBAT blocks have been successfully branched together.

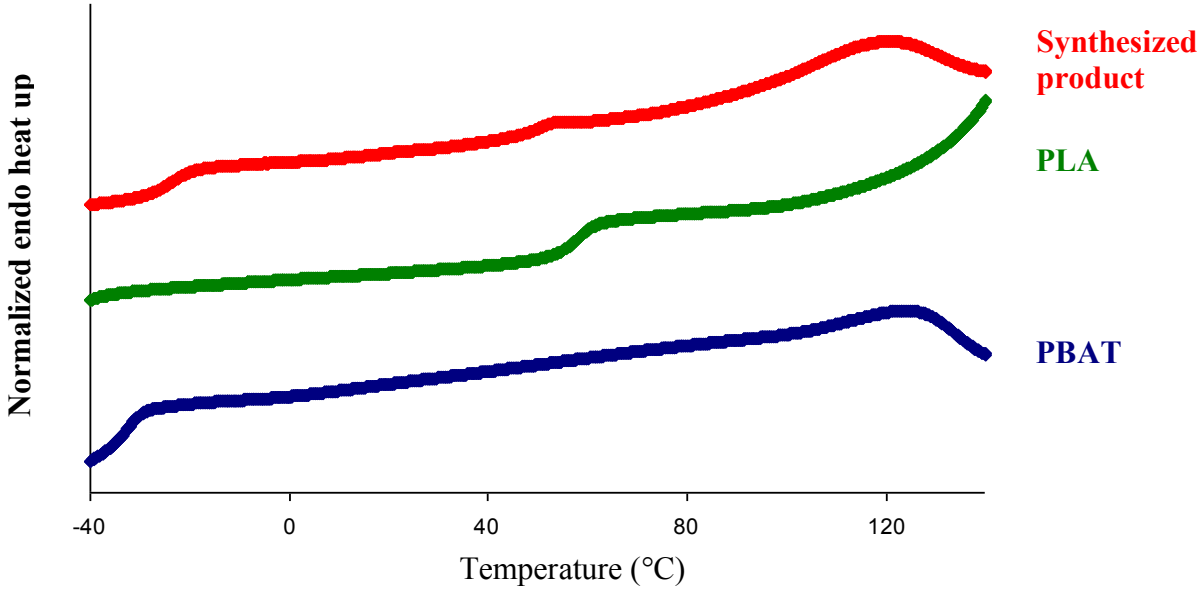

Fig. V.13 *Results of DSC test on the synthesized product, PLA and PBAT*

The synthesized PA-*b*-PBAT was also measured by DSC. The result did not show any similarity with the DSC curves of PBAT and PA respectively.

V.2.2.3 XRD

The result of X-ray diffraction is shown in Fig. V.14. From the illustration, the signal of the copolymer is almost identical to that of PBAT. This can be explained by the fact that PLA does not easily crystallise and that we may be able only to measure the response of the PBAT homopolymers.

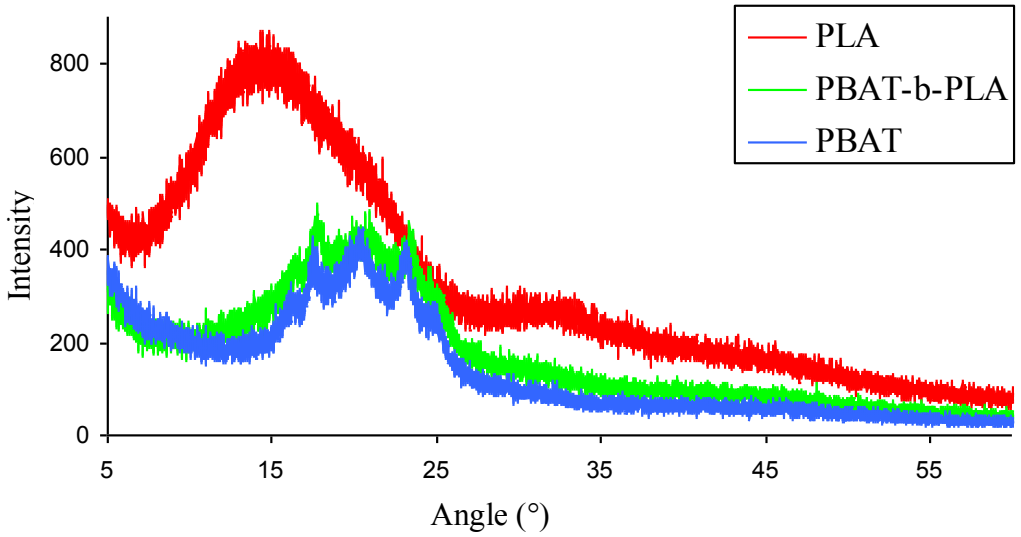

Fig. V.14 *XRD result of PLA, PBAT and copolymer PBAT-b-PLA*

V.2.2.4 Rheology

Except for the LC-CLD, none of the other characterizations above gave any proof that the PLA and PBAT blocks were linked together. In this part, rheological characterization was used to detect when PLA and PBAT blocks are successfully connected: Assuming that the PLA and PBAT blocks failed to connect during the synthesis, there should be a macrophase separation in the synthesized product. If this is the case, by testing the sample by rheology, a plateau should be observed on the G' curve due to the contribution of the interface according to the Palierne model in the case of a globular morphology [Palierne, 1990]. Based on this approach, rheological tests were conducted on two samples: one is the synthesized product, the other is a blend of the two isolated polymers with the same 40PLA/60PBAT composition. The reason to use a mass ratio of 40PLA/60PBAT is because according to the result of NMR, this is the composition of the synthesized material. The blend was prepared in the micro-compounder at 180 °C, 100 rpm for 12 min. The result is shown in Fig. V.15:

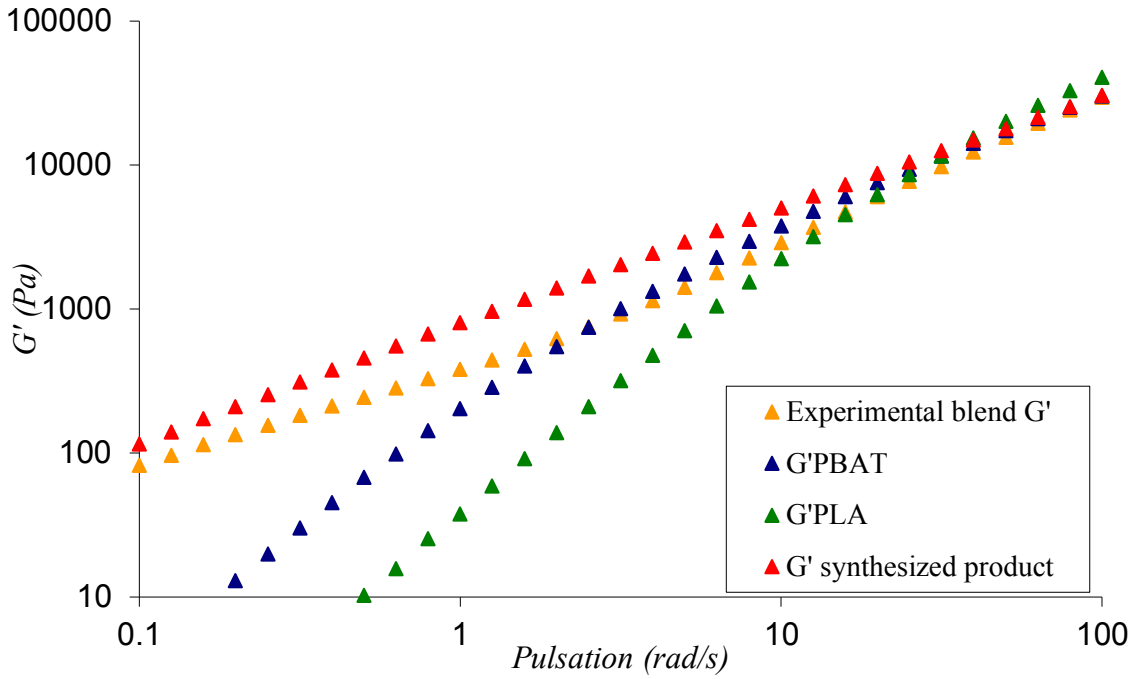

Fig. V.15 *G' curves of PLA, PBAT, the synthesized product, a blend 40PLA/60PBAT*

Fig. V.15 illustrates that there is a change of slope of G' curve of 40PLA/60PBAT blend at 1 rad/s. In the frequency range lower than 1 rad/s the curve shows a plateau, it is a clear signature of the elasticity linked to the interface between the two polymers. On the contrary, there is no sudden change of slope on curve of the synthesized product, it is an evidence that no macrophase separation exists in the synthesized product, confirming that it is most probably a block copolymer.

V.2.3 Verification of compatibilization effect of diblock copolymer

Several characterizations were conducted on the structure of the synthesized block copolymers, with a good indication that PBAT-*b*-PLA is indeed a block copolymer. What had to be checked next was that the prepared block copolymers are modifying the interfacial tension in such a way as to change the morphology obtained without compatibilizer towards the core–shell morphology shown in Fig. V.1. Therefore, in the following part the compatibilization effect of these block copolymers was investigated using different methods.

V.2.3.1 Influence on interfacial tension

The most direct indication that the synthesized products are compatibilizing agents is that they should decrease the interfacial tension [Macosko et al., 1996]. The drop retraction method was used again to measure the interfacial tension, but an alternative protocol was devised: a blend of copolymer and neat polymer was used as dispersed phase. For instance, to measure the interfacial tension between PLA and PBAT in the presence of block copolymer, a preblend of PLA and 5% block copolymer PBAT-*b*-PLA was used as dispersed phase in the drop retraction method. After this phase, the protocol was the same as the one presented in Chapter IV.

Based on retraction observations, it was found that the PBAT-*b*-PLA copolymer can reduce the interfacial tension between PLA and PBAT from 3±0.4 mN/m to 1.8±0.2 mN/m, while PA-*b*-PBAT had almost no influence on the interfacial tension between PA and PBAT: Before adding the copolymer, it was 3.3±0.4 mN/m, and after adding 5% PA-*b*-PBAT in the dispersed PBAT phase, it was 3.2±0.7 mN/m.

V.2.3.2 Influence on the size of inclusion in binary blends

Another way to verify the decrease of interfacial tension can be by observing the size of the particles in binary blends, since an effective compatibilizer should reduce the interfacial tension. Smaller interfacial tensions should lead to smaller particle sizes in binary blends under the condition that all the other parameters remain the same. From the comparison of the morphology in Fig. V.16, after the addition of 2% PBAT-*b*-PLA in the 80PLA/20PBAT blend, a clear decrease of particle size was observed. However, this is not the case for the PBAT/PA blend: the particle size in this binary blend in the presence of the PA-*b*-PBAT copolymer remains nearly the same as the one without copolymer. However, there was one indication that the PA-*b*-PBAT copolymer could behave as a compatibilizer. When PA/PBAT blends without compatibilizer were observed by SEM after cryofracture, the PA inclusions showed complete PA inclusions within the PBAT. After the addition of the copolymer, the PA particles break together with the PBAT matrix. This phenomenon can be seen as a proof of a better adhesion between the matrix and dispersed phase, due to a compatibilizing action of the block copolymer.

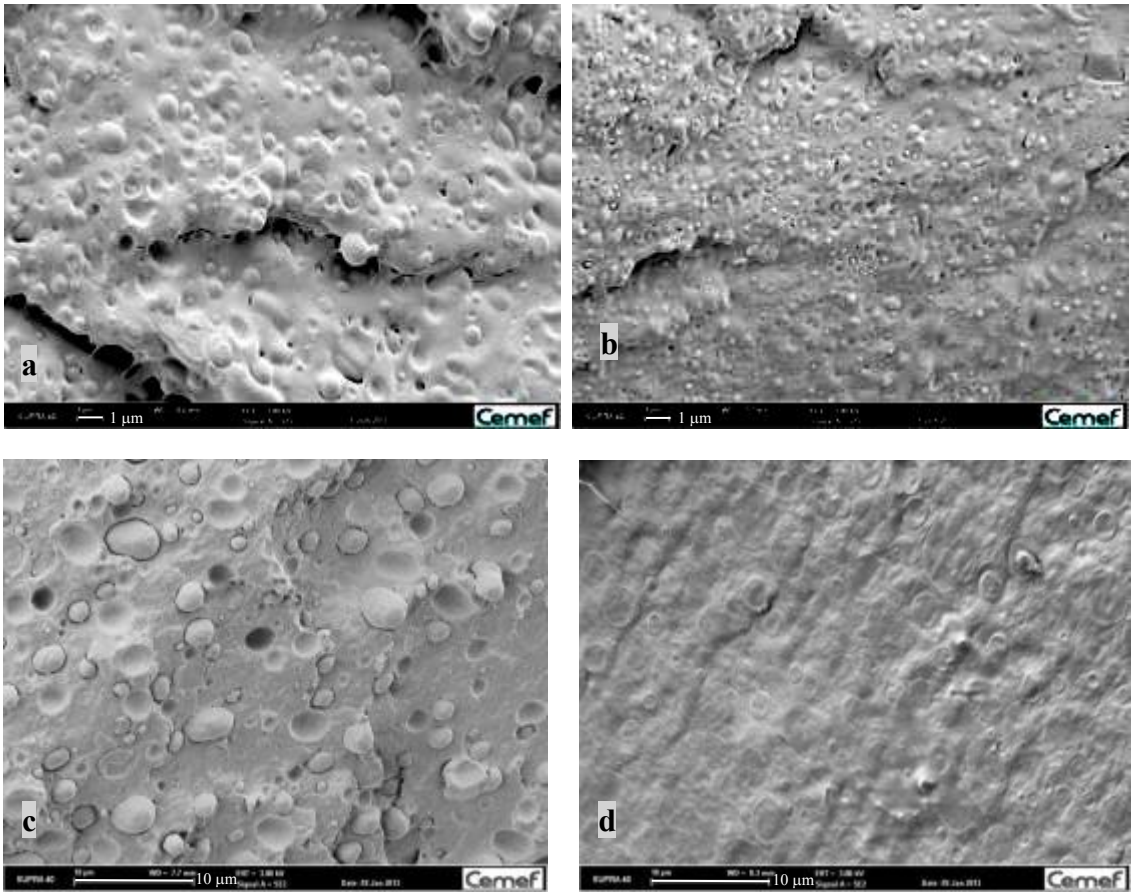

Fig. V.16 *Morphology of binary blends:* ***a****.80PLA/20PBAT;* ***b****.80PLA/18PBAT/2 PBAT-b-PLA;* ***c****.80PBAT/20PA;* ***d****.80PBAT/18PA/2PA-b-PBAT*

V.2.3.3 Influence on the hierarchy of ternary blend

After the modification of interfacial tension between the three polymers, a change in the morphology was expected: PA particles should move from the interface between PLA and PBAT inside the PBAT phase. SEM photos of the ternary blends 60PLA/27PBAT/13PA with respectively the copolymers PBAT-*b*-PLA and PA-*b*-PBAT are shown in Fig. V.17. The amount of block copolymer was added at an excess level to make sure that interfacial tension conditions were modified to influence the morphology. A larger quantity of PA-*b*-PBAT (6wt%) was added compared to PBAT-*b*-PLA (4 wt%) in order to compensate the less efficiency of the PA-*b*-PBAT copolymer following the results on binary blends. From the observation on SEM photos, clearly the PA phase is moving towards the aimed location after the addition of any of the two block copolymers.

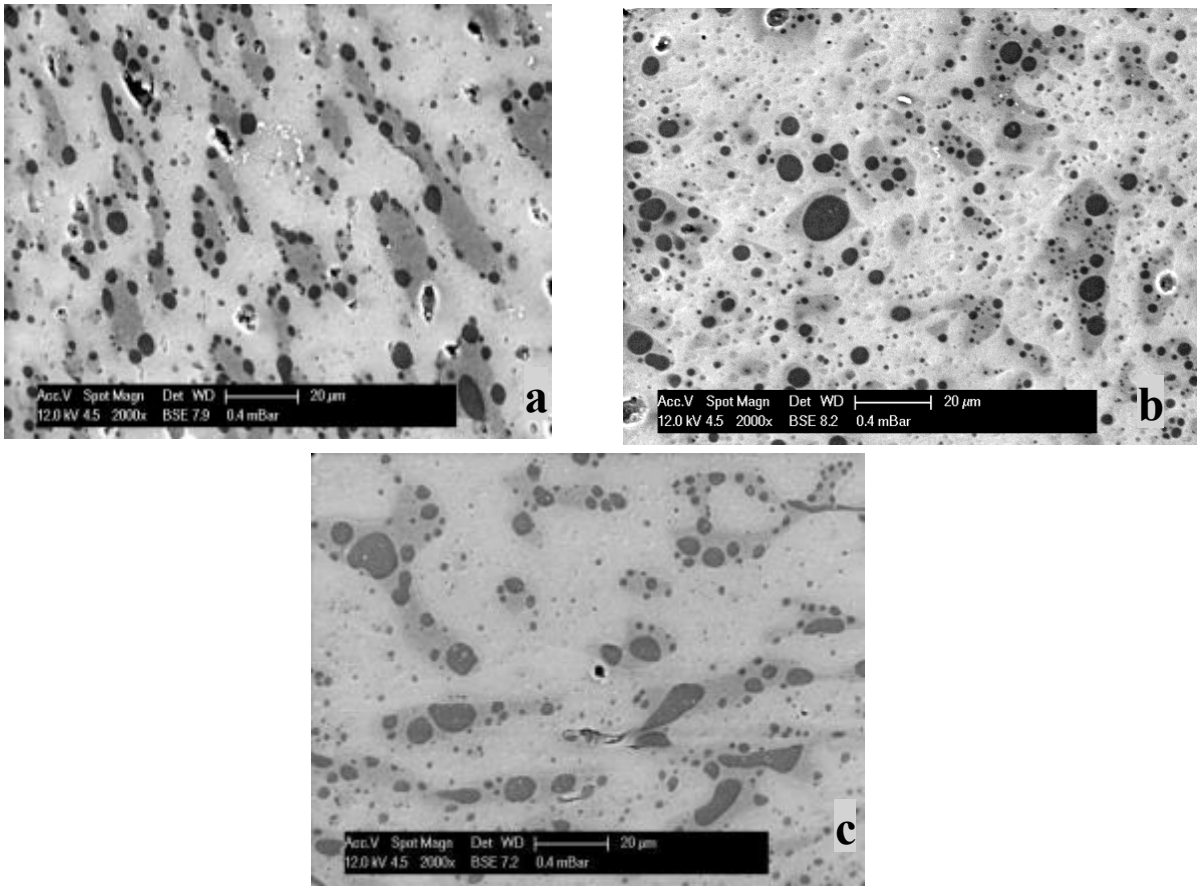

Fig. V.17 *Morphology of ternary blends:* ***a****. 60PLA/27PBAT/13PA;* ***b****. 60PLA/27PBAT/13PA + 4% PBAT-b-PLA;* ***c****. 60PLA/27PBAT/13PA + 6% PA-b-PBAT*

V.3 Compatibilized ternary blends

V.3.1 Strategy to better control the morphology of a ternary blend

Satisfying the spreading coefficient condition does not imply that a core–shell morphology is automatically achieved in the ternary blend. For instance, all the three morphologies in Fig. V.18 satisfy the interfacial condition of full encapsulation but not all of them correspond to the target morphologies.

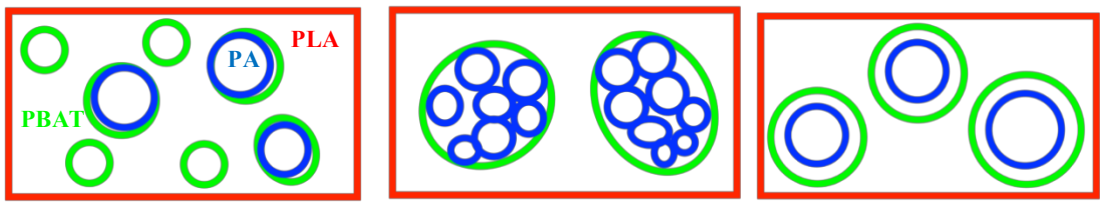

Fig. V.18 *Possible morphologies with full encapsulation*

Among the three schematic drawings, the first one is the least desirable as not all the PBAT droplets contain a PA core. To solve this problem and control the morphology of the ternary blend well, a blending strategy was set up by simplifying the ternary blend into two binary ones (Fig. V.19):

- First blend: To prepare a blend by dispersing PA droplets into the PBAT matrix;
- Second blend: To disperse the PA/PBAT as complex inclusions in the PLA matrix.

To avoid the first morphology in Fig. V.18, the size of the PA droplets in the PBAT needs to be smaller than that of the complex droplets in the second blend in Fig. V.19.

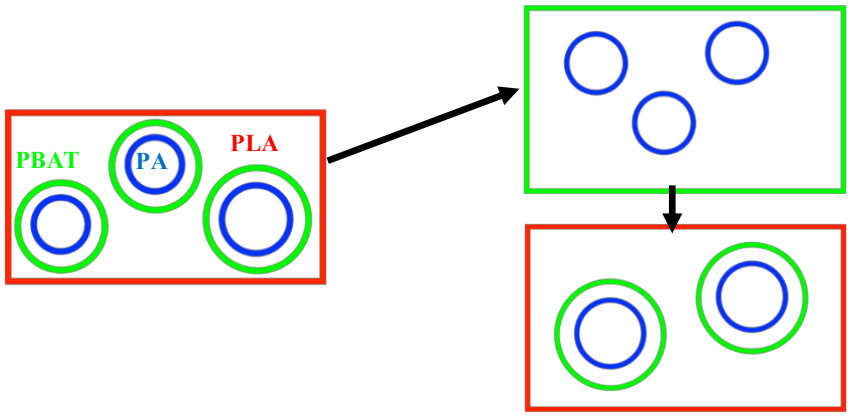

Fig. V.19 *First simplification of the ternary blend into two binary blends*

However, the size of the complex PA/PBAT droplets in the PLA matrix is quite complicated to predict. A further simplification was needed. Since the interface between the complex PBAT/PA droplets and the PLA matrix on the one hand (Fig. V.20.a) or between the PBAT and PLA (Fig. V.20.b) on the other is the same, the rheological behaviour of the PBAT alone and the PBAT/PA blend was compared in order to see if the complex PBAT/PA droplets could be simplified as PBAT droplets.

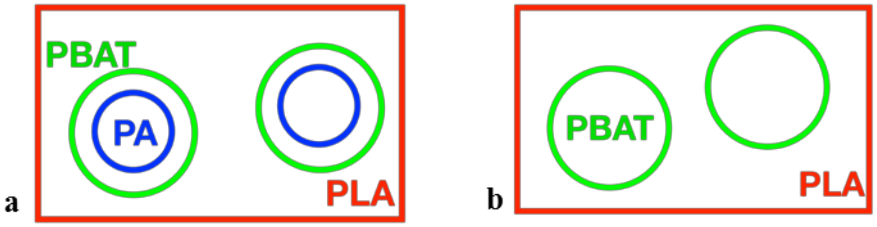

Fig. V.20 *Simplification of the ternary blend PLA/PBAT/PA (a.) into the binary blend PLA/PBAT (b.)*

Fig. V.21 shows the comparison between the viscosity curves of the neat PBAT and the 70PBAT/30PA blend, where PA droplets are dispersed in the PBAT matrix. Obviously, the viscosity curves are quite close to each other, even in the high frequency part where the largest difference is detected. The difference is less than 15%. Therefore the complex PBAT/PA droplets can roughly be regarded as neat PBAT droplets as they have the same interfacial property as PLA and similar rheological properties.

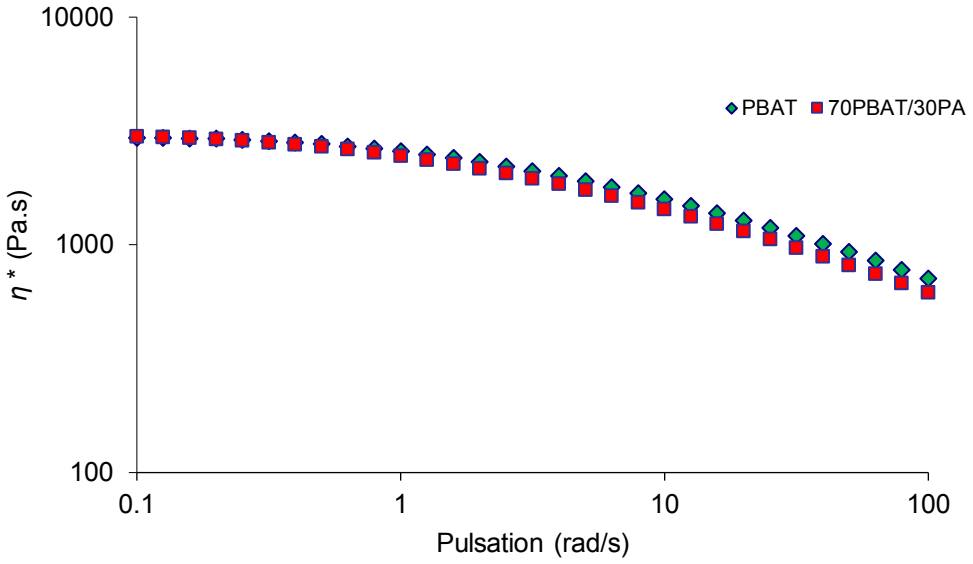

Fig. V.21 *Comparison of viscosity curves of PBAT and binary blend 70PBAT/30PA*

Now the task is to find the mixing conditions in order to prepare two binary blends: PBAT droplets dispersed in PLA and PA droplets dispersed in PBAT, with the aim of having PA droplets with a size smaller than that of the PBAT droplets, as shown in Fig. V.22.

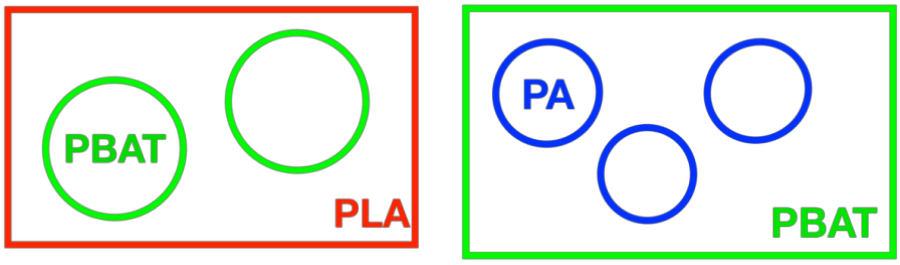

Fig. V.22 *Simplification into two binary blends*

To minimize the particle size of PA in PBAT, we considered Serpe's equation (Eq. 8, recalled here). This empirical equation gives an estimation of the particle size in binary blends:

$$R = \frac{2\gamma_{AB}(\eta_d/\eta_m)^{\pm 0.84}}{\dot{\gamma}\eta_m(1-(4\phi_d\phi_m)^{0.8}}$$

The viscosity ratio exponent is positive if $p > 1$, and negative if $p < 1$.

According to this equation, several options are available to obtain a small particle size:

1. To use a high mixing speed during blending in order to apply a high shear rate $\dot{\gamma}$ and increase the applied shear stress $\dot{\gamma}\eta_m$;
2. To reduce the concentration of the dispersed phase;
3. To have a viscosity ratio between the dispersed phase and the matrix close to 1.

The first two options are very easy to realize. For the last one, the viscosity ratio can be influenced by changing the temperature as shown in Fig. V.23:

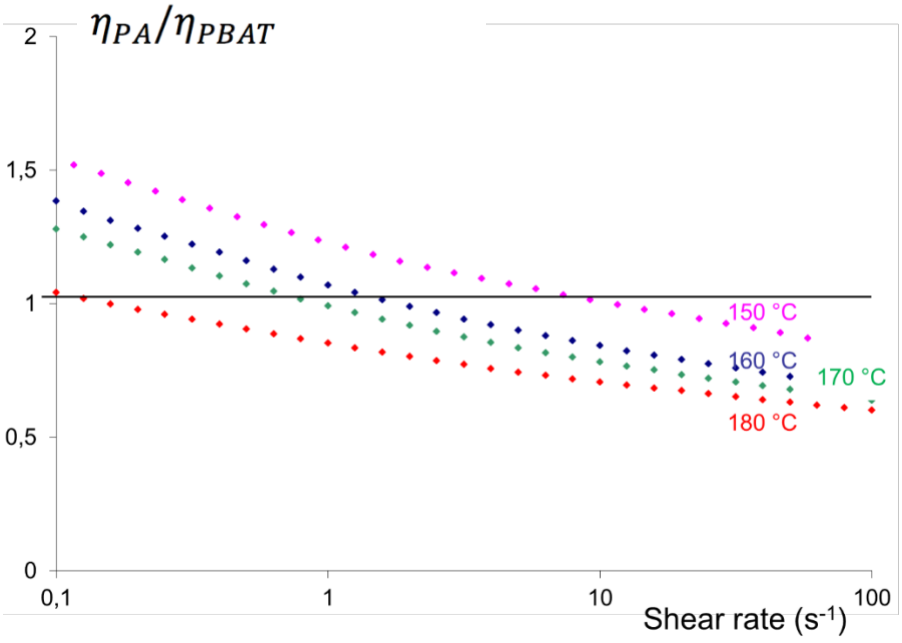

Fig. V.23 *Viscosity ratio of PA/PBAT at different temperatures*

From this figure, a high shear rate and a low temperature give a viscosity ratio between PBAT and PLA close to unity which is favourable to decrease the droplet size. Moreover, a low temperature will also lead to a higher viscosity of the matrix and thus shear stress which will also help to reduce the droplet size.

Since we are looking for larger PBAT droplets in the PLA matrix compared to PA droplets, the choice for the blending condition for the PLA/PBAT blend is in opposition: a high temperature and a low shear rate.

The following schema summarizes the strategy to obtain the core–shell morphology ternary blend. The whole strategy can be divided into three steps (Fig. V.24):

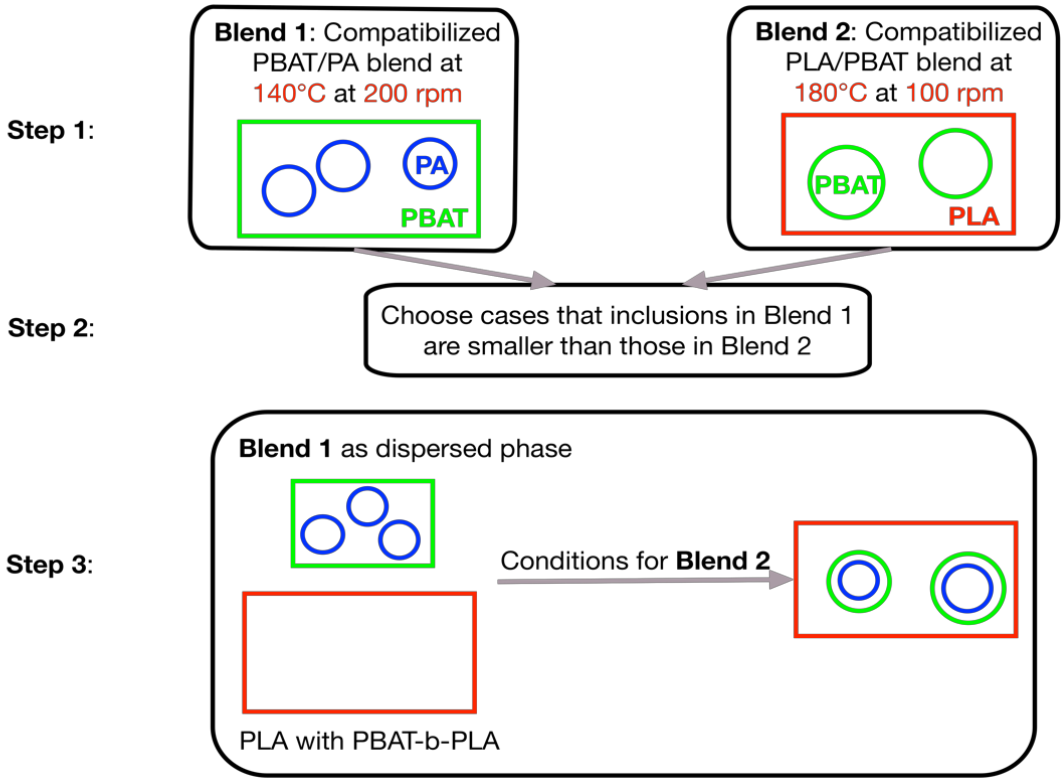

Fig. V.24 *Strategy to prepare the ternary blend PLA/PBAT/PA with the core–shell morphology*

In the first step, two binary compatibilized blends are prepared: Blend 1, PA droplets in PBAT matrix at low temperature (140 °C) and high shear rate (200 rpm in internal mixer for 12 min) as the purpose here is to obtain a small droplet size; Blend 2, with PBAT droplets dispersed in PLA matrix (180 °C, 100 rpm in internal mixer for 12 min). Both blends were prepared with various concentrations of dispersed phase.

In the second step, the droplet sizes of Blends 1 and 2 are compared and the cases where the particle size in Blend 1 is smaller than in Blend 2 are selected.

In the third step, the selected Blends 1 are used as dispersed phase in the neat PLA as matrix, while using the condition of Blend 2 to prepare the ternary blends.

V.3.2 Morphology of compatibilized ternary blends

Based on this strategy, 4 compatibilized binary blends were prepared in the first step. The compositions of the compatibilized binary blends are shown in Table V.1. For the sake of simplicity, the blend 89PBAT/10PA/1PA-*b*-PBAT is noted as compatibilized 90PBAT/10PLA blend. The weight fraction of compatibilizer was chosen as 10 wt% of the minor phase.

Composition	Notation
89PBAT/10PA/1PA-*b*-PBAT	Compatibilized 90PBAT/10PA
78PBAT/20PA/2PA-*b*-PBAT	Compatibilized 80PBAT/20PA
78PLA/20PBAT/2PLA-*b*-PBAT	Compatibilized 80PLA/20PBAT
68PLA/30PBAT/3PLA-*b*-PBAT	Compatibilized 70PLA/30PBAT

Table V.1 *Compositions and notations of the compatibilized binary blends*

The morphologies of the compatibilized binary blends are depicted in Fig. V.25.

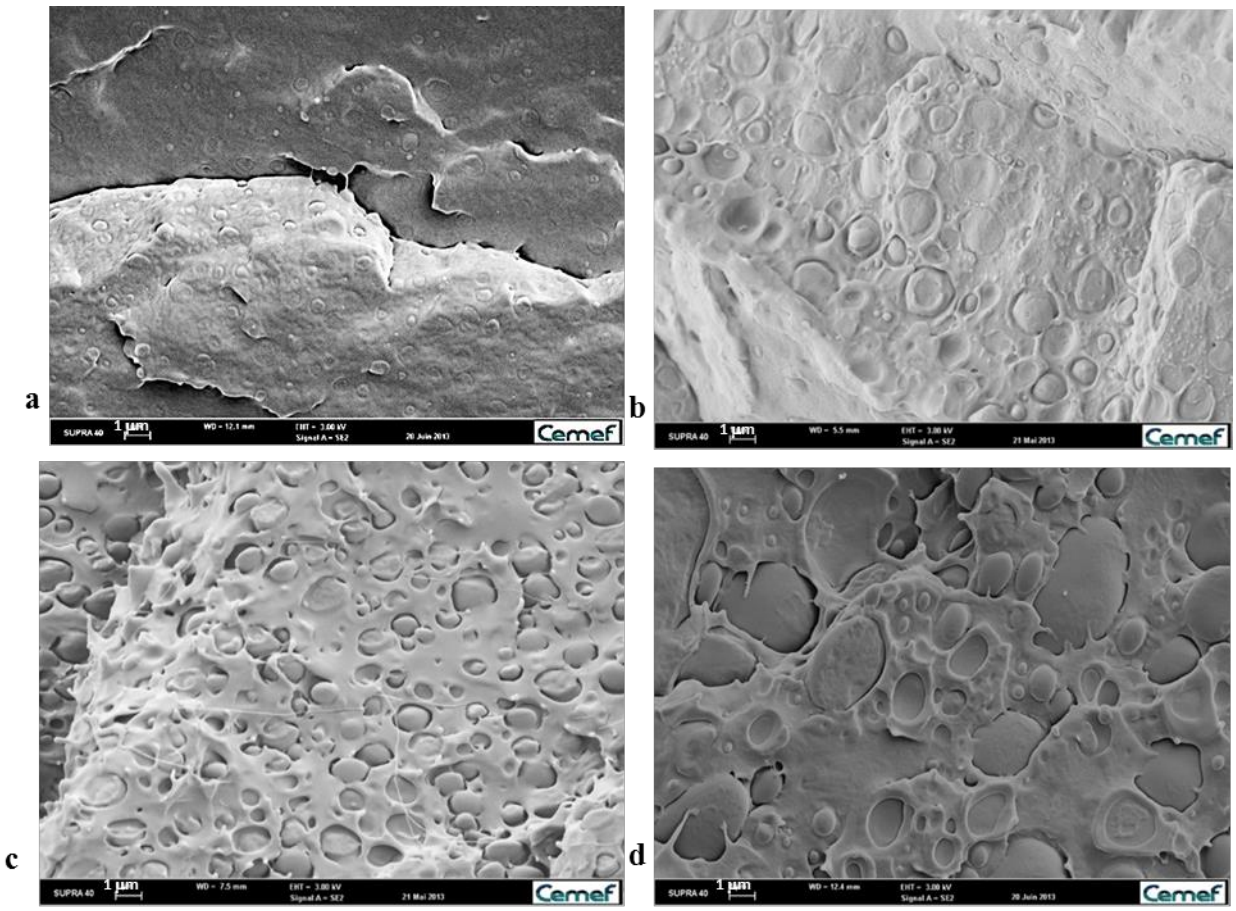

Fig. V.25 *Morphologies of compatibilized PBAT/PA blends:*
a*. 90PBAT/10PA;* ***b****. 80PBAT/20PA/;*
and compatibilized PLA/PBAT blends:
c*. 80PLA/20PBAT;* ***d****. 70PLA/30PBAT*

The droplet size of the compatibilized 70PLA/30PBAT blend (Fig. V.25.d) is obviously larger than those of both the compatibilized 80PBAT/20PA and 90PBAT/10PA blends (Fig. V.25.a and b). Hence using 30 wt% of (80PBAT/20PA or 90PBAT/10PA) as inclusions in 70 wt% PLA as matrix should lead to a core–shell morphology. Since the compatibilized 80PLA/20PBAT blend shows a similar droplet size to that of the compatibilized 80PBAT/20PA blend, it is likely that using 80 wt% of PLA as matrix and 20 wt% of compatibilized 80PBAT/20PA blend as droplets should not lead to a core–shell morphology. To verify this assumption, four ternary blends (compositions presented in Table V.2) were prepared (internal mixer, 180 °C, 100 rpm for 12 min) according to the strategy presented in Fig. V.24

Composition	Notation
78PLA/20(89PBAT/10PA /1PA-*b*-PBAT)/2PBAT-*b*-PLA	Compatibilized 80PLA/20(90PBAT/10PA)
78PLA/20(78PBAT/20PA /2PA-*b*-PBAT)/2PBAT-*b*-PLA	Compatibilized 80PLA/20(80PBAT/20PA)
67PLA/30(89PBAT/10PA /1PA-*b*-PBAT)/3PBAT-*b*-PLA	Compatibilized 70PLA/30(90PBAT/10PA)
67PLA/30(78PBAT/20PA /2PA-*b*-PBAT)/3PBAT-*b*-PLA	Compatibilized 70PLA/30(80PBAT/20PA)

Table V.2 *Compositions and notations of the compatibilized ternary blends*

The morphologies are depicted in Fig. V.26.

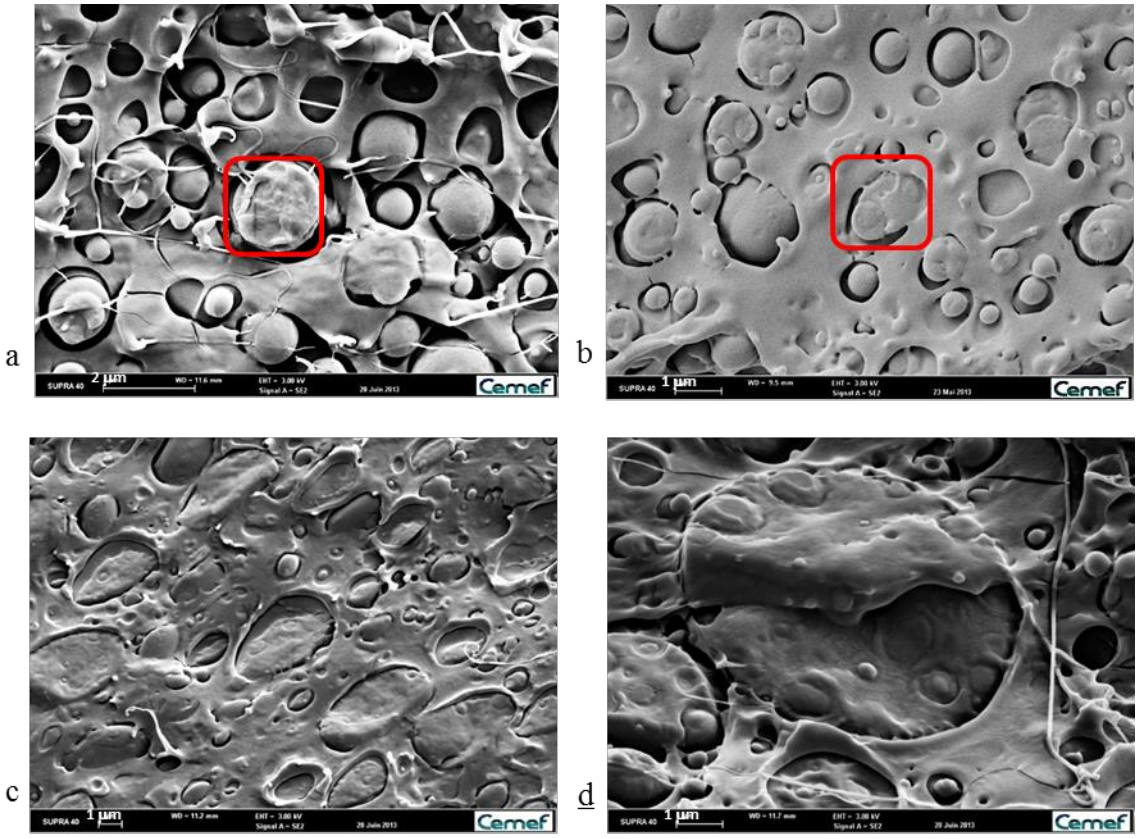

Fig. V.26 *Morphologies of the compatibilized ternary blends:*
a*. Compatibilized 80PLA/20(90PBAT/10PA) blend;*
b*. Compatibilized 80PLA/20(80PBAT/20PA) blend;*
c*. Compatibilized 70PLA/30(90PBAT/10PA) blend;*
d*. Compatibilized 70PLA/30(80PBAT/20PA) blend*

When PLA occupies 80% of the total mass in the blend, the PA phase appears to be not fully encapsulated by the PBAT phase (Fig. V.26.a and b), as marked by the red square in the SEM photos. The partial encapsulation was expected to be due to the similar size of the droplets obtained in the binary blends PBAT/PA and 80PLA/20PBAT (see comments on Fig. V.25.a, b and c). This partially encapsulated morphology may also have an effect on the mechanical performances of the blend. The PA phase is partially in contact with the PLA matrix possibly due to a lack of compatibilizer, the affinity between these two phases is very poor (high interfacial tension), and big gaps can be observed between the complex droplets and the matrix. This could lead to the deterioration of the mechanical performances.

In Fig. V.26.c and d where the PLA matrix occupies 70% of the total mass, although some PA drops are located at the border of the PBAT phase, most of them are fully encapsulated in PBAT. A core–shell morphology is observed in these two illustrations. This is because the particle sizes in Fig. V.25.a, b and d fully comply with the strategy defined in Fig. V.24. Also, as only a small fraction of the surface of PA droplets is in contact with PLA, the compatibilization between the matrix and complex inclusions is ensured. No large gap between PLA and PBAT phases is observed in Fig. V.26.c and d.

In all the blends, the sizes of the PA sub-inclusions are less than one micron. Although there is a large distribution of drop sizes of PBAT, they are all on the scale of a few microns. This order of magnitude of drop size ought to be beneficial for the impact performances. In the next step, the mechanical evaluation was carried out.

V.3.3 Mechanical properties of ternary and binary blends

As the aimed at core–shell morphology of the ternary blend has been achieved, the next interesting and logical step of the study was to investigate whether this morphology could bring further mechanical property improvement over traditional binary blends.

As the composition of ternary blends is quite complicated, the following coding system was used to refer to the different samples (Table V.3).

	Composition	First notation	Short coding
Binary blends	78PLA/20PBAT /2PBAT-*b*-PLA	Compatibilized 80PLA/20PBAT	82
	67PLA/30PBAT /3PBAT-*b*-PLA	Compatibilized 70PLA/30PBAT	73
Ternary blends	78PLA/2PBAT-*b*-PLA /20(89PBAT/10PA /1PA-*b*-PBAT)	Compatibilized 80PLA/20(90PBAT/10PA)	8291
	78PLA/2PBAT-*b*-PLA /20(78PBAT/20PA /2PA-*b*-PBAT)	Compatibilized 80PLA/20(80PBAT/20PA)	8282
	67PLA/3PBAT-*b*-PLA /30(89PBAT/10PA /1PA-*b*-PBAT)	Compatibilized 70PLA/30(90PBAT/10PA)	7391
	67PLA/3PBAT-*b*-PLA /30(78PBAT/20PA /2PA-*b*-PBAT)	Compatibilized 70PLA/30(80PBAT/20PA)	7382

Table. V.3 *Sample coding of binary and ternary blends*

The samples for mechanical characterization can be divided into 3 categories:

1. Pure PLA as reference;
2. Binary blends PLA/PBAT;
3. Ternary blend PLA/PBAT/PA to compare with binary blend samples**.**

The mechanical properties of the blends were investigated in tensile and Charpy tests.

V.3.3.1 Tensile test

Up to four tensile tests were performed for each formulation. An example of the stress–strain curve for each neat polymer (PLA, PBAT and PA) is shown in Fig. V.27 to explain how the tensile results were interpreted.

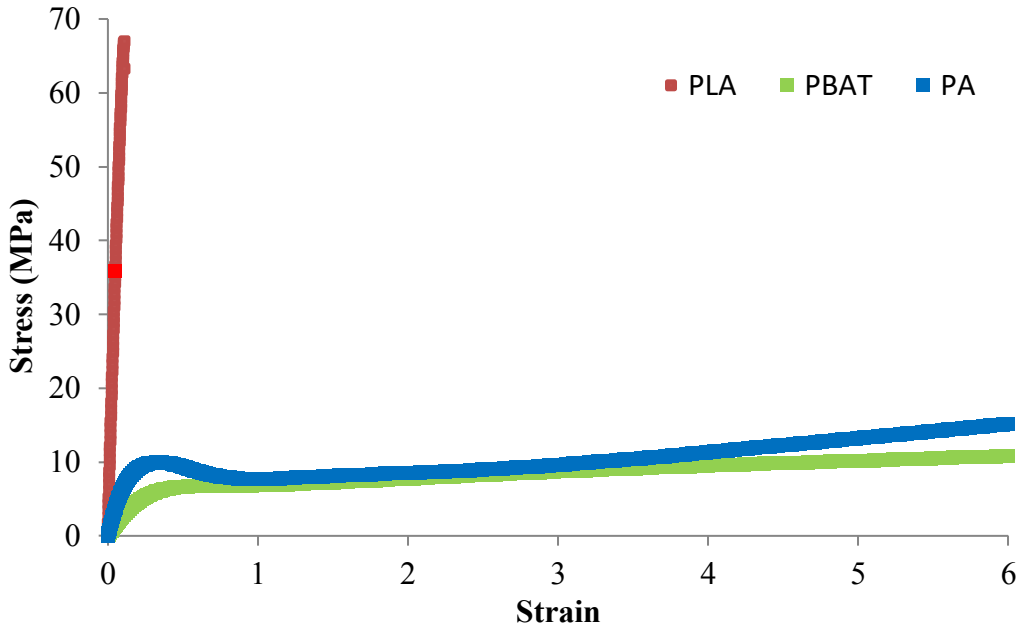

Fig. V.27 *Stress–strain curve for PLA, PBAT and PA*

From Fig. V.27, it is clear that PBAT and PA have more tenacity than PLA, as both PA and PBAT can be stretched to more than 600% of their original length without breaking. To gain more insight from the tensile measurements, three mechanical parameters were characterized:

1. Young's modulus: This parameter is determined using the slope of the first five points in the stress–strain curve to ensure the deformation is in the elastic region;
2. Yield strength: During the course of a tensile test, the nature of deformation will change from elastic to plastic. The starting sign of plastic deformation is the change of slope in a stress–strain curve. The stress at this point is the yield strength;
3. Deformation at break: The maximum strain before the sample breaks.

The results of Young's modulus are presented via the mean value and an error bar linked to the different measurements. The results are reported in Fig. V.28. The reproducibility of these measurements was good. Compared to pure PLA, binary blends showed a lower Young's modulus. The addition of a third component (PA) also led to a slight decrease.

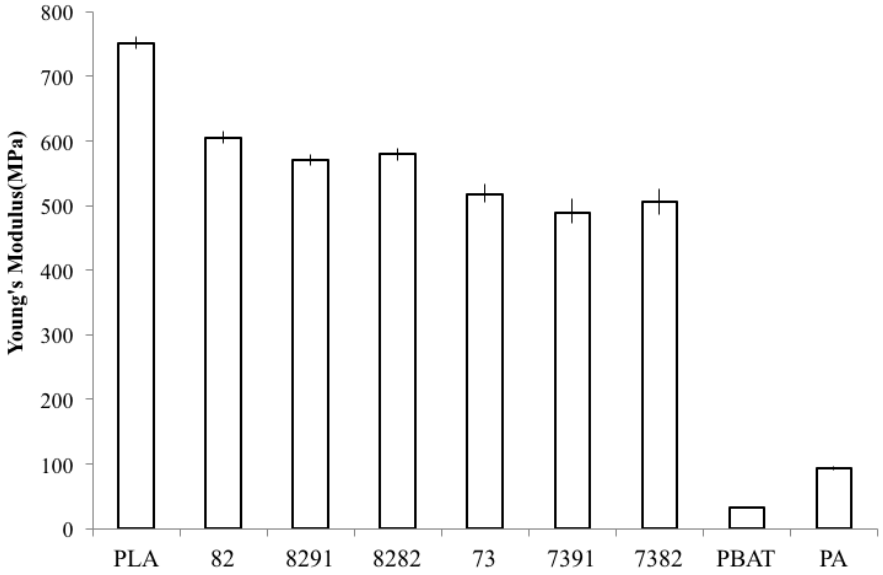

Fig. V.28 *Young's modulus of neat polymers, binary and ternary blends*

A simple mixing law (only considering the contribution of each component weighted by its volume fraction) was considered in order to estimate the modulus of a polymer blend [Voigt, 1889]. It can be expressed as:

$$G_{A/B/C} = \phi_A G_A + \phi_B G_B + \phi_C G_C$$

where G stands for Young's modulus and ϕ is the volume fraction of each component.

This equation allows us to estimate the modulus of ternary and binary blends by calculation based on the modulus of each component. The comparison between the experimental data and the calculated modulus is shown below (Table V.4).

Sample	Experimental Young's modulus (MPa)	Calculated modulus using the blending law (MPa)
82	605.2	607.4
8291	571	608.6
8282	579.5	609.8
73	517.8	535.6
7391	489	537.4
7382	506.5	539.2

Table V.4 *Comparison between experimental data of Young's modulus and calculated values using the simple mixing law*

The comparison shows that the Young's modulus measured on binary blends is in line with the estimations via the simple mixing law. However, there is a clear difference between the measured and calculated modulus in the case of ternary blends. According to the mixing law, the Young's modulus of ternary blends should be slightly larger than those of binary blends. The measurements show the contrary, with lower Young's modulus for ternary blends relative to binary blends. Based on the good estimation of the model in the case of binary blends, and also on the good efficiency of the PBAT-*b*-PLA block copolymer, the lower Young's modulus for the ternary blends could be an indication of a weaker interface between PA and PBAT.

The results of yield strength are shown in Fig. V.30. Again, little deviation is observed with all samples, which confirms again the reproducibility of the test. It is very comparable with the results for Young's modulus: PLA shows the highest yield strength of all the samples, binary blends show lower values, yet ternary blends with PA depict even lower values than binary blends.

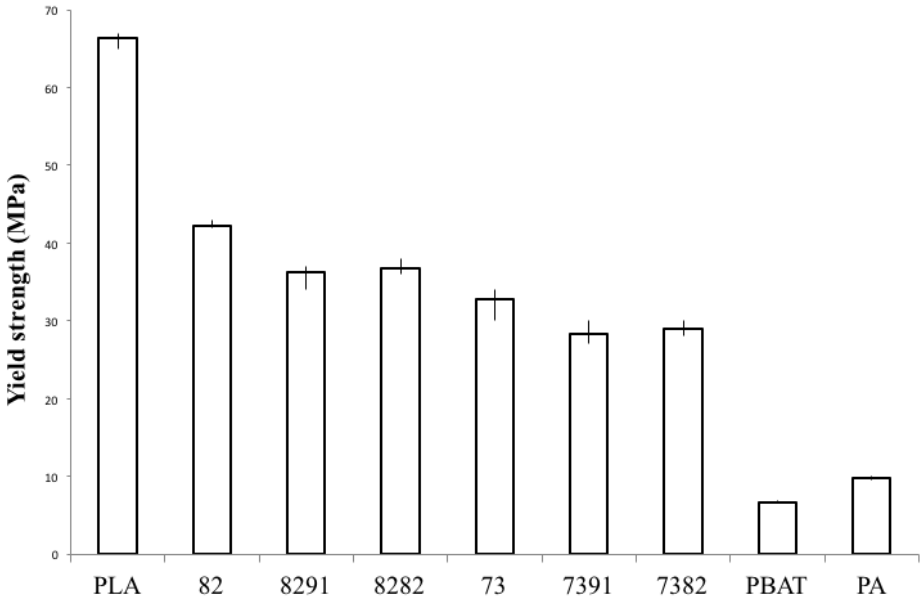

Fig. V.29 *Yield strength of neat polymers, binary and ternary blends*

The deformation at break of PLA and all the blends is shown in Fig. V.30. PA and PBAT are not plotted in this diagram as their deformation at break is higher than 6. In Fig. V.30 significant error bars are present for all the blends. Considering the reproducibility confirmed by the Young's modulus and yield strength, the reason for the instability of

these results is not the poor sample quality. The reason actually lies in the necking observed with all the blend samples during the tensile test, as the initiation of necking takes place at heterogeneous parts in the sample, such as small flaws or local variations of dimensions. These heterogeneous parts only need to be at infinitesimal scale to provoke a fluctuation in stress and strain to initiate the necking [Considère, 1885]. Therefore, even for two samples with the same composition, down to microscopic level they cannot be 100% identical and so the initiation and the development of necking will be influenced by this factor, leading to the fact that the failure strain of necking is also different.

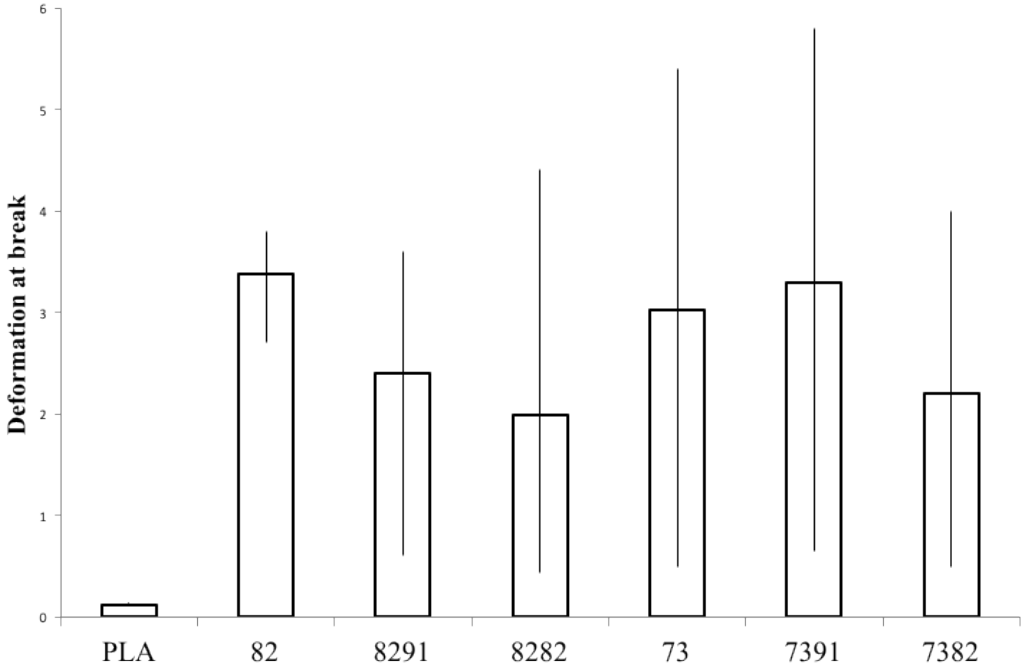

Fig. V.30 *Deformation at break of neat polymers, binary and ternary blends*

V.3.3.2 Charpy test – Impact resistance

In the case of HIPS, the core shell morphology improved tremendously the impact performance of PS. This is not the case for the present PLA/PBAT/PA system. As seen in Fig. V.31, the addition of the third component PA brings a deterioration of the impact performance compared to the binary blends. Once again, the reason could be the poor interface between the PA phase and the other phases.

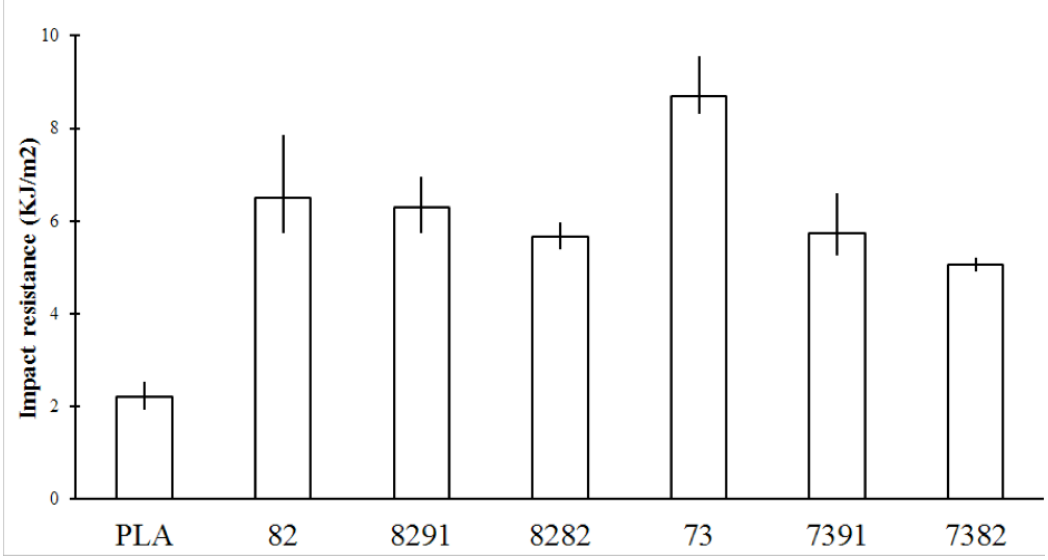

Fig. V.31 *Impact performance of PLA, binary and ternary blends*

Different reasons can be seen for the weaker interface when adding the third phase. One reason could be that the length of the blocks of the copolymer is not large enough to resist the stress transmission. This is surely the case for the block copolymer PA-*b*-PBAT used in this study. Attempts were made to synthesize longer blocks, but the synthesis resulted in non-fusible copolymers. A second reason could be linked to the morphology obtained. It is clear from Fig. V.26.d that some PA droplets are fully encapsulated, whereas some others are located at the PLA/PBAT interface, leading to large gaps with the PLA phase. This could be a sign that no PBAT-*b*-PA copolymer is present at this interface or that the PA particle size is not small enough. The reason could be that the quantity of this copolymer was not large enough. There was no time within the PhD thesis to optimize the amount of block copolymer.

V.3.3.3 Understanding the impact performance – deformation analysis during tensile test

Compared to traditional rubber reinforcement, the advantage of the core–shell morphology in HIPS is that it creates a multi-cavitation process instead of a single cavitation during the impact (Fig. II.2). The volume of cavitation generated during a tensile test in the case of a single droplet (Fig. II.2.a) or of a core–shell inclusion (Fig. II. 2.b) should be very different. In order to determine the volume variation of the blends under tension, a visual analysis system (VIC-3D) was combined with a tensile test to follow the local horizontal and vertical deformation of the sample during the tensile test. Fig. V.33 shows six pictures showing the vertical deformation during the tensile test. When the colour becomes warmer it indicates that a larger deformation is happening at

this location. The deformation concentration is obviously in the central part of the sample where the dimension is narrower (Fig. V.33.f).

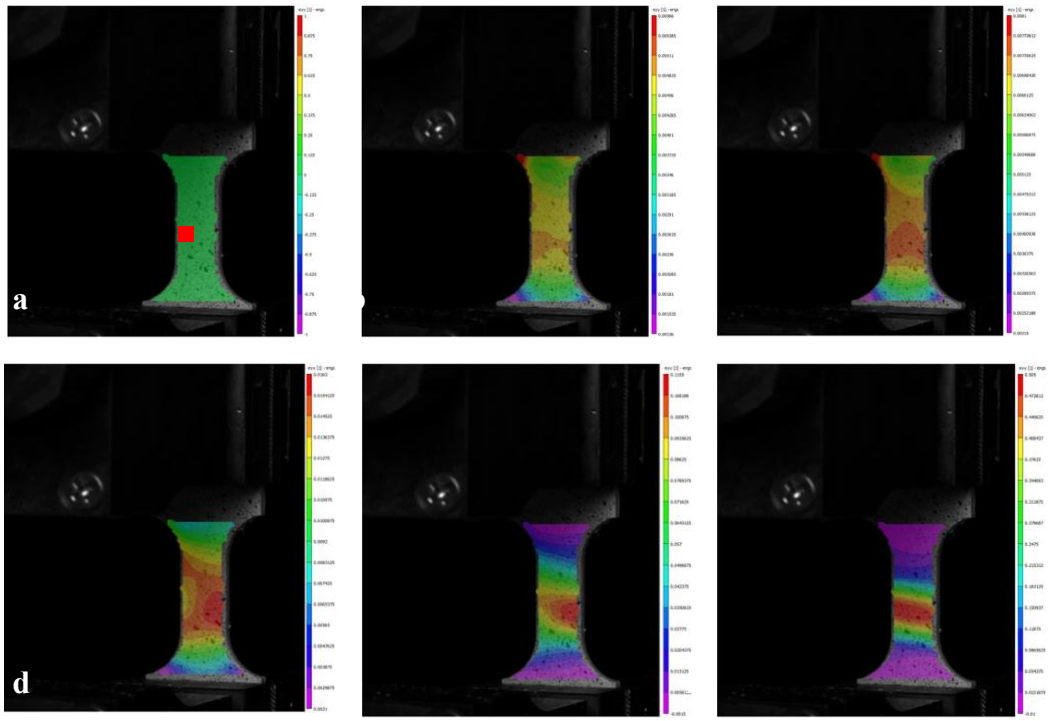

Fig. V.33 *Evolution of the iso-deformation along the tensile test using VIC3D*

To identify the volume change, a block area was selected, shown as the red square in Fig. V.33.a. The information on vertical and horizontal deformation is extracted from the deformation of this small block. A hypothesis of isotropic deformation is used for the third direction.

Based on the deformation and the hypothesis of isotropic deformation in the other direction, the volume variation along the tensile test could be determined. This analysis was restricted to deformation within the window of analysis. Fig. V.33 shows the volume variation up to 10% of strain for the different samples. Since these measurements are quite sensitive, three curves are presented for each sample:

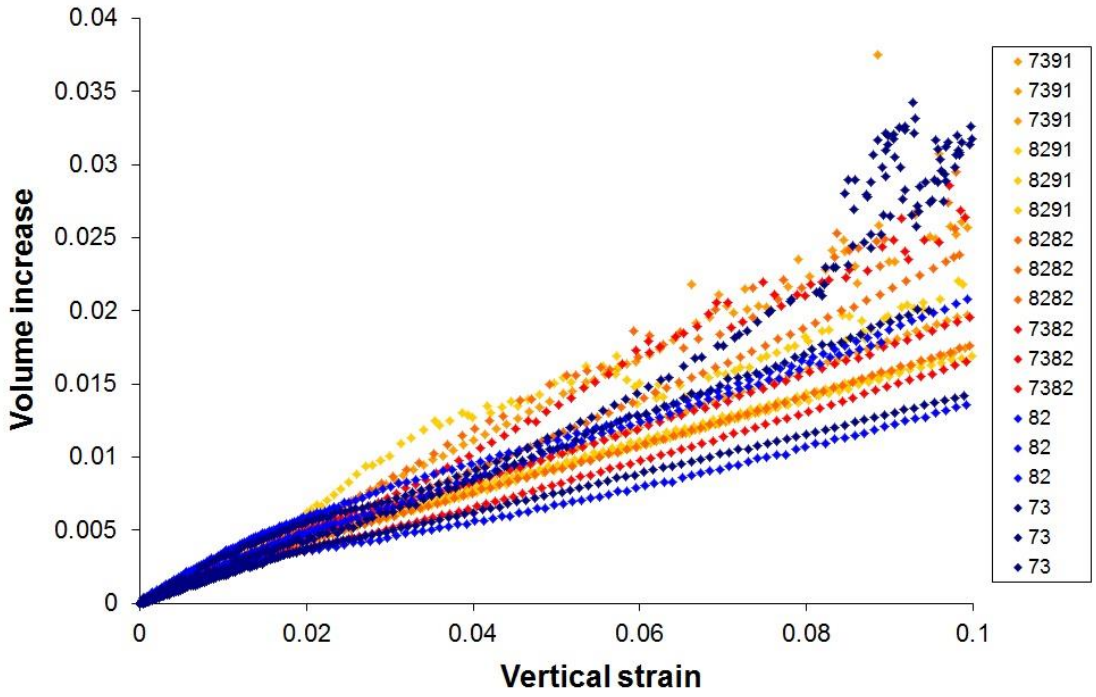

Fig. V.33 *Relationship between volume increase and vertical strain*

We can see that there is a large variation between measurements on the same blend. The reproducibility was not optimal.

The general conclusion from these measurements is that the cavitation in ternary blends developed in almost the same manner as in binary blends. So the multi-cavitation mechanism probably did not take place in the present case, by contrast with HIPS.

Different reasons (linked to defects in the morphology) could explain the large variations between different measurements for the same blend. However, the main reason for the multi-cavitation process not to happen may be linked to the modulus level of PA relative to that of the other polymers. To achieve cavitation as such, the stiffness of the core phase should be large enough to avoid any deformation during the impact. However, in the case of the PLA/PBAT/PA system, the modulus of PA is 100 MPa, which is very comparable with the modulus of PBAT which is 30 MPa. We assume that during the impact, the PA phase deforms together with PBAT and no multi-cavitation occurs.

V.3.3.4 Fracture surfaces

From the results of the impact and tensile tests, it was clear that PLA breaks in a fragile way, while the blends with PBAT are ductile. To investigate the process of breakage further, SEM observations were performed of the fracture surface after impact for the neat PLA, the compatibilized 70PLA/30PBAT binary blend, and the compatibilized 70PLA/20PBAT/10PA ternary blend.

PLA fracture showed different topographies on the fracture surface (Fig. V.34). In zone i just behind the notch, the surface was created by pure stretching and a wave pattern is observed together with a lot of fibrils along each wavy line. This wave pattern is a typical sign of a glassy polymer fracture, as it can be found with PMMA [Kusy and Turner, 1977]. However, in zones ii and iii where the fracture surface was compressed before stretching, fibrils could no longer be observed.

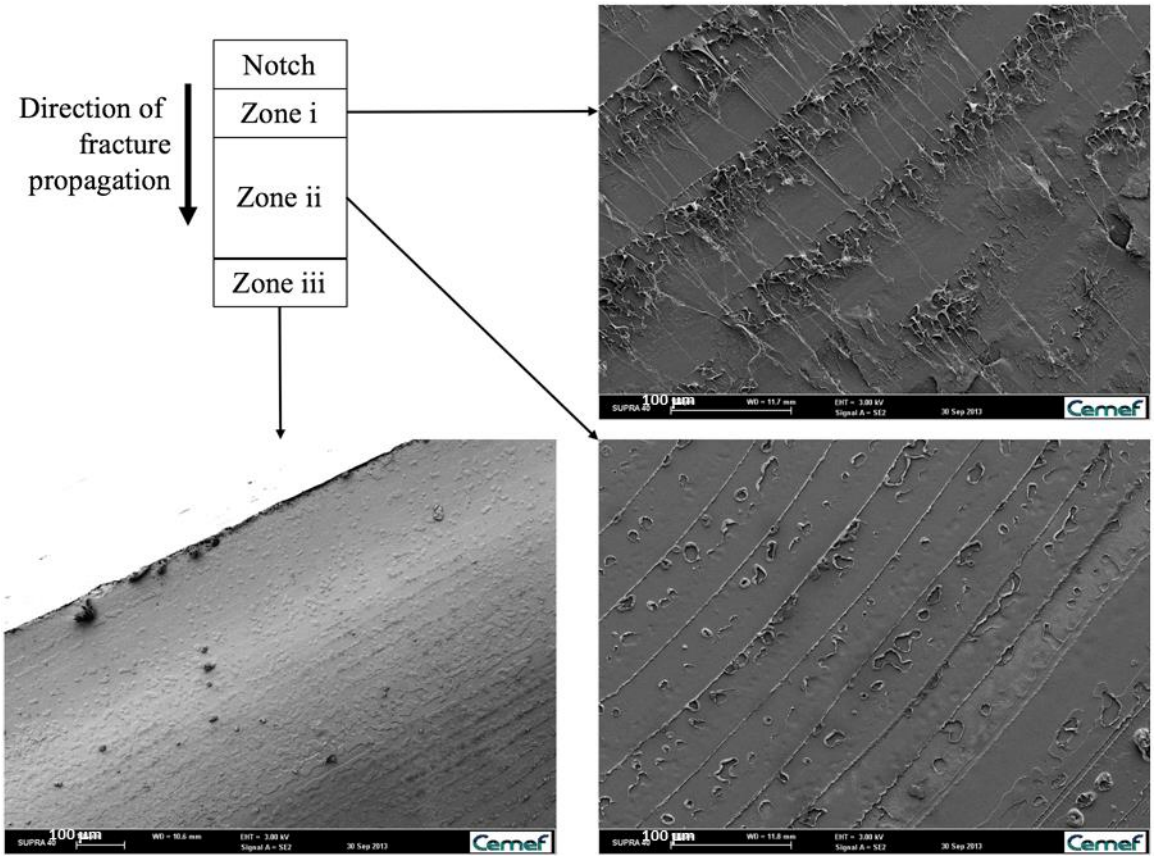

Fig. V.34 *Fracture topography of PLA after impact test*

Regarding the topography of the fracture surface of the compatibilized binary blend, most of the PBAT particles remained in a spherical shape (Fig. V.35.a). In the ternary blend (Fig. V.35.b), most of these particles were broken. This indicates the different properties of the interface quality. Also, no wavy pattern is observed in this case. Hence, both the compatibilized binary and ternary blends broke in a ductile way (as evidenced in the tensile and impact performance results).

a  b 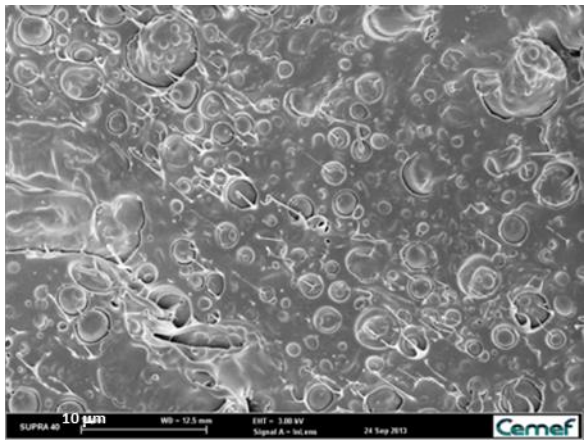

Fig. V.35 *Fracture topographies of the compatibilized binary blend 73 (**a**) and of the compatibilized of ternary blend 7391 (**b**)*

V.4 Conclusion

In this chapter, we introduced the way to synthesize two specific block copolymers designed to be localized at the PA/PBAT and PBAT/PLA interfaces. If the synthesis of the PBAT-*b*-PLA copolymer was straightforward, the one of the PA-*b*-PBAT was more delicate. The analysis of the PBAT-*b*-PLA showed that it was really a block copylmer. It was not possible to confirm the block copolymer structure in the case of the PA-*b*-PBAT. The compatibilization effect of the copolymers was verified. The PA-*b*-PBAT appeared to be less efficient. However the block copolymers indeed contributed to the surface property modification, to achieve an encapsulated morphology. Afterwards, a strategy to achieve a core–shell morphology was developed and implemented. The strategy was based on a two step blending allowing to use binary blend models to define the drop size. Micron size PBAT drops with encapsulated PA subinclusions were obtained. Morphologies were detected to be imperfect with the presence of some PA drops at the interface between PLA and PBAT. Regarding mechanical performance, the ternary blends did not show any advantage compared to the binary blends in terms of either stiffness or toughness. Two possible reasons for these poor mechanical properties of the compatibilized ternary blends were identified: the weak interface between the PA

and PBAT (poor efficiency of the PA-*b*-PBAT, the lack of efficient PA-*b*-PBAT copolymer molecules, and/or the too low value of the modulus of the PA (the core phase in our system) relative to the values of the other polymers in order to have the multi-cavitation effect as in HIPS.

References

Berek, D. (2008). Separation of parent homopolymers from diblock copolymers by liquid chromatography under limiting conditions desorption, 1 ‐ Principle of the method. *Macromolecular Chemistry and Physics*, 209(7), 695–706.

Berek, D. (2008). Separation of parent homopolymers from diblock copolymers by liquid chromatography under limiting conditions of desorption, 2 ‐ Optimization of experimental arrangement. *Macromolecular Chemistry and Physics*, 209(21) 2213-2222.

Berek, D. (2010). Separation of parent homopolymers from diblock copolymers by liquid chromatography under limiting conditions of desorption. 3 - Role of column packing. *Polymer*, 51 (3) 587-596.

Berek, D. (2010). Size exclusion chromatography–a blessing and a curse of science and technology of synthetic polymers. *Journal of Separation Science*, 33(3), 315-335.

Considère, M. (1885). Mémoire sur l'emploi du fer et de l'acier dans les constructions. *Annales des Ponts et Chaussées*, 6 Série, Tome 9, 574-775.

Gramespacher, H., & Meissner, J. (1992). Interfacial tension between polymer melts measured by shear oscillations of their blends. *Journal of Rheology*, 36, 1127-1141.

Jiang, L., Wolcott, M. P., & Zhang, J. (2006). Study of biodegradable polylactide/ poly(butylene adipate-co-terephthalate) blends. *Biomacromolecules*, 7(1), 199–207.

Kusy, R. P., Turner, D. T. (1977). Influence of the molecular weight of poly(methyl methacrylate) on fracture morphology in notched tension. *Polymer*, 18(4), 391-402.

Le Corroller, P., & Favis, B. D. (2011). Effect of viscosity in ternary polymer blends displaying partial wetting phenomena. *Polymer*, 52(17), 3827–3834.

Le Hellaye M. (2006). Synthèse et auto-assemblage de copolymères dibloc polyester-b-poly(acide-α-aminés), 2006, Ph.D thesis, Université de Bordeaux.

Macosko, C. W., Guégan, P., Khandpur, A. K., Nakayama, A., Marechal, P., & Inoue, T. (1996). Compatibilizers for melt blending: Premade block copolymers. *Macromolecules,* 29(17), 5590-5598.

Palierne, J. F. (1990). Linear rheology of viscoelastic emulsions with interfacial tension. *Rheologica Acta*, 29(3), 204–214.

Park, S., Park, I., Chang, T., & Ryu, C. Y. (2004). Interaction-controlled HPLC for block copolymer analysis and separation. *Journal of the American Chemical Society*, 126 (29), 8906-8907.

Serpe, G., Jarrin, J., & Dawans, F. (1990). Morphology-processing relationships in polyethylene-polyamide blends. *Polymer Engineering & Science*, 30(9), 553–565.

Siskova, A., Macova, E., Berek, D. (2012). Liquid chromatography under limiting conditions of desorption. 4. Separation of blends containing low-solubility polymers. *European Polymer Journal*, 48 (1) 155-162.

Voigt, W. (1889). Über die Beziehung zwischen den beiden Elasticitätsconstanten isotroper Körper. *Annalen der Physik*, 274, 573–587.

Zhang, N., Wang, Q., Ren, J., & Wang, L. (2008). Preparation and properties of biodegradable poly(lactic acid)/poly(butylene adipate-co-terephthalate) blend with glycidyl methacrylate as reactive processing agent. *Journal of Materials Science*, 44(1), 250–256.

Chapter VI

General conclusion and future outlook

VI General conclusion and future outlook

The purpose of this work was to find ways to prepare a ternary blend by melt mixing showing a core-shell morphology with three predefined polymers PLA, PBAT and PA. The objective was to improve the tenacity of the PLA matrix by mimicking the morphology of high impact polystyrene.

Two main models are able to predict the morphology of a ternary blend. The first model is based on the balance of the spreading coefficients, which are calculated from the interfacial tensions of the three pairs of polymers. The second model consists in the calculation of the free energy of the blend for each morphology in order to find the one with the lowest energy.

The first step of our work was devoted to the measurement of the interfacial tensions between PLA, PBAT and PA. Two techniques were chosen, the Palierne model and the drop retraction method. Drop retraction measurements were preferred due to their higher reliability. Interfacial tension data were then used to calculate the three spreading coefficients and to predict the morphology of our ternary blends. In order to check the theoretical predictions, blends with different compositions were prepared by melt mixing. The morphologies were in all cases in agreement with the results of the spreading coefficient model. In the case where the PLA was the matrix, a partly encapsulated morphology was observed, as predicted. However, this was not the targeted morphology.

To drive the morphology evolution towards the direction of a core–shell structure, the interfacial tensions between PLA/PBAT/PA needed to be tuned. A first trial was carried out with a commercial compatibilizer (Lotader). However, it was found that this non-selective compatibilizer could not achieve the core–shell morphology since it reduced all the three interfacial tensions in the ternary blend at the same time.

Compatibilization with selective block copolymers was then mandatory in our case to selectively modify the interfacial tensions in order to modify the spreading coefficient balance so as to obtain the desired core–shell morphology. Two block copolymers PLA-*b*-PBAT and PBAT-*b*-PA were synthesized thanks to our colleagues at the University of Aix-Marseille and characterized. The compatibilization effect of the copolymers was verified using rheology, measurements of interfacial tension and of the size of the drops in binary blends. It was concluded that the addition of block copolymers

contributed to the decrease of interfacial tensions, potentially enabling the formation of a core–shell morphology.

A strategy was then built in order to practically achieve a core–shell morphology with inclusions and sub-inclusions of the right sizes. A two-step blending procedure was adopted. In a first step, PA droplets were dispersed in the PBAT matrix. In the second step, this blend was further dispersed in the PLA matrix. Two blends were thus prepared with the targeted morphology. Defects in the core–shell morphology were noticed with the presence of a fraction of semi-encapsulated droplets of PA.

Mechanical properties: Young's modulus, yield stress and elongation at break, were measured for the neat polymers, the compatibilized PLA/PBAT blends and the compatibilized ternary blends. Regarding mechanical performance, the ternary blends did not show any advantage compared to the binary blends in terms of either stiffness or toughness. Two possible reasons for these poor mechanical properties of compatibilized ternary blends were identified: the weak interface between the PA and PBAT even if it was compatibilized and/or the too low value of the modulus of PA (the core phase in our system) relative to the values of the other polymers, in order to have the multi-cavitation effect present in HIPS.

We developed a complete methodology that is able to study immiscible ternary blends starting from fundamental considerations, the driving forces for the morphology evolution in binary and ternary blends, and down to the preparation of the blends. This methodology has a general validity and can be widely applied. This work can be used as a reference for future work on ternary blends.

Future outlook

Several further studies could be beneficial for the study of ternary polymer blends:

A first point concerns interfacial tension measurements. It is always surprising to find such different interfacial tension measurements even on the same couple of polymers. It would be interesting to run round-robin tests on the same polymers in different labs to see if the difference arises from differences in the polymers, the methodologies or other causes.

Due to the restricted time for a PhD work, there were different aspects that we were unable to optimize for the development of a ternary blend with improved mechanical properties. Several such aspects are indicated in the following:

- The choice of polymers should take into account morphology considerations but also the intrinsic properties of interest of the polymers (in the present case the mechanical properties). We did not pay enough attention to this aspect.
- The strategy of using diblock copolymers for a selective compatibilization was a good choice. This work clearly showed the role of these copolymers. The amount and the size of the blocks in the copolymers were not optimized. Their role is twofold. They should be efficient for the morphology development but also for stress transmission during mechanical testing.
- The characterization of the morphology was not easy. Mechanical etching has very severe limits when the droplet size becomes too small. It would have been better to apply a selective dissolution of one phase to better visualize the morphology. TEM could be another way to observe this kind of complex morphology.
- In our case, blends were prepared in an internal mixer. A further step would be to study the elaboration of such blends by twin-screw extrusion. This should produce a more homogeneous morphology.
- We did not check if this type of morphology is stable. We assumed it is because it is driven by thermodynamics. However, it would be interesting to check this point by submitting the blend to other processing steps like injection moulding.
- The characterization of the rheological response of such materials with complex morphologies would be of interest in the linear domain, evaluating the effect of time and temperature to probe the morphology stability, transients under constant shear rate and relaxation.
- The mechanical evaluation part of our study was very limited. It would have been interesting to perform a more complete characterization in order to better understand the reinforcement mode: load and unload tensile tests, measurements at different temperatures for tensile and impact tests in order to investigate whether the brittle-toughness transition temperature can be shifted, changing the compositions.

Résumé

Ce travail vise à obtenir une morphologie cœur-peau directement lors du mélangeage à l'état fondu de mélanges de trois polymères, l'acide polylactique (PLA), le poly(butylène adipate-co-téréphtalate) (PBAT) et un copolyamide (PA). Le but final est d'améliorer la ténacité de l'acide polylactique. La morphologie de mélanges de polymères multiphasiques est contrôlée par la thermodynamique du système. La morphologie des mélanges ternaires peut être prédite à partir des valeurs relatives des trois coefficients d'étalement caractérisant le triplet de polymères. Les coefficients d'étalement sont calculés à partir des tensions interfaciales entre les composants pris deux à deux. La détermination des tensions interfaciales entre le PLA, le PBAT et lePA prédit une morphologie dispersée complexe dans la matrice PLA où les sous-inclusions de PA sont partiellement encapsulées dans la phase PBAT. Cette morphologie a bien été obtenue par mélange à l'état fondu des trois composants (observations en microscopie électronique à balayage). Dans une seconde étape, une compatibilisation sélective a été utilisée pour modifier l'emplacement des sous-inclusions de PA. A cette fin, deux copolymères diblocs PBAT-*b*-PLA, PA-*b*-PBAT ont été synthétisés. La présence des copolymères a permis de modifier la tension interfaciale des couples PLA/PBAT et PA/PBAT. Cette modification de l'équilibre des tensions interfaciales a été la clef pour passer d'une semi-encapsulation à une encapsulation complète des sous-inclusions de PA dans les gouttes de PBAT. La performance mécanique de ce mélange ternaire a été évaluée.

Mots Clés

Polymères bio-sourcés, tension interfaciale, mélanges ternaires, morphologie cœur-peau

Abstract

This work aims at achieving direct core-shell morphologies by melt mixing in blends with three polymers, polylactic acid (PLA). poly(butylene adipate-co-terephthalate) (PBAT) and a copolyamide (PA). The final goal is to improve the toughness of PLA. The morphology of multi-phase polymer blends is controlled by interfacial tensions between the components. The morphology of ternary blends can be predicted from the relative values of the three spreading coefficients characterizing the triplet of polymers. Spreading coefficients are calculated from interfacial tensions of couples of components. The determination of interfacial tensions between PLA, PBAT and PA predicts a complex dispersed morphology in the PLA matrix where PA sub-inclusions are partly encapsulated in the PBAT phase. Such a morphology was indeed obtained by melt mixing of the three components (scanning electron microscopy observations). In a second step, selective compatibilization was used to modify the PA sub-inclusion location. To this end, PBAT-*b*-PLA and PA-*b*-PBAT di-block copolymers were synthesized. The presence of the di-block copolymers enabled to modify the interfacial tension in PLA/PBAT and PA/PBAT. The modification of the interfacial tension balance was shown to successfully change the morphology from semi-encapsulation to full encapsulation of PA sub-inclusions in the PBAT drops. The mechanical performance of this ternary blend was evaluated.

Keywords

Biobased polymers, interfacial tension, ternary blends, core shell morphology